Enhanced Multicarrier Techniques for Professional Ad-Hoc and Cell-Based Communications

(EMPhAtiC)

Document Number D6.2

Coordinated multipoint and distributed beamforming

Contractual date of delivery to the CEC:	31/12/2014
Actual date of delivery to the CEC:	09/01/2015
Project Number and Acronym:	318362 EMPhAtiC
Editor:	Jérôme Louveaux
Authors:	Yao Cheng (ITU), Martin Haardt (ITU), Leonardo Baltar (TUM), Oliver De Candido (TUM), Yahia Medjahdi (UCL), Francois Rottenberg (UCL)
Participants:	ITU, TUM, UCL
Workpackage:	WP6
Security:	Public(PU)
Nature:	Report
Version:	2.1
Total Number of Pages:	84

Abstract:

This deliverable presents the results related to task 6.2 on coordinated multipoint and distributed beamforming. The issue of coordinated beamforming design for distributed multi-user MIMO systems using FBMC/OQAM is investigated. New methods are developed to alleviate the dimensionality constraint imposed on the number of antennas in state-of-the art solutions. Both cases of full coordination and partial coordination are considered. Furthermore, solutions are also investigated for highly selective channels where other methods, which are based on the usual assumption of an approximatively flat channel across subcarriers, fail to provide satisfactory results. Finally, the related issue of MIMO channel estimation is investigated. Preamble-based estimation is first analyzed for synchronized and unsynchronized scenarios. Then, a tracking method based on SNR measurements is presented.

Document Revision History

Version	Date	Author	Summary of main changes
0.1	20/12	all involved partners	
2.1	05/01	all involved partners	Glossary, Conclusions, Harmonization of notations

Table of Contents

1. Introduction

The objective of this deliverable is to focus on how multi-user MIMO (multiple-input multiple-output) strategies, and in particular CoMP (coordinated multi-point) and distributed beamforming techniques, can be applied in a PMR scenario using FBMC/OQAM modulation. The implementation of several MIMO techniques, which are fairly simple in CP-OFDM systems, can become much more complex when using the FBMC/OQAM modulation, due to the so-called *intrinsic interference*. This has been an important issue investigated in the literature in the last years. For instance, [1] and [2] have developed receive processing techniques for MIMO FBMC/OQAM systems, when it is assumed that the channel frequency responses of adjacent subcarriers do not vary. On the other hand, to the best of our knowledge, most of the FBMC/OQAM related literature has focused on the centralized scenario where all the (downlink) transmitting antennas are collocated at a single base-station. However in the context of CP-OFDM, the coordinated multi-point technique is known as one of the advanced communication techniques that are able to provide benefits of reduced intercell interference and enhanced cell edge throughput. It has generated a very fruitful research [3], [4], [5], [6], [7]. It is therefore important to investigate the corresponding scenario for FBMC/OQAM-based systems and identify if efficient algorithms can also be designed to benefit from the same advantages.

In this deliverable, we focus on downlink CoMP and the schemes that belong to the category of joint transmission [3]. When the full cooperation between the base stations of adjacent cells is assumed, the channel state information (CSI) and signals for all users are shared by the base stations. In this case, a virtual multi-user MIMO downlink setting is formed, where the transmit antennas are geographically separated. Thereby, the transmission strategies that have been developed for the single cell multi-user MIMO downlink can be employed. Nevertheless, such a full cooperation scheme is not practical due to issues such as it requires excessive information exchange resulting in a large signaling overhead, and the CSI of all users is very hard to acquire [5].

In section 2, the design of beamforming schemes is investigated for downlink CoMP. The state-of-the art techniques are first presented. These techniques provide good results when the channel has low frequency selectivity and when the total number of transmit antenas is (strictly) larger than the total number of receive antennas. This is however not always the case in a distributed scenario, for instance when base stations can help edge users of adjacent cells. Several new methods are then proposed to cope with the case where the total number of receive antennas of the different users served is larger or equal to the total number of transmit antennas. Simulation results show that these methods are able to mitigate the intrinsic interference of FBMC/OQAM and can also cope with medium frequency selectivity.

In section 3, the case of high frequency selectivity is investigated. In that case, all existing methods exhibit an error floor as they are not able to remove all intrinsic interference. For this reason, new multi-tap joint beamforming and equalization schemes are proposed and designed. Due to the inter-dependencies between the precoder filters at the transmitter of an FBMC system, straight MMSE design is quite complex. Hence two methods are proposed to deal with the issue. The first method is iterative and successively optimizes the precoder and equalizer using the uplink-downlink duality. The second method is based on a signal-to-leakage criterion. Simulation results show that these methods significantly outperform stat-of-the-art techniques in high selective scenarios.

Section 4 and 5 tackle the issue of distributed MIMO channel estimation, which is a requirement in order to implement the beamforming techniques presented in sections 2 and 3. Section 4 focuses on the analysis of preamble-based techniques. Two channel estimation meth-

ods are presented and compared. It is suggested to perform a subcarrier assignment during the preamble and two subcarrier assignment schemes are compared, both in synchronized and unsynchronized scenarios. Simulation results are provided for both CP-OFDM and FBMC/OQAM modulations. Results show that the equispaced assignment performs better in most situations.

Finally, section 5 investigates the tracking of MIMO channel estimation. A method is proposed that does not rely on scattered pilots but only requires the feedback of SNR measurements. The method is based on small perturbations applied to the transmitted signal. Results show that, despite the small amount of feedback needed, the method is still able to provide accurate estimation results in a tracking scenario (i.e. when a coarse estimation has already been performed).

2. Intrinsic interference mitigating coordinated beamforming (IIM-CBF) for the downlink of FBMC/OQAM based multi-user MIMO systems and coordinated multi-point systems

We propose intrinsic interference mitigating coordinated beamforming (IIM-CBF) based transmission strategies for the downlink of multi-user MIMO systems and coordinated multi-point (CoMP) systems where filter bank based multi-carrier with offset quadrature amplitude modulation (FBMC/OQAM) is employed. Our goal is to alleviate the dimensionality constraint imposed on the state-of-the-art solutions for FBMC/OQAM based space division multiple access (SDMA) that the total number of receive antennas of the users must not exceed the number of transmit antennas at the base station. First, a single-cell multi-user MIMO downlink system is considered, and two IIM-CBF algorithms are proposed for the case where the number of transmit antennas at the base station is equal to the total number of receive antennas of the users and the case where the former is smaller than the latter, respectively. The central idea is to jointly and iteratively calculate the precoding matrix and the decoding matrix for each subcarrier to mitigate the multi-user interference as well as the intrinsic interference inherent in FBMC/OQAM based systems. Second, for a CoMP downlink scenario where partial coordination among the base stations is considered, the application of coordinated beamforming based transmission schemes is further investigated. An appropriate IIM-CBF technique is proposed. Simulation results show that when the number of transmit antennas at the base station is equal to the total number of receive antennas of the users, the proposed IIM-CBF algorithm outperforms the existing transmission strategies for FBMC/OQAM based multi-user MIMO downlink systems. Moreover, we evaluate the performances of the IIM-CBF strategies in the downlink of multi-user MIMO systems and CoMP systems where the total number of receive antennas of the users exceeds the number of transmit antennas at the base station. It is observed that by employing the proposed IIM-CBF schemes, the FBMC/OQAM systems achieve a similar bit error rate (BER) performance as its orthogonal frequency division multiplexing with the cyclic prefix insertion (CP-OFDM) based counterpart while exhibiting superiority in terms of a higher spectral efficiency, a greater robustness against synchronization errors, and a lower out-of-band radiation. In the presence of residual carrier frequency offsets, the superiority of the FBMC/OQAM systems over the CP-OFDM based systems is demonstrated, which corroborates the theoretical analysis that the FBMC/OQAM systems are more immune to the lack of perfect synchronization. In addition, numerical results with respect to the convergence behavior of the proposed IIM-CBF techniques are presented, and the computational complexity issue is also addressed.

2.1 Introduction

Filter bank based multi-carrier modulation (FBMC) is widely known as a promising alternative to orthogonal frequency division multiplexing with the cyclic prefix insertion (CP-OFDM). Thanks to the use of spectrally well-contained synthesis and analysis filter banks at the transmitter and at the receiver [8], [9], FBMC features a concentrated spectrum and a much lower out-of-band radiation compared to CP-OFDM. Consequently, it is beneficial to choose FBMC over CP-OFDM for asynchronous scenarios [10], [11], or to achieve an effective utilization of spectrum holes [12], [13]. Moreover, in systems where filter bank based multi-carrier with offset

quadrature amplitude modulation (FBMC/OQAM) is employed, the insertion of the CP is not needed as in CP-OFDM based systems, leading to a higher spectral efficiency.

In FBMC/OQAM systems, the real and imaginary parts of each complex-valued data symbol are staggered by half of the symbol period [8], [14] such that the desired signal and the intrinsic interference are separated in the real domain and in the pure imaginary domain, respectively. Different approaches of canceling the intrinsic interference have been proposed based on different assumptions on the frequency selectivity of the channel. In [1] and [2] where receive processing techniques have been developed for multiple-input-multiple-out (MIMO) FBMC/OQAM systems, it is assumed that the channel frequency responses of adjacent subcarriers do not vary. Consequently, the intrinsic interference is canceled by taking the real part of the resulting signal after the equalization.

To alleviate the constraint on the frequency selectivity of the channel, a zero forcing (ZF) based approach has been proposed in [15] for multi-stream transmissions in a MIMO FBMC/OQAM system where the channel is not restricted to flat fading. More details of the performance analysis of this algorithm have been presented in [16]. However, the work in [15] and [16] is limited to the case where the number of receive antennas does not exceed the number of transmit antennas. In addition, the authors have shown numerically and have also pointed out that their proposed approach only provides a satisfactory performance in an asymmetric configuration, i.e., when the number of transmit antennas is larger than the number of receive antennas. Based on the concept of mitigating the intrinsic interference mentioned above for point-to-point MIMO FBMC/OQAM systems, the authors in [17] have adapted the conventional spatial Tomlinson Harashima precoder (STHP) to an FBMC/OQAM based multiple-input-single-output broadcast channel (MISO-BC) which results in a new non-linear precoder. It is known that non-linear precoders have a higher computational complexity compared to linear precoders. Moreover, the non-linear precoding technique in [17] is restricted to the case where each user is equipped with only a single receive antenna. On the other hand, a block diagonalization (BD) based linear precoder has been developed in [18] for the FBMC/OQAM based multi-user MIMO downlink with space division multiple access (SDMA). It adopts the central idea of BD [19] to mitigate the multi-user interference and then uses the ZF based approach [15] to deal with the intrinsic interference cancellation for the resulting equivalent single-user transmissions. Consequently, this algorithm inherits the drawback of the ZF based scheme such that it also fails to achieve a good performance in a symmetric multi-user MIMO downlink setting, where the number of transmit antennas at the base station is equal to the total number of receive antennas of the users. In addition, this linear precoder suffers from the dimensionality constraint that the total number of receive antennas of the users must not exceed the number of transmit antennas at the base station. Note that similarly as in these publications, we focus on scenarios where the channel on each subcarrier is flat fading in this chapter. However, we will consider more critical downlink settings of multi-user PMR scenarios where the channels exhibit severe frequency selectivity in Chapter 3. In addition, in the aforementioned publications on the FBMC/OQAM based multi-user downlink, the impact of the residual carrier frequency offsets (CFOs) has not been investigated.

To the best of our knowledge, FBMC/OQAM based coordinated multi-point (CoMP) techniques have not been studied in the literature. In the context of CP-OFDM the corresponding research has been very fruitful, and CoMP is known as one of the advanced communication techniques that are able to provide benefits of reduced intercell interference and enhanced cell edge throughput [3], [4], [5], [6], [7]. In this work, we focus on downlink CoMP and the schemes that belong to the category of joint transmission [3]. When the full cooperation between the base stations of adjacent cells is assumed, the channel state information (CSI) and signals for all

users are shared by the base stations. In this case, a virtual multi-user MIMO downlink setting is formed, where the transmit antennas are geographically separated. Thereby, the transmission strategies that have been developed for the single cell multi-user MIMO downlink can be employed. Nevertheless, such a full cooperation scheme is not practical due to issues such as it requires excessive information exchange resulting in a large signaling overhead, and the CSI of all users is very hard to acquire [5]. As a more realistic solution, partial cooperation schemes have been proposed in [5], [6], [20], where the users are classified into two categories, cell [or in some papers [5], [6] cluster that consists of multiple cells] interior users and cell (cluster) edge users. The base stations of adjacent cells (clusters) transmit the same signals to the cell (cluster) edge users, and coordinated beamforming techniques that rely on the limited cooperation between the cells (clusters) (e.g., the exchange of the beamforming matrices for cell (cluster) edge users) are employed to suppress the intra-cell (cluster) and inter-cell (cluster) interference. For these downlink CoMP scenarios, it is more likely that the total number of receive antennas of the users served by one base station is larger than the number of transmit antennas. Thus, transmission strategies that are able to tackle such a case are required. Note that in the aforementioned publications on CP-OFDM based downlink CoMP, perfect synchronization is assumed. However, the asynchronous nature of the interference in the downlink CoMP setting is emphasized in [21]. It has been shown in [21] that the lack of perfect synchronization causes a performance degradation. Such a fact greatly motivates the use of FBMC as a replacement of CP-OFDM, as FBMC is more robust against synchronization errors compared to CP-OFDM.

In this report, we present intrinsic interference mitigating coordinated beamforming (IIM-CBF) schemes that we have designed for the FBMC/OQAM based multi-user MIMO downlink systems and CoMP downlink systems without restricting the configuration with respect to the number of transmit antennas and the number of receive antennas. First, considering the symmetric single-cell multi-user MIMO downlink setting where the number of transmit antennas at the base station is equal to the total number of receive antennas of the users, we propose to compute the precoding matrix and the decoding matrix jointly in an iterative procedure for each subcarrier. Different choices of the decoding matrix in the initialization step are recommended for different scenarios. For CP-OFDM based multi-user MIMO downlink systems, there have been some publications on coordinated beamforming techniques [22], [5] proposed to cope with the dimensionality constraint imposed on BD based precoding algorithms [19]. Inspired by these works, an IIM-CBF scheme specifically for FBMC/OQAM based systems is developed to alleviate the same dimensionality constraint that all state-of-the-art transmission strategies for FBMC/OQAM based multi-user downlink settings suffer from. It handles the mitigation of the multi-user interference as well as the intrinsic interference. Moreover, we investigate FBMC/OQAM based CoMP techniques for the first time and provide an extension of the IIM-CBF scheme designed for the FBMC/OQAM based multi-user MIMO downlink system. To evaluate the performance of the proposed IIM-CBF algorithms, we have performed extensive simulations. The BER as well as sum rate performances are shown, and the convergence behavior of the developed coordinated beamforming techniques is also investigated via numerical results. It can be observed that the number of iterations required for the convergence in these IIM-CBF schemes is acceptable. Thus, the additional computational complexity is not prohibitive compared to the close-form algorithms which fail in scenarios where the total number of receive antennas of the users exceeds the number of transmit antennas. In the deliverable D4.3, some results with respect to IIM-CBF 1 and IIM-CBF 2 have been reported. The impact of imperfect channel state state information on the performance of these two schemes has been studied as well. In this document, on the other hand, we investigate the effects of the residual CFOs and demonstrate the superiority of the FBMC/OQAM based system over its CP-OFDM

based counterpart in the tolerance of the synchronization errors.

In the sequel, the data model of a single-cell multi-user MIMO FBMC/OQAM system is first introduced, and two state-of-the-art transmission strategies for such a system are reviewed. Then, we describe the two proposed algorithms IIM-CBF 1 and IIM-CBF 2 in detail for the case where the number of transmit antennas at the base station is equal to the total number of receive antennas of the users and the case where the former is smaller than the latter, respectively. With our focus on the CoMP downlink, we further present another coordinated beamforming based transmission scheme, namely "IIM-CBF 3". Finally, numerical results are shown, before conclusions are drawn.

2.2 System model

In a multi-user MIMO downlink system where SDMA is employed, one base station equipped with $M_{\mathrm{T}}^{(\mathrm{BS})}$ transmit antennas transmits to Q users at the same time and on the same frequency. The number of receive antennas of the qth user is denoted by M_{R_q}, and the total number of receive antennas of all users severed simultaneously is then $M_{\mathrm{R}}^{(\mathrm{tot})} = \sum_{q=1}^{Q} M_{\mathrm{R}_q}$. Assuming that the channel on each subcarrier can be treated as flat fading [15], [16], [18], the combined receive vector on the kth subcarrier and at the nth time instant is denoted by $\boldsymbol{y}_k[n] = \begin{bmatrix} \boldsymbol{y}_{1,k}^{\mathrm{T}}[n] & \boldsymbol{y}_{2,k}^{\mathrm{T}}[n] & \cdots & \boldsymbol{y}_{Q,k}^{\mathrm{T}}[n] \end{bmatrix}^{\mathrm{T}} \in \mathbb{C}^{M_{\mathrm{R}}^{(\mathrm{tot})}}$ where the received signals of all Q users are stacked and can be represented by

$$\begin{aligned} \boldsymbol{y}_k[n] =& \boldsymbol{H}_k[n]\boldsymbol{F}_k[n]\boldsymbol{d}_k[n] + \sum_{i=n-3}^{n+3} \sum_{\ell=k-1}^{k-+1} \boldsymbol{H}_\ell[i]\boldsymbol{F}_\ell[i] c_{i\ell} \boldsymbol{d}_\ell[i] \\ &+ \boldsymbol{n}_k[n], \quad (\ell, i) \neq (k, n). \end{aligned} \tag{2.1}$$

Here $\boldsymbol{H}_k[n] \in \mathbb{C}^{M_{\mathrm{R}}^{(\mathrm{tot})} \times M_{\mathrm{T}}^{(\mathrm{BS})}}$ denotes the combined channel matrix of all Q users[1] and is written as

$$\boldsymbol{H}_k[n] = \begin{bmatrix} \boldsymbol{H}_{1,k}^{\mathrm{T}}[n] & \boldsymbol{H}_{2,k}^{\mathrm{T}}[n] & \cdots & \boldsymbol{H}_{Q,k}^{\mathrm{T}}[n] \end{bmatrix}^{\mathrm{T}}, \tag{2.2}$$

where $\boldsymbol{H}_{q,k}[n] \in \mathbb{C}^{M_{\mathrm{R}_q} \times M_{\mathrm{T}}^{(\mathrm{BS})}}$ represents the channel frequency response between the base station and the qth user, $q = 1, 2, \ldots, Q$. The data vector $\boldsymbol{d}_k[n] \in \mathbb{R}^d$ with the total number of spatial streams $d = \sum_{q=1}^{Q} d_q$ is expressed as

$$\boldsymbol{d}_k[n] = \begin{bmatrix} \boldsymbol{d}_{1,k}^{\mathrm{T}}[n] & \boldsymbol{d}_{2,k}^{\mathrm{T}}[n] & \cdots & \boldsymbol{d}_{Q,k}^{\mathrm{T}}[n] \end{bmatrix}^{\mathrm{T}}, \tag{2.3}$$

where $\boldsymbol{d}_{q,k}[n] \in \mathbb{R}^{d_q}$ denotes the desired signal for the qth user on the kth subcarrier and at the nth time instant when $(k+n)$ is even[2], and d_q denotes the number of spatial streams sent to the qth user. The terms $c_{i\ell}\boldsymbol{d}_\ell[i]$ in (2.1) contribute to the intrinsic interference and

[1] Here we only provide the formulas of the channel matrices, precoding matrices, and data vectors on the kth subcarrier and at the nth time instant explicitly due to limited space. In case of the ℓth subcarrier and the ith time instant, the corresponding expressions can be obtained by replacing k and n with ℓ and i, respectively.

[2] For the case where $(k+n)$ is odd, the desired signal on the kth subcarrier and at the nth time instant is pure imaginary, while the intrinsic interference is real providing that the prototype pulse satisfies the perfect reconstruction property [14], [17]. As the two cases are essentially equivalent to each other, we only take the case where $(k+n)$ is even to describe the proposed algorithm in this document. In addition, each entry in the data vector corresponds to either the in-phase component or the quadrature component of a QAM symbol that is assumed to have unit energy.

are pure imaginary if the prototype pulse satisfies the perfect reconstruction property [14], [17], where $\ell = k-1,\ k,\ k+1,\ i = n-3,\ldots,n+3$, and $(\ell,i) \neq (k,n)$. The coefficients $c_{i\ell}$ (cf. Table 2-1) represent the system impulse response determined by the synthesis and analysis filters. The PHYDYAS prototype filter [23] is used, and the overlapping factor is chosen to be $K = 4$. For more details about FBMC/OQAM systems, the reader is referred to [14]. Moreover, $\boldsymbol{n}_k[n] \in \mathbb{C}^{M_{\mathrm{R}}^{(\mathrm{tot})}}$ denotes the combined additive white Gaussian noise vector with variance σ_n^2, and the noise is assumed to be spatially uncorrelated. For the qth user, the noise autocorrelation matrix is written as $\sigma_n^2 \boldsymbol{I}_{M_{\mathrm{R}_q}}$.

	$n-3$	$n-2$	$n-1$	n	$n+1$	$n+2$	$n+3$
$k-1$	$0.043\jmath$	-0.125	$-0.206\jmath$	0.239	$0.206\jmath$	-0.125	$-0.043\jmath$
k	-0.067	0	0.564	1	0.564	0	-0.067
$k+1$	$-0.043\jmath$	-0.125	$0.206\jmath$	0.239	$-0.206\jmath$	-0.125	$0.043\jmath$

Table 2-1: Coefficients $c_{i\ell}$ representing the system impulse response determined by the synthesis and analysis filters [14] (the PHYDYAS prototype filter [23] used with the overlapping factor $K = 4$)

Furthermore, $\boldsymbol{F}_k[n] \in \mathbb{C}^{M_{\mathrm{T}}^{(\mathrm{BS})} \times d}$ contains the precoding matrices for all users

$$\boldsymbol{F}_k[n] = \begin{bmatrix} \boldsymbol{F}_{1,k}[n]\boldsymbol{G}_{1,k}[n] & \boldsymbol{F}_{2,k}[n]\boldsymbol{G}_{2,k}[n] & \cdots & \boldsymbol{F}_{Q,k}[n]\boldsymbol{G}_{Q,k}[n] \end{bmatrix}, \tag{2.4}$$

where $\boldsymbol{F}_{q,k}[n] \in \mathbb{C}^{M_{\mathrm{T}}^{(\mathrm{BS})} \times M_{\mathrm{T}_q}^{(\mathrm{eq})}}$, $q = 1,2,\ldots,Q$, are calculated to mitigate the multi-user interference by employing, e.g., block diagonalization (BD) [19] such that a multi-user MIMO downlink system is decoupled into parallel equivalent single-user transmissions. Here $M_{\mathrm{T}_q}^{(\mathrm{eq})}$ symbolizes the resulting equivalent number of transmit antennas for the qth user. It is determined by the precoding scheme employed to suppress the multi-user interference, which will be explained in detail in Section 2.3. In addition, $\boldsymbol{G}_{q,k}[n] \in \mathbb{C}^{M_{\mathrm{T}_q}^{(\mathrm{eq})} \times d_q}$, $q = 1,2,\ldots,Q$, are the transmit beamforming matrices for the equivalent single-user systems. Note that throughout this work equal power allocation on the spatial streams and subcarriers is assumed.

2.2.1 Straightforward extension of the transmission strategy as in case of CP-OFDM

In some publications on MIMO FBMC/OQAM systems, such as [1] and [2], it is assumed that the channel stays constant across adjacent subcarriers and during consecutive symbol periods, i.e.,

$$\begin{gathered} \boldsymbol{H}_k[n] = \boldsymbol{H}_\ell[i], \\ \ell = k-1,\ k,\ k+1, \quad i = n-3,\ldots,n+3. \end{gathered}$$

Since the precoding is performed on a per-subcarrier basis, i.e., the calculation of the precoding matrices for a certain subcarrier is solely determined by the channel on the same subcarrier, the precoding matrices are also the same on adjacent subcarriers. Therefore, the combined received signal on the kth subcarrier and at the nth time instant can be expressed as

$$\boldsymbol{y}_k[n] = \boldsymbol{H}_k[n]\boldsymbol{F}_k[n]\widetilde{\boldsymbol{d}}_k[n] + \boldsymbol{n}_k[n], \tag{2.5}$$

where $\widetilde{\boldsymbol{d}}_k[n]$ contains the real-valued desired signal and the pure imaginary intrinsic interference

$$\widetilde{\boldsymbol{d}}_k[n] = \boldsymbol{d}_k[n] + \sum_{i=n-3}^{n+3} \sum_{\ell=k-1}^{k+1} c_{i\ell} \boldsymbol{d}_\ell[i], \quad (\ell, i) \neq (k, n). \tag{2.6}$$

Considering $\widetilde{\boldsymbol{d}}_k[n]$ as an equivalent transmitted signal, (2.5) resembles the data model of a CP-OFDM based multi-user MIMO downlink system. Consequently, transmission strategies that have been developed for multi-user MIMO CP-OFDM downlink systems can be straightforwardly extended to their FBMC/OQAM based counterparts where only one additional step is required, i.e., taking the real part of the resulting signal after the multiplication by the decoding matrix

$$\hat{\boldsymbol{d}}_k[n] = \mathrm{Re}\left\{ \boldsymbol{D}_k^{\mathrm{H}}[n] \boldsymbol{y}_k[n] \right\}, \tag{2.7}$$

where $\boldsymbol{D}_k[n] \in \mathbb{C}^{M_{\mathrm{R}}^{(\mathrm{tot})} \times d}$ is the combined block-diagonal decoding matrix on the kth subcarrier and at the nth time instant that contains the decoding matrices $\boldsymbol{D}_{q,k}[n] \in \mathbb{C}^{M_{\mathrm{R}_q} \times d_q}$, $q = 1, 2, \ldots, Q$, for the Q users, respectively. It is worth mentioning that there is no cooperation among the users, and the decoding matrix for each user is computed separately. Here $\mathrm{Re}\{\cdot\}$ symbolizes the real part of the input argument, while $\mathrm{Im}\{\cdot\}$ represents the imaginary part.

The concept of this transmission scheme is simple, does not induce much additional processing compared to CP-OFDM based systems, and directly applies the state-of-the-art transmit as well as receive processing techniques developed for the CP-OFDM based multi-user MIMO downlink. Nevertheless, it relies on the impractical assumption that the channel is flat fading and time invariant. In case of frequency selective channels, this transmission strategy fails to completely eliminate the intrinsic interference inherent in FBMC/OQAM systems and thus suffers from a performance degradation as also shown in the simulations section.

2.2.2 Block diagonalization based approach

In [18] a BD based precoding algorithm has been proposed for FBMC/OQAM based multi-user MIMO downlink systems, where $M_{\mathrm{T}}^{(\mathrm{BS})} \geq M_{\mathrm{R}}^{(\mathrm{tot})}$. First, the BD algorithm [19] is used to calculate the first part of the precoding matrix $\boldsymbol{F}_{q,k}[n]$, $q = 1, 2, \ldots, Q$, for the Q users to mitigate the multi-user interference. By rendering $\boldsymbol{F}_{q,k}[n]$ for the qth user to lie in the null space of all the other users' combined channel matrix, it is ensured that

$$\boldsymbol{H}_{g,k}[n] \cdot \boldsymbol{F}_{q,k}[n] = \boldsymbol{0} \quad \in \mathbb{C}^{M_{\mathrm{R}_q} \times M_{\mathrm{T}_q}^{(\mathrm{eq})}}, \quad g \neq q. \tag{2.8}$$

Consequently, the received signal of the qth user is expressed as

$$\begin{aligned} \boldsymbol{y}_{q,k}[n] =& \boldsymbol{H}_{q,k}[n] \boldsymbol{F}_{q,k}[n] \boldsymbol{G}_{q,k} \boldsymbol{d}_{q,k}[n] \\ &+ \sum_{i=n-3}^{n+3} \sum_{\ell=k-1}^{k+1} \boldsymbol{H}_{q,\ell}[i] \boldsymbol{F}_{q,\ell}[i] \boldsymbol{G}_{q,\ell}[i] c_{i\ell} \boldsymbol{d}_{q,\ell}[i] \\ &+ \boldsymbol{n}_{q,k}[n], \quad (\ell, i) \neq (k, n), \end{aligned} \tag{2.9}$$

where $\boldsymbol{H}_{q,k}[n] \boldsymbol{F}_{q,k}[n] \in \mathbb{C}^{M_{\mathrm{R}_q} \times M_{\mathrm{T}_q}^{(\mathrm{eq})}}$, $q = 1, 2, \ldots, Q$, can be treated as the equivalent channels for parallel single-user transmissions. Let us expand the real part of the received signal of the

qth user

$$\begin{aligned}\mathrm{Re}\left\{\boldsymbol{y}_{q,k}[n]\right\} =& \mathrm{Re}\left\{\boldsymbol{H}_{q,k}[n]\boldsymbol{F}_{q,k}[n]\boldsymbol{G}_{q,k}\right\}\boldsymbol{d}_{q,k}[n] \\ &+ (-1)\cdot\sum_{i=n-3}^{n+3}\sum_{\ell=k-1}^{k+1}\mathrm{Im}\left\{\boldsymbol{H}_{q,\ell}[i]\boldsymbol{F}_{q,\ell}[i]\boldsymbol{G}_{q,\ell}[i]\right\}\mathrm{Re}\left\{c_{i\ell}\boldsymbol{d}_{q,\ell}[i]\right\} \\ &+ \mathrm{Re}\left\{\boldsymbol{n}_{q,k}[n]\right\}, \quad (\ell,i)\neq(k,n). \end{aligned} \tag{2.10}$$

To cancel the intrinsic interference, the second term on the right hand side of (2.10) should be rendered as zero. This can be achieved by computing the second part of the precoding matrix suth that [18]

$$\mathrm{Im}\left\{\boldsymbol{H}_q\boldsymbol{F}_q\boldsymbol{G}_q\right\} = \boldsymbol{0} \quad \in \mathbb{C}^{M_{\mathrm{R}_q}\times d_q}, \tag{2.11}$$

where $\boldsymbol{F}_q\boldsymbol{G}_q$ represents the precoding matrix for the qth user on a certain subcarrier and at a certain time instant, and $\boldsymbol{H}_q$ denotes the channel matrix for the qth user on the same subcarrier and at the same time instant. From now on, the time and frequency indices are ignored as the precoding is performed on a per-subcarrier basis. It should be noted that the optimization of the power allocation is originally incorporated in the BD based technique [18]. Nevertheless, this part of the algorithm is not reviewed in detail here, since optimizing the power allocation is beyond our scope and equal power allocation is assumed. In the simulations section, when using the BD based technique as a benchmark scheme, equal power allocation is also adopted to ensure a fair comparison.

This approach outperforms the straightforward extension of the CP-OFDM case in the sense that it is able to tolerate a certain level of the frequency selectivity of the channel. However, it suffers from the dimensionality constraint that the number of transmit antennas at the base station has to be larger than or equal to the total number of receive antennas of the users, i.e., $M_{\mathrm{T}}^{(\mathrm{BS})} \geq M_{\mathrm{R}}^{(\mathrm{tot})}$. For the case where $M_{\mathrm{T}}^{(\mathrm{BS})} = M_{\mathrm{R}}^{(\mathrm{tot})}$, this scheme is not able to provide a satisfactory performance as shown later in the simulation section.

2.3 Coordinated beamforming for the single-cell multi-user MIMO downlink

Based on the philosophy on the precoding design for multi-user MIMO downlink settings first proposed in [24], the precoding matrix for each user is decomposed into two parts as already shown in (2.4). For the qth user, the first part $\boldsymbol{F}_q$ eliminates the multi-user interference[3]. The second part $\boldsymbol{G}_q$ plays the role of the transmit beamforming matrix for each equivalent single-user transmission after the multi-user interference cancellation. Due to the fact that the intrinsic interference resides in FBMC/OQAM based systems, we propose to further decouple $\boldsymbol{G}_q$ into two parts, i.e.,

$$\boldsymbol{G}_q = \boldsymbol{G}_{q,1}\boldsymbol{G}_{q,2} \in \mathbb{C}^{M_{\mathrm{T}_q}^{(\mathrm{eq})}\times d_q}, \tag{2.12}$$

where $\boldsymbol{G}_{q,1} \in \mathbb{C}^{M_{\mathrm{T}_q}^{(\mathrm{eq})}\times M_{x_q}}$ is computed to suppress the intrinsic interference, and $\boldsymbol{G}_{q,2} \in \mathbb{R}^{M_{x_q}\times d_q}$ is used for the spatial mapping.

[3] In IIM-CBF 3 for the CoMP downlink, $\boldsymbol{F}_q$ suppresses both the intra-cell interference and the inter-cell interference.

2.3.1 The IIM-CBF 1 algorithm

We first propose a coordinated beamforming based transmission scheme IIM-CBF 1 for symmetric multi-user MIMO downlink settings where $M_{\mathrm{T}}^{(\mathrm{BS})} = M_{\mathrm{R}}^{(\mathrm{tot})}$. BD [19] is employed to calculate the first part of the precoding matrices $\boldsymbol{F}_q \in \mathbb{C}^{M_{\mathrm{T}}^{(\mathrm{BS})} \times M_{\mathrm{T}_q}^{(\mathrm{eq})}}$, $q = 1, 2, \ldots, Q$. For the qth user, define a matrix $\widetilde{\boldsymbol{H}}_{\mathrm{e}} \in \mathbb{C}^{(M_{\mathrm{R}}^{(\mathrm{tot})} - M_{\mathrm{R}_q}) \times M_{\mathrm{T}}^{(\mathrm{BS})}}$ as

$$\widetilde{\boldsymbol{H}}_{\mathrm{e}} = \left[\begin{array}{ccccccc} \boldsymbol{H}_1^{\mathrm{T}} & \cdots & \boldsymbol{H}_{q-1}^{\mathrm{T}} & \boldsymbol{H}_{q+1}^{\mathrm{T}} & \cdots & \boldsymbol{H}_Q^{\mathrm{T}} \end{array} \right]^{\mathrm{T}}, \tag{2.13}$$

which contains the channel matrices of all the other users. The precoding matrix $\boldsymbol{F}_q$ for the qth user is obtained as $\boldsymbol{F}_q = \widetilde{\boldsymbol{V}}_{\mathrm{e}_{(q,0)}} \in \mathbb{C}^{M_{\mathrm{T}}^{(\mathrm{BS})} \times M_{\mathrm{T}_q}^{(\mathrm{eq})}}$, where $\widetilde{\boldsymbol{V}}_{\mathrm{e}_{(q,0)}}$ contains the last $M_{\mathrm{T}_q}^{(\mathrm{eq})}$ right singular vectors that form an orthonormal basis for the null space of $\widetilde{\boldsymbol{H}}_{\mathrm{e}}$ [19]. The resulting equivalent number of transmit antennas $M_{\mathrm{T}_q}^{(\mathrm{eq})} = M_{\mathrm{T}}^{(\mathrm{BS})} - \sum_{g=1, g\neq q}^{Q} M_{\mathrm{R}_g}$ is equal to M_{R_q}. The reader is referred [19] for more details of the BD algorithm.

For the qth user, we propose to jointly and iteratively update the second part of its precoding matrix $\boldsymbol{G}_q$ and its decoding matrix. An equivalent channel matrix $\boldsymbol{H}_{\mathrm{e}_q}$ is defined as

$$\boldsymbol{H}_{\mathrm{e}_q} = \boldsymbol{D}_q^{\mathrm{T}} \boldsymbol{H}_q \boldsymbol{F}_q \in \mathbb{C}^{d_q \times M_{\mathrm{T}_q}^{(\mathrm{eq})}}, \tag{2.14}$$

where $\boldsymbol{D}_q \in \mathbb{R}^{M_{\mathrm{R}_q} \times d_q}$ is the real-valued decoding matrix. The proposed coordinated beamforming algorithm is summarized as follows:

- **Step 1**: Initialize the decoding matrix $\boldsymbol{D}_q^{(0)} \in \mathbb{R}^{M_{\mathrm{R}_q} \times d_q}$, set the iteration index p to zero, and set a threshold ϵ for the stopping criterion. The decoding matrix is generated randomly if the current subcarrier is the first one; otherwise set the decoding matrix as the one calculated for the previous subcarrier [22].

- **Step 2**: Set $p \leftarrow p + 1$ and calculate the equivalent channel matrix $\boldsymbol{H}_{\mathrm{e}_q}^{(p)}$ in the pth iteration as

  $$\boldsymbol{H}_{\mathrm{e}_q}^{(p)} = \boldsymbol{D}_q^{(p-1)^{\mathrm{T}}} \boldsymbol{H}_q \boldsymbol{F}_q \in \mathbb{C}^{d_q \times M_{\mathrm{T}_q}^{(\mathrm{eq})}}. \tag{2.15}$$

  Define a matrix

  $$\check{\boldsymbol{H}}_{\mathrm{e}_q}^{(p)} = \left[\begin{array}{cc} \mathrm{Im}\left\{ \boldsymbol{H}_{\mathrm{e}_q}^{(p)} \right\} & \mathrm{Re}\left\{ \boldsymbol{H}_{\mathrm{e}_q}^{(p)} \right\} \end{array} \right] \in \mathbb{R}^{d_q \times 2M_{\mathrm{T}_q}^{(\mathrm{eq})}}. \tag{2.16}$$

- **Step 3**: Calculate the precoding matrix $\boldsymbol{G}_q^{(p)} = \boldsymbol{G}_{q,1}^{(p)} \boldsymbol{G}_{q,2}^{(p)}$ for the pth iteration. First, we perform the singular value decomposition (SVD) of $\check{\boldsymbol{H}}_{\mathrm{e}_q}^{(p)}$ as

  $$\check{\boldsymbol{H}}_{\mathrm{e}_q}^{(p)} = \boldsymbol{U}_{q,1}^{(p)} \boldsymbol{\Sigma}_{q,1}^{(p)} \boldsymbol{V}_{q,1}^{(p)^{\mathrm{T}}}. \tag{2.17}$$

  Denoting the rank of $\check{\boldsymbol{H}}_{\mathrm{e}_q}^{(p)}$ as $r_q^{(p)}$, we define $\boldsymbol{V}_{q,1,0}^{(p)} \in \mathbb{R}^{2M_{\mathrm{T}_q}^{(\mathrm{eq})} \times M_{x_q}}$ as containing the last $M_{x_q} = 2M_{\mathrm{T}_q}^{(\mathrm{eq})} - r_q^{(p)}$ right singular vectors that form an orthonormal basis for the null space of $\check{\boldsymbol{H}}_{\mathrm{e}_q}^{(p)}$. Hence, $\boldsymbol{G}_{q,1}^{(p)}$ for the pth iteration can be obtained via

  $$\boldsymbol{V}_{1,0}^{(p)} = \left[\begin{array}{c} \mathrm{Re}\left\{ \boldsymbol{G}_{q,1}^{(p)} \right\} \\ \mathrm{Im}\left\{ \boldsymbol{G}_{q,1}^{(p)} \right\} \end{array} \right] \in \mathbb{R}^{2M_{\mathrm{T}_q}^{(\mathrm{eq})} \times M_{x_q}}. \tag{2.18}$$

To further calculate $\boldsymbol{G}_{q,2}^{(p)}$, the following equivalent channel matrix after the cancellation of the intrinsic interference for the pth iteration is defined as

$$\widetilde{\boldsymbol{H}}_{\mathrm{e}_q}^{(p)} = \mathrm{Re}\left\{\boldsymbol{H}_{\mathrm{e}_q}^{(p)}\boldsymbol{G}_{q,1}^{(p)}\right\} \in \mathbb{R}^{d_q \times M_{x_q}}. \tag{2.19}$$

Further calculate the SVD of $\widetilde{\boldsymbol{H}}_{\mathrm{e}_q}^{(p)}$, and define $\boldsymbol{V}_{q,2,1}^{(p)} \in \mathbb{R}^{M_{x_q}\times d_q}$ as containing the first d_q right singular vectors. Thereby, $\boldsymbol{G}_{q,2}^{(p)}$ is obtained as $\boldsymbol{G}_{q,2}^{(p)} = \boldsymbol{V}_{q,2,1}^{(p)}$.

- **Step 4**: Update the decoding matrix based on the equivalent channel matrix after the cancellation of the intrinsic interference where only the processing at the transmitter is considered

$$\widetilde{\boldsymbol{H}}_{\mathrm{etx}_q}^{(p)} = \mathrm{Re}\left\{\boldsymbol{H}_q\boldsymbol{F}_q\boldsymbol{G}_q^{(p)}\right\} \in \mathbb{R}^{M_{\mathrm{R}_q}\times d_q}. \tag{2.20}$$

When the MMSE receiver[4] is used, the decoding matrix has the following form

$$\boldsymbol{D}_q^{(p)} = \widetilde{\boldsymbol{H}}_{\mathrm{etx}_q}^{(p)}\left(\widetilde{\boldsymbol{H}}_{\mathrm{etx}_q}^{(p)^{\mathrm{T}}}\widetilde{\boldsymbol{H}}_{\mathrm{etx}_q}^{(p)} + \sigma_n^2\boldsymbol{I}_{d_q}\right)^{-1}. \tag{2.21}$$

- **Step 5**: Calculate the term $\Delta(\boldsymbol{G}_q)$ defined as

$$\Delta(\boldsymbol{G}_q) = \left\|\boldsymbol{G}_q^{(p)} - \boldsymbol{G}_q^{(p-1)}\right\|_{\mathrm{F}}^2, \tag{2.22}$$

which measures the change of the precoding matrix $\boldsymbol{G}_q$. If $\Delta(\boldsymbol{G}_q) < \epsilon$, the convergence is achieved, and the iterative procedure terminates. Otherwise go back to **Step 2**.

It is important to note that in the special case where $M_{\mathrm{T}_q}^{(\mathrm{eq})} = M_{\mathrm{R}_q} = d_q + 1$, we propose to compute the decoding matrix in the initialization step as follows. Then it is observed that the coordinated beamforming technique only needs two iterations to converge. First, calculate the SVD of $\check{\boldsymbol{H}}_q \in \mathbb{R}^{M_{\mathrm{R}_q}\times 2M_{\mathrm{T}_q}^{(\mathrm{eq})}}$

$$\check{\boldsymbol{H}}_q = \left[\begin{array}{cc} \mathrm{Im}\left\{\boldsymbol{H}_q\boldsymbol{F}_q\right\} & \mathrm{Re}\left\{\boldsymbol{H}_q\boldsymbol{F}_q\right\}\end{array}\right], \tag{2.23}$$

and let $\boldsymbol{V}_{q,1,0}^{(0)}$ contain the last $(2M_{\mathrm{T}_q}^{(\mathrm{eq})} - M_{\mathrm{R}_q})$ right singular vectors. Defining $\boldsymbol{G}_{q,1}^{(0)}$ via

$$\boldsymbol{V}_{q,1,0}^{(0)} = \left[\begin{array}{c} \mathrm{Re}\left\{\boldsymbol{G}_{q,1}^{(0)}\right\} \\ \mathrm{Im}\left\{\boldsymbol{G}_{q,1}^{(0)}\right\}\end{array}\right], \tag{2.24}$$

we compute $\boldsymbol{U}_{q,2,1}^{(0)} \in \mathbb{R}^{M_{\mathrm{R}_q}\times d_q}$ from the SVD of $\mathrm{Re}\left\{\boldsymbol{H}_q\boldsymbol{F}_q\boldsymbol{G}_{q,1}^{(0)}\right\}$ such that it contains the first d_q left singular vectors. Then the decoding matrix for the initialization step is chosen as

$$\boldsymbol{D}_q^{(0)} = \boldsymbol{U}_{q,2,1}^{(0)}. \tag{2.25}$$

[4]Other receivers, such as zero forcing or maximum ratio combining, can also be employed in this coordinated beamforming algorithm.

2.3.2 The IIM-CBF 2 algorithm

In multi-user MIMO FBMC/OQAM downlink systems where the total number of receive antennas of the users exceeds the number of transmit antennas at the base station, the BD algorithm [19] or the BD based technique [18] cannot be employed to achieve the multi-user interference or the intrinsic interference suppression. Therefore, we propose another iterative procedure to jointly compute the precoding matrix and the decoding matrix. Let us first define an equivalent combined channel matrix after the decoding at the user terminals as

$$\boldsymbol{H}_{\mathrm{e}} = \begin{bmatrix} \boldsymbol{D}_1^{\mathrm{T}} \boldsymbol{H}_1 \\ \boldsymbol{D}_2^{\mathrm{T}} \boldsymbol{H}_2 \\ \vdots \\ \boldsymbol{D}_Q^{\mathrm{T}} \boldsymbol{H}_Q \end{bmatrix} \in \mathbb{C}^{d \times M_{\mathrm{T}}^{(\mathrm{BS})}}. \tag{2.26}$$

Unlike the coordinated beamforming schemes in [5] or [22], the decoding matrices $\boldsymbol{D}_q \in \mathbb{R}^{M_{\mathrm{R}_q} \times d_q}$, $q = 1, 2, \ldots, Q$, are forced to be real-valued. Although the BD based concept cannot be employed on the physical channel due to the dimensionality constraint, it can be used on this equivalent channel. The proposed IIM-CBF 2 algorithm for the FBMC/OQAM based multi-user MIMO downlink system is described in detail as follows:

- **Step 1**: Initialize the decoding matrices $\boldsymbol{D}_q^{(0)} \in \mathbb{R}^{M_{\mathrm{R}_q} \times d_q}$ $(q = 1, \ldots, Q)$, set the iteration index p to zero, and set a threshold ϵ for the stopping criterion. If the current subcarrier is the first one, the decoding matrices are generated randomly; otherwise, set the decoding matrices as those calculated for the previous subcarrier [22].

- **Step 2**: Set $p \leftarrow p + 1$ and calculate the equivalent channel matrix $\boldsymbol{H}_{\mathrm{e}}^{(p)}$ in the pth iteration as

$$\boldsymbol{H}_{\mathrm{e}}^{(p)} = \begin{bmatrix} \boldsymbol{H}_{\mathrm{e}_1}^{(p)^{\mathrm{T}}} & \boldsymbol{H}_{\mathrm{e}_2}^{(p)^{\mathrm{T}}} & \cdots & \boldsymbol{H}_{\mathrm{e}_Q}^{(p)^{\mathrm{T}}} \end{bmatrix}^{\mathrm{T}}, \tag{2.27}$$

  where $\boldsymbol{H}_{\mathrm{e}_q}^{(p)} = \boldsymbol{D}_q^{(p-1)^{\mathrm{T}}} \boldsymbol{H}_q$ is the equivalent channel matrix for the qth user in the pth iteration.

- **Step 3**: Calculate the precoding matrices $\boldsymbol{F}_q^{(p)}$ $(q = 1, \ldots, Q)$ in the pth iteration to cancel the multi-user interference based on the BD algorithm [19]. For the qth user, define a matrix $\widetilde{\boldsymbol{H}}_{\mathrm{e}_q}^{(p)} \in \mathbb{C}^{(d-d_q) \times M_{\mathrm{T}}^{(\mathrm{BS})}}$ as

$$\widetilde{\boldsymbol{H}}_{\mathrm{e}_q}^{(p)} = \begin{bmatrix} \boldsymbol{H}_{\mathrm{e}_1}^{(p)^{\mathrm{T}}} & \cdots & \boldsymbol{H}_{\mathrm{e}_{q-1}}^{(p)^{\mathrm{T}}} & \boldsymbol{H}_{\mathrm{e}_{q+1}}^{(p)^{\mathrm{T}}} & \cdots & \boldsymbol{H}_{\mathrm{e}_Q}^{(p)^{\mathrm{T}}} \end{bmatrix}^{\mathrm{T}}, \tag{2.28}$$

  which contains the equivalent channel matrices of all the other users that are calculated in **Step 2**. The precoding matrix $\boldsymbol{F}_q^{(p)}$ for the qth user in the pth iteration is obtained as $\boldsymbol{F}_q^{(p)} = \widetilde{\boldsymbol{V}}_{\mathrm{e}_{(q,0)}}^{(p)} \in \mathbb{C}^{M_{\mathrm{T}}^{(\mathrm{BS})} \times M_{\mathrm{T}_q}^{(\mathrm{eq})}}$, where $\widetilde{\boldsymbol{V}}_{\mathrm{e}_{(q,0)}}^{(p)}$ contains the last $M_{\mathrm{T}_q}^{(\mathrm{eq})}$ right singular vectors that form an orthonormal basis for the null space of $\widetilde{\boldsymbol{H}}_{\mathrm{e}_q}^{(p)}$ [19]. To this end, the multi-user MIMO downlink transmission is decoupled into parallel equivalent single-user MIMO transmissions that will be considered in the following steps.

- **Step 4**: Define a matrix $\check{\boldsymbol{H}}_{\mathrm{e}_q}^{(p)} \in \mathbb{R}^{d_q \times 2M_{\mathrm{T}_q}^{(\mathrm{eq})}}$ for the qth user based on its equivalent channel matrix $\boldsymbol{H}_{\mathrm{e}_q}^{(p)} \boldsymbol{F}_q^{(p)}$ after the cancellation of the multi-user interference

$$\check{\boldsymbol{H}}_{\mathrm{e}_q}^{(p)} = \begin{bmatrix} \mathrm{Im}\left\{ \boldsymbol{H}_{\mathrm{e}_q}^{(p)} \boldsymbol{F}_q^{(p)} \right\} & \mathrm{Re}\left\{ \boldsymbol{H}_{\mathrm{e}_q}^{(p)} \boldsymbol{F}_q^{(p)} \right\} \end{bmatrix}. \tag{2.29}$$

- **Step 5**: Calculate the precoding matrix $\boldsymbol{G}_q^{(p)} = \boldsymbol{G}_{q,1}^{(p)}\boldsymbol{G}_{q,2}^{(p)}$ for the qth user in the pth iteration. First, we perform the singular value decomposition (SVD) of $\check{\boldsymbol{H}}_{\mathrm{e}_q}^{(p)}$ and obtain $\boldsymbol{V}_{q,1,0}^{(p)} \in \mathbb{R}^{2M_{\mathrm{T}_q}^{(\mathrm{eq})} \times M_{x_q}}$ as containing the last $M_{x_q} = 2M_{\mathrm{T}_q}^{(\mathrm{eq})} - r_q^{(p)}$ right singular vectors that form an orthonormal basis for the null space of $\check{\boldsymbol{H}}_{\mathrm{e}_q}^{(p)}$, where $r_q^{(p)}$ denotes the rank of $\check{\boldsymbol{H}}_{\mathrm{e}_q}^{(p)}$. Hence, $\boldsymbol{G}_{q,1}^{(p)} \in \mathbb{C}^{M_{\mathrm{T}_q}^{(\mathrm{eq})} \times M_{x_q}}$ can be obtained via

$$\boldsymbol{V}_{q,1,0}^{(p)} = \begin{bmatrix} \mathrm{Re}\left\{\boldsymbol{G}_{q,1}^{(p)}\right\} \\ \mathrm{Im}\left\{\boldsymbol{G}_{q,1}^{(p)}\right\} \end{bmatrix} \in \mathbb{R}^{2M_{\mathrm{T}_q}^{(\mathrm{eq})} \times M_{x_q}} \tag{2.30}$$

such that (2.11) is fulfilled to achieve the mitigation of the intrinsic interference.

Now we define the following equivalent channel matrix after canceling the intrinsic interference for the qth user in the pth iteration

$$\bar{\boldsymbol{H}}_{\mathrm{e}_q}^{(p)} = \mathrm{Re}\left\{\boldsymbol{H}_{\mathrm{e}_q}^{(p)}\boldsymbol{F}_q^{(p)}\boldsymbol{G}_{q,1}^{(p)}\right\} \in \mathbb{R}^{d_q \times M_{x_q}}. \tag{2.31}$$

Further calculate the SVD of $\bar{\boldsymbol{H}}_{\mathrm{e}_q}^{(p)}$ and define $\boldsymbol{V}_{q,2,1}^{(p)} \in \mathbb{R}^{M_{x_q} \times d_q}$ as containing the first d_q right singular vectors. Then $\boldsymbol{G}_{q,2}^{(p)}$ is obtained as $\boldsymbol{G}_{q,2}^{(p)} = \boldsymbol{V}_{q,2,1}^{(p)}$.

- **Step 6**: Update the decoding matrix for each user based on the real-valued equivalent channel matrix where the processing at the transmitter and the procedure of taking the real part of the receive signal are taken into account

$$\boldsymbol{H}_{\mathrm{etx}_q}^{(p)} = \mathrm{Re}\left\{\boldsymbol{H}_q\boldsymbol{F}_q^{(p)}\boldsymbol{G}_q^{(p)}\right\} \in \mathbb{R}^{M_{\mathrm{R}_q} \times d_q}, \quad q = 1, \ldots, Q. \tag{2.32}$$

When the MMSE receiver is used, the update of the decoding matrix in the pth iteration for the qth user has the following form:

$$\boldsymbol{D}_q^{(p)} = \boldsymbol{H}_{\mathrm{etx}_q}^{(p)}\left(\boldsymbol{H}_{\mathrm{etx}_q}^{(p)^{\mathrm{T}}}\boldsymbol{H}_{\mathrm{etx}_q}^{(p)} + \sigma_n^2\boldsymbol{I}_{d_q}\right)^{-1}. \tag{2.33}$$

- **Step 7**: Calculate the term $\xi^{(p)}$ that measures the residual multi-user and the inter-stream interference for the pth iteration defined as

$$\xi^{(p)} = \left\|\mathrm{off}\left(\boldsymbol{D}^{(p)^{\mathrm{T}}}\mathrm{Re}\left\{\boldsymbol{H}\boldsymbol{F}^{(p)}\right\}\right)\right\|_{\mathrm{F}}^2, \tag{2.34}$$

where off$(\cdot)$ indicates an operation of keeping all off-diagonal elements of its input matrix while setting its diagonal elements to zero. If $\xi^{(p)} < \epsilon$, the convergence is achieved, and the iterative procedure terminates. Otherwise go back to **Step 2**.

Note that the stopping criterion similar as (2.22) that tracks the change of the precoding matrix can also be adopted[5]. In addition, for both IIM-CBF schemes proposed in this section and Section 2.3.1, it is not required that the users are informed of the decoding matrices that are obtained at the base station while computing the precoding matrices. After the users acquire the information of the effective channel via channel estimation, the receive processing can be performed. For example, the MMSE receiver of the effective channel for each user can be employed.

[5]These two stopping criteria require different thresholds for the convergence. In this work, we only present numerical results obtained when the stopping criterion as in (2.34) is employed, and the threshold ϵ is set to 10^{-5}.

2.4 Coordinated beamforming for the CoMP downlink

In this section, we focus on a CoMP downlink setting based on [5]. Note that in [5] a clustered cellular scenario is considered where each cluster contains multiple cells. Since full cooperation is assumed in each cluster, the downlink transmissions for each cluster resemble those of the single-cell multi-user MIMO downlink. Thereby, we simplify the scenario description of the CoMP downlink and only consider joint transmission of adjacent cells. It is assumed that the cell interior users only receive signals from their own base station and suffer only from the intra-cell interference, i.e., the multi-user interference as in the single-cell multi-user MIMO downlink scenarios. On the other hand, both the intra-cell interference and the inter-cell interference have an impact on the cell edge users. To assist the cell edge users to combat the interference and also deal with the greater path loss compared to the cell interior users, the base stations of the adjacent cells transmit the same signals to each cell edge user. An example of a two-cell FBMC/OQAM based CoMP downlink scenario is illustrated in Fig. 2-1. Assume that Cell 1

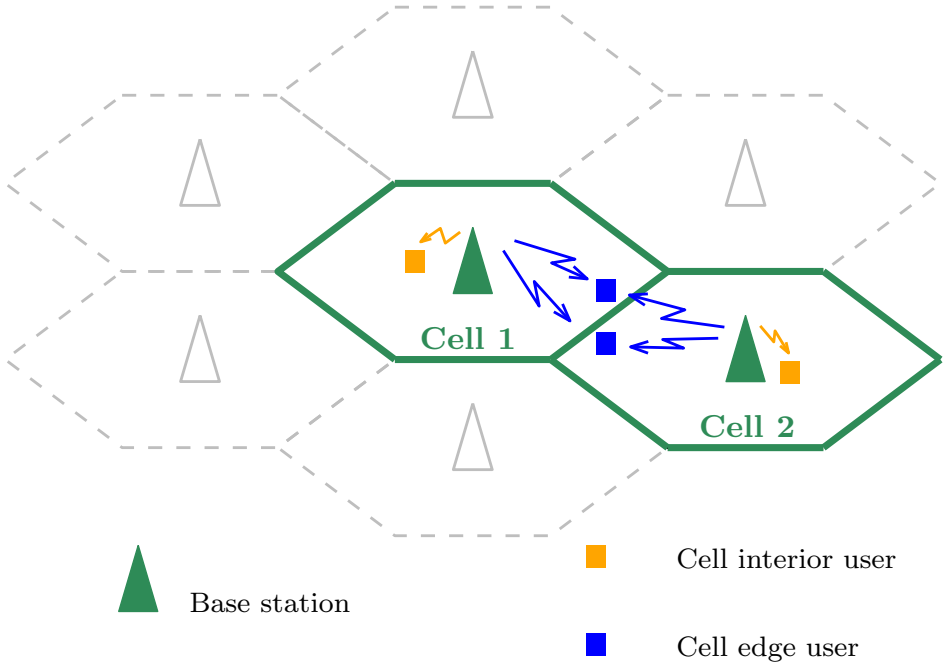

Figure 2-1: An example of a two-cell CoMP downlink scenario where a cell interior user and two cell edge users are served in each cell

and Cell 2 are equipped with $M_{\mathrm{T}}^{(\mathrm{BS1})}$ and $M_{\mathrm{T}}^{(\mathrm{BS2})}$ transmit antennas, respectively. The number of users served by each cell is denoted as Q. The received signal on the kth subcarrier and at the nth time instant of the qth user of Cell 1 as a cell interior user is expressed as

$$\begin{aligned}\boldsymbol{y}_{q,k}[n] =& \boldsymbol{H}_{q,k,(1)}[n]\boldsymbol{F}_{k,(1)}[n]\boldsymbol{d}_{k,(1)}[n] + \sum_{i=n-3}^{n+3}\sum_{\ell=k-1}^{k+1}\boldsymbol{H}_{q,\ell,(1)}[i]\boldsymbol{F}_{\ell,(1)}[i]c_{i\ell}\boldsymbol{d}_{\ell,(1)}[i] \\ &+ \boldsymbol{n}_{q,k}[n], \quad (\ell,i)\neq(k,n),\end{aligned} \tag{2.35}$$

where $\boldsymbol{H}_{q,k,(1)}[n] \in \mathbb{C}^{M_{\mathrm{R}_q}\times M_{\mathrm{T}}^{(\mathrm{BS1})}}$ represents the channel matrix between the base station of Cell 1 and the qth user with M_{R_q} receive antennas, $\boldsymbol{F}_{k,(1)}[n]$ symbolizes the precoding matrix for Cell 1, and $\boldsymbol{d}_{k,(1)}[n]$ contains the signals for all users served by Cell 1. It can be seen that for

a cell interior user, assuming that the inter-cell interference is negligible, the transmission from the base station in its own cell is the same as in a single-cell multi-user MIMO downlink system. For the gth user that is a cell edge user and receives the same signals from both Cell 1 and Cell 2, its received signal on the kth subcarrier and at the nth time instant has the following form

$$\begin{aligned}\boldsymbol{y}_{g,k}[n] =&\boldsymbol{H}_{g,k,(1)}[n]\boldsymbol{F}_{k,(1)}[n]\boldsymbol{d}_{k,(1)}[n] + \sum_{i=n-3}^{n+3}\sum_{\ell=k-1}^{k+1}\boldsymbol{H}_{g,\ell,(1)}[i]\boldsymbol{F}_{\ell,(1)}[i]c_{i\ell}\boldsymbol{d}_{\ell,(1)}[i]+\\ &\boldsymbol{H}_{g,k,(2)}[n]\boldsymbol{F}_{k,(2)}[n]\boldsymbol{d}_{k,(2)}[n] + \sum_{i=n-3}^{n+3}\sum_{\ell=k-1}^{k+1}\boldsymbol{H}_{g,\ell,(2)}[i]\boldsymbol{F}_{\ell,(2)}[i]c_{i\ell}\boldsymbol{d}_{\ell,(2)}[i]\\ &+\boldsymbol{n}_{g,k}[n], \quad (\ell,i)\neq(k,n). \end{aligned} \tag{2.36}$$

Here the channel matrix, precoding matrix, and the data vector with respect to Cell 2 are denoted similarly as in (2.35) only with "(2)" in the subscripts. Note that $\boldsymbol{d}_{g,k,(1)}[n] = \boldsymbol{d}_{g,k,(2)}[n]$, i.e., the signals from Cell 1 and Cell 2 transmitted to the gth user[6] are the same. To enable such FBMC/OQAM based CoMP downlink transmissions, the mitigation of the intra-cell, inter-cell, and intrinsic interference has to be achieved. Therefore, we propose the following IIM-CBF scheme that is an extension of the approach described in Section 2.3.2 and is also the outcome of adapting the Extended FlexCoBF algorithm for CP-OFDM based systems in [5] to FBMC/OQAM based systems.

Consider M cells, and the mth cell serves Q_m users simultaneously, $m = 1, 2, \ldots, M$. It is assumed that for the mth cell the users $1, 2, \ldots, L_m$ are cell interior users, while the remaining $(Q_m - L_m)$ users are cell edge users. The proposed IIM-CBF 3 scheme is summarized as follows:

- **Step 1**: Initialize the real-valued decoding matrices $\boldsymbol{D}_q^{(0)}$ $(q = 1, \ldots, Q_m)$ for the mth cell, where $m = 1, \ldots, M$. Set the iteration index p to zero, and set a threshold ϵ for the stopping criterion. If the current subcarrier is the first one, the decoding matrices are generated randomly; otherwise, set the decoding matrices as those calculated for the previous subcarrier [22].

- **Step 2**: Set $p \leftarrow p + 1$ and calculate the equivalent channel matrix $\boldsymbol{H}_{\mathrm{e}_m}^{(p)}$ in the pth iteration as

$$\boldsymbol{H}_{\mathrm{e}_m}^{(p)} = \left[\begin{array}{cccc}\boldsymbol{H}_{\mathrm{e}_{(1,m)}}^{(p)^{\mathrm{T}}} & \boldsymbol{H}_{\mathrm{e}_{(2,m)}}^{(p)^{\mathrm{T}}} & \cdots & \boldsymbol{H}_{\mathrm{e}_{(Q_m,m)}}^{(p)^{\mathrm{T}}}\end{array}\right]^{\mathrm{T}}, \tag{2.37}$$

  where $\boldsymbol{H}_{\mathrm{e}_{(q,m)}}^{(p)} = \boldsymbol{D}_q^{(p-1)^{\mathrm{T}}}\boldsymbol{H}_{q,m}$ is the equivalent channel matrix for the qth user in the pth iteration.

- **Step 3**: Calculate the precoding matrices $\boldsymbol{F}_{q,m}^{(p)}\boldsymbol{G}_{q,m}^{(p)}$ $(q = 1, \ldots, Q_m)$ following **Step 3** - **Step 5** of Section 2.3.2 to achieve the suppression of the multi-user interference and the intrinsic interference.

- **Step 4**: Update the decoding matrix for each user based on the real-valued equivalent channel matrix where the processing at the transmitter and the procedure of taking the real part of the receive signal are taken into account.

  1. For the qth user that is a cell interior user of the mth cell, its equivalent channel matrix $\boldsymbol{H}_{\mathrm{etx}_{(q,m)}}^{(p)}$ is calculated as

$$\boldsymbol{H}_{\mathrm{etx}_{(q,m)}}^{(p)} = \mathrm{Re}\left\{\boldsymbol{H}_{q,m}\boldsymbol{F}_{q,m}^{(p)}\boldsymbol{G}_{q,m}^{(p)}\right\}. \tag{2.38}$$

[6] In this example, we assume that the indices of each cell edge user in Cell 1 and Cell 2 are the same to facilitate the description of the scenario.

2. For the qth user that is a cell edge user, define a set $\mathcal{S}_{q,m}$ that contains the indices of the cells that simultaneously transmit the same signals to the qth user. Then its equivalent channel matrix is expressed as

$$\boldsymbol{H}_{\mathrm{etx}_{(q,m)}}^{(p)} = \sum_{r \in \mathcal{S}_{q,m}} \mathrm{Re}\left\{ \boldsymbol{H}_{q_r,r} \boldsymbol{F}_{q_r,r}^{(p)} \boldsymbol{G}_{q_r,r}^{(p)} \right\}, \tag{2.39}$$

where q_r represents the index of the qth user of the mth cell in the rth cell, and $q_m = q$ following this definition. It is required that the base station of the mth cell is informed by the rth cell, $r \in \mathcal{S}_{q,m}$ and $r \neq m$, of the corresponding real-valued equivalent channel matrices after the precoding and the operation of taking the real part of the received signal. In a summary, the cooperation of the adjacent cells involves the knowledge of the signals for cell edge users. It also requires the exchange of these real-valued equivalent channel matrices that are used to compute the decoding matrix for each cell edge user, which can be achieved by adopting the two exchange mechanisms proposed in [5].

Afterwards, when a single data stream is transmitted to each user, the decoding matrix for the qth user in the pth iteration can be obtained by employing the MRC receiver or the MMSE receiver of the its equivalent channel matrix $\boldsymbol{H}_{\mathrm{etx}_{(q,m)}}^{(p)}$. On the other hand, when there exist users to which multiple data streams are transmitted, we propose to use the ZF receiver[7]

$$\boldsymbol{D}_{q,m}^{(p)} = \boldsymbol{H}_{\mathrm{etx}_{(q,m)}}^{(p)} \left(\boldsymbol{H}_{\mathrm{etx}_{(q,m)}}^{(p)^{\mathrm{T}}} \boldsymbol{H}_{\mathrm{etx}_{(q,m)}}^{(p)} \right)^{-1}. \tag{2.40}$$

- **Step 5**: Calculate the term $\xi_m^{(p)}$ for the mth cell that measures the residual multi-user and the inter-stream interference for the pth iteration. When a single data stream is transmitted to each user, $\xi_m^{(p)}$ is defined as

$$\xi_m^{(p)} = \left\| \mathrm{off}\left(\boldsymbol{D}_m^{(p)^{\mathrm{T}}} \cdot \mathrm{Re}\left\{ \boldsymbol{H}_m \boldsymbol{F}_m^{(p)} \right\} \right) \right\|_{\mathrm{F}}^2, \tag{2.41}$$

where $\mathrm{off}(\cdot)$ indicates an operation of keeping all off-diagonal elements of its input matrix while setting its diagonal elements to zero. Moreover, $\boldsymbol{D}_m^{(p)}$, $\boldsymbol{H}_m$, and $\boldsymbol{F}_m^{(p)}$ denote the block diagonal combined decoding matrix in the pth iteration, the combined channel matrix, and the precoding matrix in the pth iteration for the mth cell, respectively.

When multiple data streams are transmitted to at least one of the cell edge users, we propose to express the term $\xi_m^{(p)}$ as

$$\begin{aligned}
\xi_m^{(p)} = & \sum_{q=1}^{L_m} \left(\left\| \mathrm{off}\left(\boldsymbol{D}_q^{(p)^{\mathrm{T}}} \cdot \mathrm{Re}\left\{ \boldsymbol{H}_{q,m} \boldsymbol{F}_{q,m}^{(p)} \boldsymbol{G}_{q,m}^{(p)} \right\} \right) \right\|_{\mathrm{F}}^2 + \sum_{g=1, g\neq q}^{Q_m} \left\| \boldsymbol{D}_q^{(p)^{\mathrm{T}}} \cdot \mathrm{Re}\left\{ \boldsymbol{H}_{q,m} \boldsymbol{F}_{g,m}^{(p)} \boldsymbol{G}_{g,m}^{(p)} \right\} \right\|_{\mathrm{F}}^2 \right) \\
& + \sum_{q=L_m+1}^{Q_m} \left(\left\| \mathrm{off}\left(\boldsymbol{D}_q^{(p)^{\mathrm{T}}} \cdot \sum_{r \in \mathcal{S}_{q,m}} \mathrm{Re}\left\{ \boldsymbol{H}_{q_r,r} \boldsymbol{F}_{q_r,r}^{(p)} \boldsymbol{G}_{q_r,r}^{(p)} \right\} \right) \right\|_{\mathrm{F}}^2 \right. \\
& \left. + \sum_{g=1, g\neq q}^{Q_m} \left\| \boldsymbol{D}_q^{(p)^{\mathrm{T}}} \cdot \mathrm{Re}\left\{ \boldsymbol{H}_{q,m} \boldsymbol{F}_{g,m}^{(p)} \boldsymbol{G}_{g,m}^{(p)} \right\} \right\|_{\mathrm{F}}^2 \right).
\end{aligned} \tag{2.42}$$

[7] In such scenarios where multiple data streams are transmitted to at least one user, by employing the MMSE or the MRC criterion to update the decoding matrices in IIM-CBF 3, convergence cannot be achieved.

Table 2-2: Acronyms of the proposed intrinsic interference mitigating coordinated beamforming (IIM-CBF) schemes and the corresponding scenarios

Acronyms	Configurations	Interference Type
IIM-CBF 1	multi-user MIMO downlink, $M_{\mathrm{T}}^{(\mathrm{BS})} = M_{\mathrm{R}}^{(\mathrm{tot})}$	intrinsic, multi-user
IIM-CBF 2	multi-user MIMO downlink, $M_{\mathrm{T}}^{(\mathrm{BS})} < M_{\mathrm{R}}^{(\mathrm{tot})}$	intrinsic, multi-user
IIM-CBF 3	CoMP downlink	intrinsic, intra/inter-cell

On the right-hand side of (2.42), the first term corresponds to the residual inter-stream interference of each cell interior user, while the second term represents the residual multi-user interference that it still suffers from. For each cell edge user, the third term on the right-hand side of (2.42) measures its residual inter-stream interference. Here we take into account the fact that coordinated adjacent cells transmit the same signals to the cell edge user simultaneously. Recall that $\mathcal{S}_{q,m}$ contains the indices of the cells that serve the qth user of the mth cell. Moreover, the forth term corresponds to the residual multi-user interference that affects each cell edge user.

If $\xi_m^{(p)} < \epsilon$, the convergence is achieved, and the iterative procedure terminates. Otherwise go back to **Step 2**.

As mentioned before, this coordinated beamforming scheme is designed based on the CoMP technique in [5]. Nevertheless, due to the fact that the intrinsic interference is inherent in FBMC/OQAM systems, we have proposed to incorporate the additional processing to suppress the intrinsic interference. Moreover, different choices of the stopping criterion are recommended for single-stream transmissions and multiple-stream transmissions, respectively.

Finally, we summarize the proposed IIM-CBF schemes in Table 2-2. These three algorithms are all based on the concept of jointly and iteratively computing the precoding matrix and decoding matrix. In addition, they mitigate the intra-cell and inter-cell interference as well as the intrinsic interference in a ZF fashion. Nevertheless, the three schemes are designed for different configurations and deal with different types of interference. IIM-CBF 1 is developed for symmetric single-cell FBMC/OQAM based multi-user MIMO downlink settings. In this scenario, BD can still be employed to cancel the multi-user interference. Therefore, in IIM-CBF 1 only the precoding matrix for each equivalent single user transmission (i.e., $\boldsymbol{G}_q$ for the qth user) is computed via the iterative procedure to suppress the intrinsic interference. On the other hand, IIM-CBF 2 is proposed to overcome the dimensionality constraint that $M_{\mathrm{R}}^{(\mathrm{tot})}$ must not exceed $M_{\mathrm{T}}^{(\mathrm{BS})}$ in the single-cell FBMC/OQAM based multi-user MIMO downlink. The complete precoding matrix (i.e., for the qth user $\boldsymbol{F}_q\boldsymbol{G}_q$) that mitigates the multi-user interference and the intrinsic interference is computed iteratively and jointly with the decoding matrix. Unlike the first two schemes, IIM-CBF 3, as a novel FBMC/OQAM based CoMP technique, is devised to enable the joint transmission of adjacent cells and to mitigate both the intra-cell interference and the inter-cell interference. In the meantime, it is able to achieve the suppression of the intrinsic interference inherent in FBMC/OQAM based systems. Although the three IIM-CBF schemes exhibit satisfactory capabilities in alleviating the dimensionality constraint and in combating different types of interference, a complete elimination of the intrinsic interference that is inherent in FBMC/OQAM based systems is not achieved. We revisit this issue in Section 2.5.2. It is worth noting that compared to the transmission strategy reviewed in Section 2.2.1, the residual intrinsic interference in case of the IIM-CBF schemes is much smaller, which is reflected in the performance comparison in Section 2.5. Throughout this chapter, equal power alloca-

tion is considered. A direct implementation of optimal power allocation schemes developed for CP-OFDM based systems suffers from the loss of optimality due to the residual intrinsic interference existing in FBMC/OQAM based multi-user MIMO downlink systems where the IIM-CBF algorithms are employed. Although the power optimization issue is beyond our scope, it is of interest to devise power allocation schemes which are tailored for FBMC/OQAM based multi-user MIMO downlink systems by taking into account the methods of the multi-user and intrinsic interference mitigation as well as possible residual interference.

2.5 Simulation results

2.5.1 Single-cell multi-user MIMO downlink

In this section, we evaluate the BER performances of the proposed IIM-CBF techniques in various simulation settings. For all examples, the total number of subcarriers is 128, and the subcarrier spacing is 15 kHz. In case of CP-OFDM, the length of the CP is set to $1/8$ of the symbol period. The ITU Ped-A channel [25] is adopted. Moreover, the PHYDYAS prototype filter [23] with the overlapping factor $K = 4$ is employed. The data symbols are drawn from a 16 QAM constellation. Perfect CSI is assumed at the transmitter and at the receiver.

In the first experiment, a symmetric multi-user MIMO downlink setting is considered, where the base station is equipped with $M_{\mathrm{T}}^{(\mathrm{BS})} = 8$ transmit antennas, each of the two users has four receive antennas, and the number of spatial streams transmitted to each user is 3. The BER performances of the three schemes for FBMC/OQAM based systems are presented and also compared to that of a CP-OFDM based system in Fig. 2-2. It can be found that IIM-CBF 1 described in Section 2.3.1 yields the best performance. The multi-user interference is first mitigated by using the BD algorithm [19], and the precoding matrix and the decoding matrix are computed jointly and iteratively for each of the resulting 4×4 equivalent point-to-point transmissions. Note that the decoding matrix is initialized as (2.25). In this case, we observe that it takes only two iterations to converge. On the other hand, the transmission scheme that is a straightforward extension of BD [19] for the CP-OFDM case as described in Section 2.2.1 relies on the assumption that the channel frequency responses remain the same across adjacent subcarriers. As the ITU Ped-A channel exhibits frequency selectivity and such an assumption is therefore violated, the performance of this scheme degrades especially in the high signal-to-noise ratio (SNR) regime. We can also observe that in this symmetric scenario, the BD based precoding algorithm[8] proposed in [18] performs much worse compared to the other schemes.

In the second and the third examples, we consider multi-user MIMO downlink settings where the base station equipped with $M_{\mathrm{T}}^{(\mathrm{BS})} = 8$ transmit antennas simultaneously serves two users and three users , i.e., $Q = 2$ and 3, respectively. Each of the two users in the second scenario has five receive antennas, and the number of data streams transmitted to each user is 3. On the other hand, the three users in the third scenario are equipped with three receive antennas each, and two data streams are transmitted to each of the three users. Note that for such $M_{\mathrm{R}}^{(\mathrm{tot})} > M_{\mathrm{T}}^{(\mathrm{BS})}$ configurations, the transmission strategy proposed in [18] and briefly reviewed in Section 2.2.2 cannot be employed. Fig. 2-3 and Fig. 2-4 show the BER curves for these two scenarios, respectively. Two techniques are considered for the FBMC/OQAM based system,

[8] In the implementation of this algorithm, after the cancellation of the multi-user interference by using BD, only the ZF based step that ensures the cancellation of the intrinsic interference is considered. The remaining part of the transmit processing (spatial mapping) and the receive processing (MMSE receiver) are chosen to be the same as the other schemes for the purpose of a fair comparison. Note that the precoding algorithm proposed in [18] is dominated by the BD and ZF based steps.

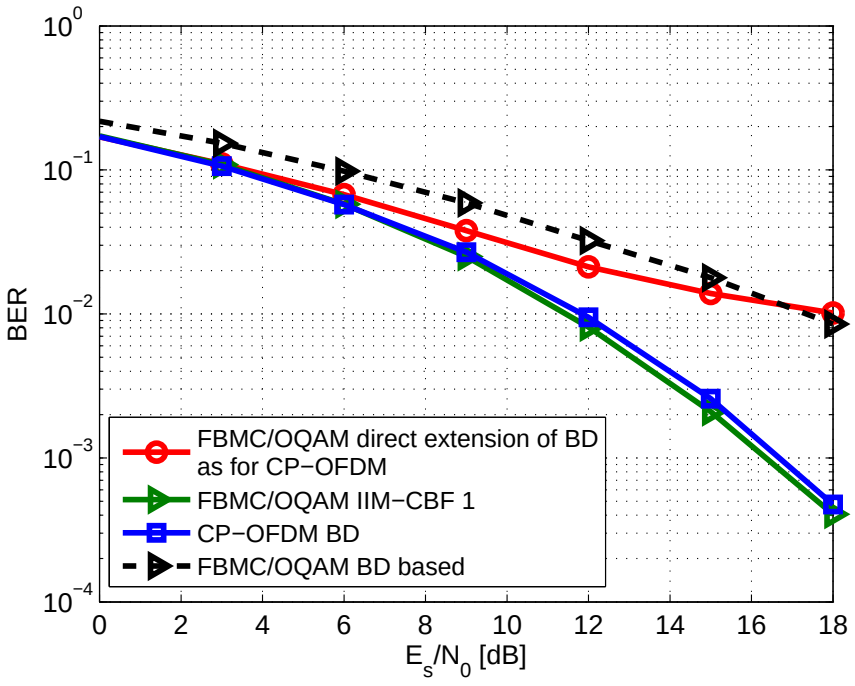

Figure 2-2: Comparison of the BER performances of different schemes in a multi-user MIMO system where $Q = 2$, $M_{\mathrm{T}}^{(\mathrm{BS})} = M_{\mathrm{R}}^{(\mathrm{tot})} = 8$, $d = 6$, the ITU Ped-A channel is considered; E_{s} denotes the energy of each 16 QAM symbol, and N_0 represents the noise power spectral density

i.e., IIM-CBF 2 presented in Section 2.3.2 and a direct extension (cf. Section 2.2.1) of the LoCCoBF algorithm [22] originally designed for the case of CP-OFDM. For the purpose of comparison, we also present the BER performance of a CP-OFDM based system with the same configuration where LoCCoBF is employed. For both the proposed IIM-CBF 2 scheme and LoCCoBF, ϵ for the stopping criterion is set to 10^{-5}, and the maximum number of iterations[9] is 50. It can be observed that the performance of the FBMC/OQAM based multi-user MIMO downlink system where IIM-CBF 2 is employed is slightly better than its CP-OFDM based counterpart due to the fact that no insertion of the CP is required. The other transmission scheme for the FBMC/OQAM based system suffers from a performance degradation due to the frequency selectivity of the channel. By assuming that the channel stays constant across the neighboring subcarriers, the multi-user interference and the intrinsic interference cannot be eliminated even for high SNRs.

In addition, the convergence behavior of IIM-CBF 2 for the multi-user MIMO FBMC/OQAM downlink system where $M_{\mathrm{R}}^{(\mathrm{tot})} > M_{\mathrm{T}}^{(\mathrm{BS})}$ is investigated. The complimentary cumulative dis-

[9]Via numerical simulations, it has been observed that there exist rare cases where it takes a large number of iterations for the stopping criteria of the IIM-CBF schemes to be fulfilled. Therefore, a maximum number of iterations is set to handle these cases. The iterative procedure is manually terminated if the stopping criteria are not fulfilled when the number of iterations reaches this maximum number. Taking IIM-CBF 2 as an example, its stopping criterion corresponds to the residual interference. We have observed that when the algorithm is manually terminated, though the residual interference is above the threshold, its value is already so small that the performance is not affected much. Except for this simple way of setting a maximum number of iterations, the termination of the iterative procedure can also be determined based on the variation of the residual interference (in case of IIM-CBF 2 and IIM-CBF 3) or the change of the precoding matrix (in case of IIM-CBF 1) as the number of iterations increases.

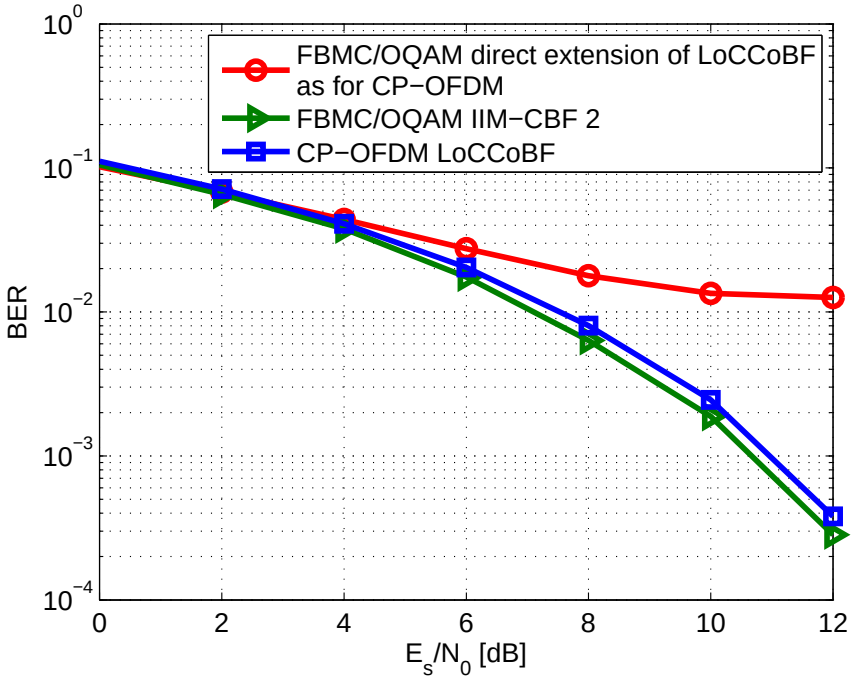

Figure 2-3: Comparison of the BER performances of different schemes in a multi-user MIMO downlink system where $Q = 2$, $M_{\mathrm{T}}^{(\mathrm{BS})} = 8$, $M_{\mathrm{R}}^{(\mathrm{tot})} = 10$, $d = 6$, and the ITU Ped-A channel is considered; E_{s} denotes the energy of each 16 QAM symbol, and N_0 represents the noise power spectral density

tribution function (CCDF) of the number of iterations required to achieve the convergence of the IIM-CBF 2 scheme presented in Section 2.3.2 and LoCCoBF for the case of CP-OFDM is illustrated in Fig. 2-5. The three-user scenario used for Fig. 2-4 is considered. By comparison, we also plot the same set of results for a four-user case, i.e., $Q = 4$. The base station has 8 transmit antennas, and each of the four users is equipped with 3 receive antennas and is sent to 2 data streams. Thereby, the total number of the receive antennas of the users $M_{\mathrm{R}}^{(\mathrm{tot})} = 12$, and all spatial degrees of freedom are exploited. It can be observed that for the three-user scenario IIM-CBF 2 converges within 6 iterations in almost all of the cases. As the number of users and consequently the total number of receive antennas increase, the number of iterations needed for the convergence becomes slightly larger. Nevertheless, the convergence is achieved within 10 iterations. Moreover, we can see from the comparison of the proposed IIM-CBF 2 technique for the FBMC/OQAM based system and LoCCoBF for the case of CP-OFDM that the number of iterations required for the convergence for both schemes are similar. Hence, compared to the CP-OFDM based multi-user MIMO downlink setting, employing such an IIM-CBF technique in the FBMC/OQAM based system where $M_{\mathrm{R}}^{(\mathrm{tot})} > M_{\mathrm{T}}^{(\mathrm{BS})}$ does not result in an increased number of iterations for the convergence. Only the processing dedicated to the elimination of the intrinsic interference contributes to a slight additional complexity.

Furthermore, we consider again the four-user single-cell multi-user MIMO downlink system (as used for Fig. 2-5) and investigate the impact of the residual CFO. The IIM-CBF 2 scheme for the FBMC/OQAM based system and LoCCoBF for CP-OFDM are considered. In addition, it is assumed that the residual CFO (normalized by the subcarrier spacing) ranges[10] either from

[10] In the simulations, the residual CFO is drawn uniformly from the range $(0, 0.1)$ or $(0, 0.15)$

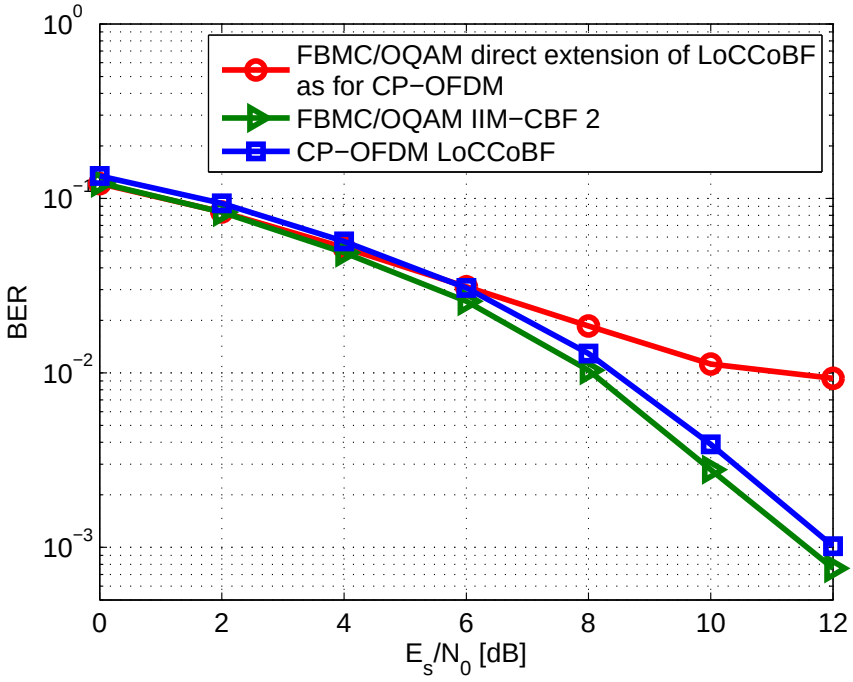

Figure 2-4: Comparison of the BER performances of different schemes in a multi-user MIMO downlink system where $Q = 3$, $M_{\mathrm{T}}^{(\mathrm{BS})} = 8$, $M_{\mathrm{R}}^{(\mathrm{tot})} = 9$, $d = 6$, and the ITU Ped-A channel is considered; E_{s} denotes the energy of each 16 QAM symbol, and N_0 represents the noise power spectral density

0 to 0.1 or from 0 to 0.15. Fig. 2-6 illustrates the corresponding BER performances of these two schemes in the presence of the residual CFO. Notice that the CP-OFDM based system suffers from a severe performance degradation. In contrast, the FBMC/OQAM based system with IIM-CBF 2 significantly outperforms its CP-OFDM based counterpart, and it exhibits a greater robustness against the synchronization errors in the frequency domain.

2.5.2 CoMP downlink

In the sequel, the performance of the FBMC/OQAM based CoMP downlink is assessed. Instead of the BER, we choose to use the sum rate performance as the evaluation approach. We start with a two-cell scenario consisting of 5 users in total. Each cell equipped with 4 transmit antennas serves 3 users each with 2 receive antennas, which forms a 4×6 multi-user downlink setting. Among the three users, two are cell interior users, and one is a cell edge user. A single data stream is transmitted to each cell interior user, and two data streams are transmitted to the cell edge use, i.e., for each cell full spatial multiplexing is considered. The pathloss of the transmission to the cell edge users is assumed to be 10 times bigger than that for the cell interior users [5]. To calculate the sum rate for both the FBMC/OQAM and the CP-OFDM cases, we first compute an instantaneous signal-to-interference-plus-noise-ratio (SINR) on each data stream for each subcarrier. In case of the FBMC/OQAM based multi-user MIMO downlink

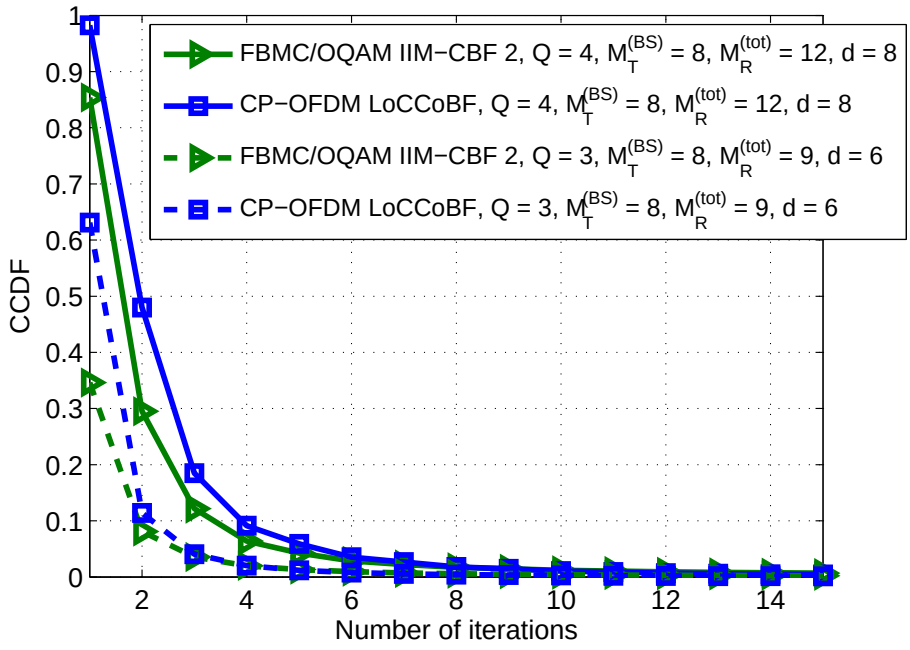

Figure 2-5: CCDF of the number of iterations required for IIM-CBF 2 and LoCCoBF in multi-user MIMO FBMC/OQAM and CP-OFDM based downlink systems with different settings, respectively, and the ITU Ped-A channel is considered

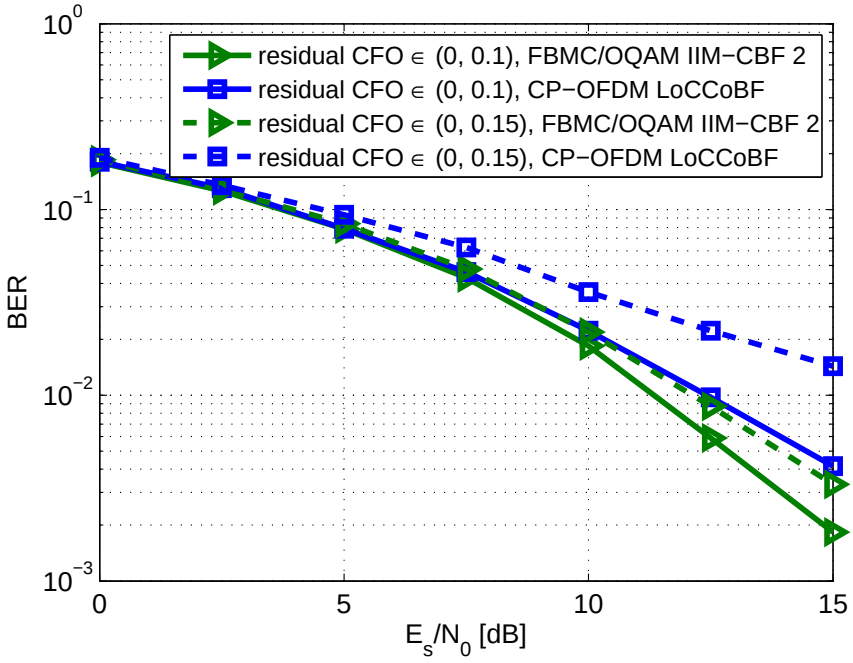

Figure 2-6: Comparison of the BER performances of different schemes in a multi-user MIMO downlink system in the presence of residual CFO (unit: subcarrier spacing) where $Q = 4$, $M_{\mathrm{T}}^{(\mathrm{BS})} = 8$, $M_{\mathrm{R}}^{(\mathrm{tot})} = 12$, $d = 8$, and the ITU Ped-A channel is considered; E_{s} denotes the energy of each 16 QAM symbol, and N_0 represents the noise power spectral density

where IIM-CBF 2 is employed, the decoded signal is written as

$$\begin{aligned}\hat{\boldsymbol{d}}_k[n] &= \boldsymbol{D}_k^{\mathrm{T}}[n] \cdot \mathrm{Re}\left\{ \boldsymbol{H}_k[n]\boldsymbol{F}_k[n]\boldsymbol{d}_k[n] + \sum_{i=n-3}^{n+3} \sum_{\ell=k-1}^{k+1} \boldsymbol{H}_\ell[i]\boldsymbol{F}_\ell[i] c_{i\ell} \boldsymbol{d}_\ell[i] + \boldsymbol{n}_k[n] \right\} \\ &= \boldsymbol{D}_k^{\mathrm{T}}[n] \cdot \mathrm{Re}\left\{\boldsymbol{H}_k[n]\boldsymbol{F}_k[n]\right\} \boldsymbol{d}_k[n] + \boldsymbol{D}_k^{\mathrm{T}}[n] \cdot \mathrm{Im}\left\{ - \sum_{i=n-3}^{n+3} \sum_{\ell=k-1}^{k+1} \boldsymbol{H}_\ell[i]\boldsymbol{F}_\ell[i] \right\} \bar{c}_{i\ell} \bar{\boldsymbol{d}}_\ell[i] \\ &+ \boldsymbol{D}_k^{\mathrm{T}}[n] \cdot \mathrm{Re}\left\{\boldsymbol{n}_k[n]\right\}, \quad (\ell, i) \neq (k, n). \end{aligned} \tag{2.43}$$

where

$$\begin{aligned} \bar{c}_{i\ell} &= \mathrm{Im}\left\{c_{i\ell}\right\}, \quad \bar{\boldsymbol{d}}_\ell[i] = \boldsymbol{d}_\ell[i], \quad \text{when} \quad (\ell + i) \quad \text{is even}, \\ \bar{c}_{i\ell} &= c_{i\ell}, \quad \bar{\boldsymbol{d}}_\ell[i] = \mathrm{Im}\left\{\boldsymbol{d}_\ell[i]\right\}, \quad \text{when} \quad (\ell + i) \quad \text{is odd}. \end{aligned}$$

Note that as mentioned in Section 2.2, for the case where $(\ell + i)$ is even, the signal $\boldsymbol{d}_\ell[i]$ on the ℓth subcarrier and at the ith time instant is real, while the corresponding coefficient $c_{i\ell}$ is pure imaginary. On the contrary, when $(\ell + i)$ is odd, $\boldsymbol{d}_\ell[i]$ and $c_{i\ell}$ are pure imaginary and real, respectively. This explains the definitions of $\bar{c}_{i\ell}$ and $\bar{\boldsymbol{d}}_\ell[i]$ shown above. Let us further write (2.43) as

$$\hat{\boldsymbol{d}}_k[n] = \boldsymbol{H}_k^{(\mathrm{eff})}[n]\boldsymbol{d}_k[n] + \sum_{i=n-3}^{n+3} \sum_{\ell=k-1}^{k+1} \boldsymbol{H}_\ell^{(\mathrm{inf})}[i] \bar{\boldsymbol{d}}_\ell[i] + \widetilde{\boldsymbol{n}}_k[n], \quad (\ell, i) \neq (k, n), \tag{2.44}$$

where

$$\begin{aligned} \boldsymbol{H}_k^{(\mathrm{eff})}[n] &= \boldsymbol{D}_k^{\mathrm{T}}[n] \cdot \mathrm{Re}\left\{\boldsymbol{H}_k[n]\boldsymbol{F}_k[n]\right\} \in \mathbb{R}^{d \times d}, \\ \boldsymbol{H}_\ell^{(\mathrm{inf})}[i] &= \boldsymbol{D}_k^{\mathrm{T}}[n] \cdot \mathrm{Im}\left\{-\boldsymbol{H}_\ell[i]\boldsymbol{F}_\ell[i]\right\} \bar{c}_{i\ell} \in \mathbb{R}^{d \times d}, \\ \widetilde{\boldsymbol{n}}_k[n] &= \boldsymbol{D}_k^{\mathrm{T}}[n] \cdot \mathrm{Re}\left\{\boldsymbol{n}_k[n]\right\}. \end{aligned}$$

To calculate the SINR denoted by $\gamma_{r,k}$ for the rth data stream on the kth subcarrier, where $r = 1, \ldots, d$, the entry (r, r) of $\boldsymbol{H}_k^{(\mathrm{eff})}[n]$ determines the effective gain for the rth data stream, while the entries (r, u) $(u = 1, \ldots, d, u \neq r)$ of $\boldsymbol{H}_k^{(\mathrm{eff})}[n]$ determine the residual multi-user and inter-stream interference. In addition, the elements of the rth row of $\boldsymbol{H}_\ell^{(\mathrm{inf})}[i]$ provide a measure of the residual intrinsic interference. Notice that only when $\boldsymbol{D}_k[n] = \boldsymbol{D}_\ell[i]$ $(\ell = k-1,\ k,\ k+1,\ i = n-3, \ldots, n+3$, and $(\ell, i) \neq (k, n))$, $\boldsymbol{H}_\ell^{(\mathrm{inf})}[i]$ is rendered as zero, and the intrinsic interference is completely eliminated. Due to the fact that the channel is not flat fading, the aforementioned condition is not fulfilled, leading to the existence of the residual intrinsic interference. The noise component can be extracted from the covariance matrix of $\widetilde{\boldsymbol{n}}_k[n]$

$$\boldsymbol{R}_{\widetilde{n}\widetilde{n}_k}[n] = \boldsymbol{D}_k^{\mathrm{T}}[n] \cdot \frac{N_0}{2} \boldsymbol{I}_{M_{\mathrm{R}}} \cdot \boldsymbol{D}_k[n]. \tag{2.45}$$

Therefore, $\gamma_{r,k}$ is computed as[11]

$$\gamma_{r,k} = \frac{\left(\boldsymbol{H}_k^{(\mathrm{eff})}[n](r,r)\right)^2}{\sum_{u=1, u\neq r}^{d} \left(\boldsymbol{H}_k^{(\mathrm{eff})}[n](r,u)\right)^2 + \sum_{\substack{i=n-3 \\ (\ell,i)\neq(k,n)}}^{n+3} \sum_{\ell=k-1}^{k+1} \sum_{u=1}^{d} \left(\boldsymbol{H}_\ell^{(\mathrm{inf})}[i](r,u)\right)^2 + \left(\boldsymbol{R}_{\widetilde{n}\widetilde{n}_k}[n](r,r)\right)^2}. \tag{2.46}$$

[11] For a matrix $\boldsymbol{A}$, $\boldsymbol{A}(m, n)$ denotes its (m, n)th entry.

The sum rate is then approximated as

$$R_{\text{sum}} = \frac{1}{N_{\text{c}}} \sum_{k=1}^{N_{\text{c}}} \sum_{r=1}^{d} \log_2(1 + \gamma_{r,k}), \tag{2.47}$$

where N_{c} is the total number of subcarriers. For the case of CP-OFDM, the sum rate can be computed similarly, but the residual intrinsic interference term does not exist. Moreover, the $\text{Re}\{\cdot\}$ operation is not used. On the other hand, when a transmission scheme that is a straightforward extension of the CP-OFDM case (cf. Section 2.2.1) is adopted, the residual intrinsic interference results from the violation of the assumption that the channels of adjacent subcarriers are the same. Therefore, the effective channel that determines the intrinsic interference caused by the signal on the ℓth subcarrier and at the ith time instant to that on the kth subcarrier and at the nth time instant, where $(\ell, i) \neq (k, n)$ is expressed as

$$\boldsymbol{H}_{\ell}^{(\text{inf})}[i] = \text{Im}\left\{ \boldsymbol{D}_k^{\text{H}}[n] \boldsymbol{H}_{\ell}[i] \boldsymbol{F}_{\ell}[i] - \boldsymbol{D}_k^{\text{H}}[n] \boldsymbol{H}_k[n] \boldsymbol{F}_k[n] \right\} \bar{c}_{i\ell}. \tag{2.48}$$

Then the sum rate for this case can be calculated accordingly. It is worth mentioning that in case of the downlink of the CoMP system, the fact that adjacent cells send the same signal to each cell edge user should be taken into account in the sum rate calculation, while the rest resembles the aforementioned case of the multi-user MIMO downlink system.

To this end, we use Fig. 2-7 to illustrate the sum rate performances of two transmission schemes for the FBMC/OQAM based CoMP downlink systems described at the beginning of this section. Here $\text{SNR} = P_{\text{T}}/\sigma_n^2$, where P_{T} is the transmit power of each cell. The CP-OFDM based system where Extended FlexCoBF[12] is employed is also considered for comparison. It can be seen that IIM-CBF 3 leads to a slightly better performance of the FBMC/OQAM based system in contrast to the CP-OFDM based system. The reason is that the former has a higher spectral efficiency compared to the latter, since no cyclic prefix is required. This observation also implies the effectiveness of the proposed transmission strategy IIM-CBF 3 in mitigating the intra-cell and inter-cell interference as well as the intrinsic interference. By comparison, when a transmission strategy originally designed for CP-OFDM, here Extended FlexCoBF, is straightforwardly extended to the FBMC/OQAM system, and the channel is frequency selective, the performance is much worse than that of the proposed IIM-CBF 3 scheme due to a much higher level of the residual interference.

Moreover, Fig. 2-8 depicts the CCDF of the number of iterations required for the IIM-CBF 3 technique to converge. For all the evaluated schemes, ϵ used for the stopping criterion is set to 10^{-5}, and the iterative procedure is manually terminated when the number of iterations reaches 50. Two types of the frequency selective channel, ITU Ped-A and Veh-A are considered. Recall that in the initialization step of IIM-CBF 3, the decoding matrices calculated for the previous subcarrier are used to initialize the decoding matrices for the current subcarrier. Thereby, the lower the frequency selectivity of the channel is, the more effective becomes such a choice of the initial decoding matrices, which leads to a smaller number of iterations required for the convergence of the coordinated beamforming algorithm. Consequently, we observe in Fig. 2-8 that compared to the case of the ITU Veh-A channel which is more frequency selective, the number of iterations that are needed by the coordinated beamforming schemes to converge in case of the ITU Ped-A channel is slightly smaller. However, even when the ITU Veh-A is considered as the propagation channel, the proposed IIM-CBF 3 technique converges within 15 iterations in almost all of the cases.

[12] In the implementation of Extended FlexCoBF [5], we adopt the same mechanism of initializing the decoding matrices as in the LoCCoBF algorithm [22] such that the correlation of the channels of adjacent subcarriers is exploited, and consequently the number of iterations required for the convergence is reduced.

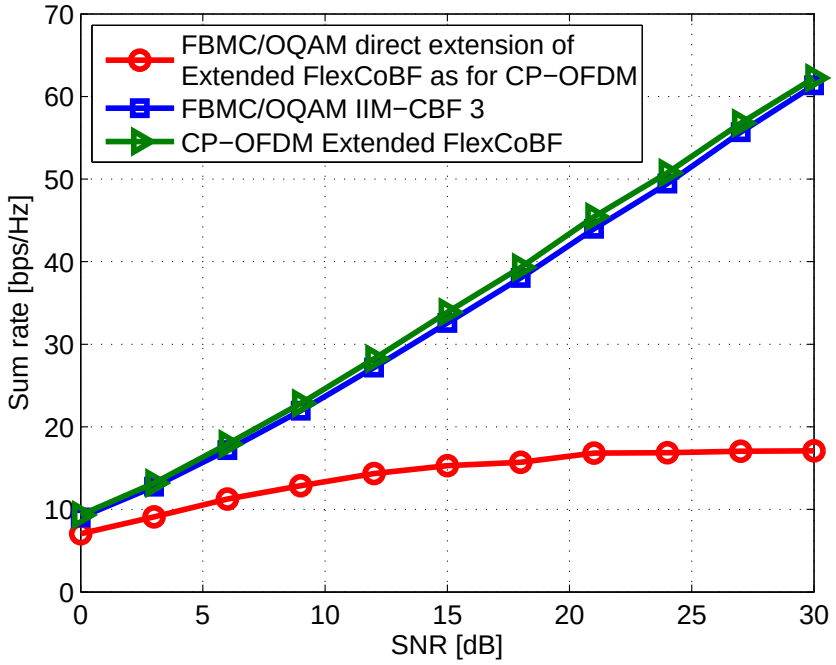

Figure 2-7: Comparison of the sum rate performances of different schemes in the CoMP downlink where the total number of users in two adjacent cells is 5, and the ITU Ped-A channel is considered

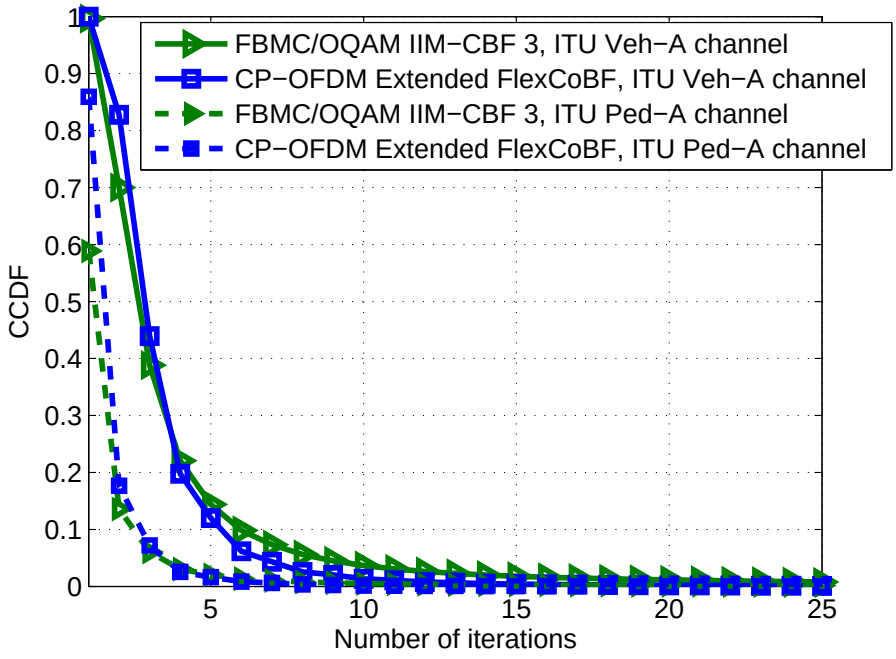

Figure 2-8: CCDF of the number of iterations required for different coordinated beamforming schemes in the CoMP downlink system where the total number of users in two adjacent cells is 5, and the ITU Ped-A channel or the ITU Veh-A channel is considered

Finally, a three-cell CoMP downlink scenario is considered. Each cell equipped with 4 transmit antennas serves 3 users each with 2 receive antennas. This leads to a 4×6 multi-user downlink setting. Among the three users, two are cell interior users, and one is a cell edge user. A single data stream is transmitted to each cell interior user, and two data streams are transmitted to the cell edge user. Similar observations are obtained as in Fig. 2-7.

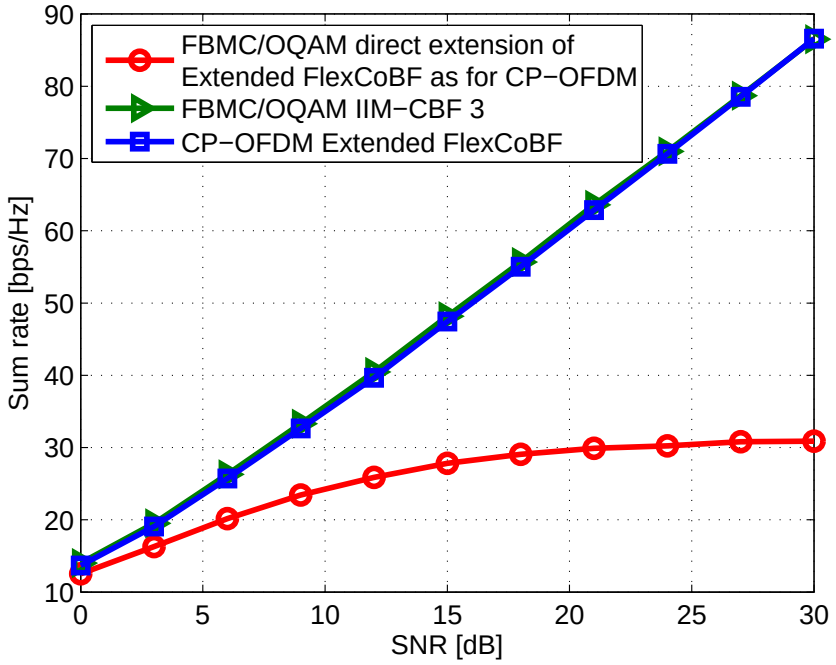

Figure 2-9: Comparison of the sum rate performances of different coordinated beamforming schemes in the CoMP downlink where the total number of users in three adjacent cells is 7, and the ITU Ped-A channel is considered

2.6 Summary

We have developed three IIM-CBF based transmission schemes for the downlink of FBMC/OQAM based multi-user MIMO systems and CoMP systems. The first algorithm that is called IIM-CBF 1 is designed for a multi-user MIMO FBMC/OQAM downlink system where $M_{\mathrm{T}}^{(\mathrm{BS})} = M_{\mathrm{R}}^{(\mathrm{tot})}$. We have employed an iterative procedure to jointly compute the precoding matrix and the decoding matrix of each equivalent single-user transmission that results from the elimination of the multi-user interference. On the other hand, the IIM-CBF 2 technique has been proposed as a solution to the problem that the state-of-the-art transmission strategies for the downlink of FBMC/OQAM based multi-user MIMO systems fail to work when $M_{\mathrm{R}}^{(\mathrm{tot})} > M_{\mathrm{T}}^{(\mathrm{BS})}$. Moreover, we have conducted an investigation of FBMC/OQAM based CoMP downlink systems for the first time. With a focus on the case of partial cooperation of adjacent cells, the scheme, IIM-CBF 3, has been designed to enable the joint transmission of base stations in adjacent cells and combat both the intra-cell and the inter-cell interference. It is worthing noting that in addition to the suppression of the multi-user interference, these three proposed IIM-CBF schemes are effective in mitigating the intrinsic interference that is inherent in FBMC/OQAM based systems without assuming that the propagation channel is almost flat fading. To demonstrate the advantages of the three IIM-CBF algorithms, their BER and sum rate performances

have been shown in different settings. Via the simulation results, it has been shown that the FBMC/OQAM based multi-user MIMO and CoMP downlink systems where IIM-CBF 1, IIM-CBF 2, or IIM-CBF 3 is employed achieve a similar performance compared to their CP-OFDM based counterparts but with a higher spectral efficiency and a greater robustness against misalignments in the frequency domain. In addition, we have numerically analyzed the convergence of the IIM-CBF techniques. It leads to the conclusion that the additional complexity is quite acceptable as the price of alleviating the aforementioned dimensionality constraint.

3. Transmission strategies for multi-user MIMO FBMC/OQAM systems in highly frequency selective channels

To exploit the benefits of both the advanced multi-carrier scheme, FBMC, and the multi-user downlink with space division multiple access (SDMA), there have been several proposals in the literature that shed light on appropriate designs of transmission strategies for FBMC/OQAM based multi-user downlink settings. As reviewed in Chapter 2, most of these state-of-the-art solutions rely on the assumption that the channel on each subcarrier can be treated as flat fading. Among them, the spatial Tomlinson Harashima precoder based non-linear precoding scheme in [17] allows only one receive antenna at each user terminal and is more prone to a high computational complexity compared to linear precoders. On the other hand, a block diagonalization (BD) based linear precoder has been developed in [18] for the FBMC/OQAM based multi-user MIMO downlink. It adopts the central idea of BD [19] to mitigate the multi-user interference (MUI) and then uses the zero forcing based approach [15] to deal with the intrinsic interference cancellation for the resulting equivalent single-user transmissions. Furthermore, the coordinated beamforming based transmission strategies devised in [26], [27] and described in Chapter 2 have the advantage of alleviating the dimensionality constraint such that the number of receive antennas is not restricted. Nevertheless, the violation of the assumption that the channel on each subcarrier is flat fading results in performance degradation of the aforementioned techniques.

Focusing on the case of highly frequency selective channels, the linear precoder in [28] has a structure of a filter applied on each subcarrier and its two adjacent subcarriers at twice the symbol rate. In [29], two different *quasi* minimum mean square error (MMSE) based approaches have been devised for FBMC/OQAM based multi-user multiple-input-single-output (MISO) downlink systems also considering highly frequency selective channels. A closed-form solution is provided in the first scheme, where one complex-valued fractionally spaced multi-tap precoder for each user on each subcarrier is applied at the transmitter and a single-tap real-valued weight at the receiver. The second scheme involves a joint transmitter and receiver design via an iterative procedure, where now the equalizer at the receiver side is also complex-valued fractionally spaced multi-tap. The corresponding results have been reported in the deliverable D4.3. Similar to [28], the two methods in [29] are restricted to the case where each user is equipped with a single receive antenna.

In this chapter, we present the design of linear precoding and equalization schemes for the downlink of critical multi-user MISO and MIMO PMR scenarios under highly frequency selective propagation conditions.

Due to the inter-dependencies and inter-coupling between the precoder filters at the transmitter of a FBMC system an MMSE-based precoder design is quite complex. Although we only consider ICI with the neighboring sub-carriers, in a MU-FBMC system the precoder design must additionally consider the precoder filters of all other users and also the neighboring sub-carriers. In a dual MMSE-based equalizer this inter-coupling is not present and therefore the design is simpler. We will use the *quasi* MMSE-based precoder design of [29] as a benchmark for the MSE-duality based MISO precoder designs introduced in this chapter. It should be noted that the numerical calculation of the precoder filters in [29] suffered from ill conditioned matrices which is not the case in the new proposed method.

Moreover, stemming from the problem formulation in [29], we first develop an iterative approach, where MMSE based multi-tap precoders are designed to effectively mitigate the MUI, inter-symbol interference (ISI), and inter-carrier interference (ICI). At each user terminal equipped with multiple antennas, only a receive spatial filter is applied. Via an iterative design,

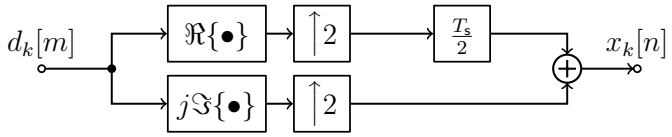

Figure 3-1: OQAM Staggering for even indexed subcarriers

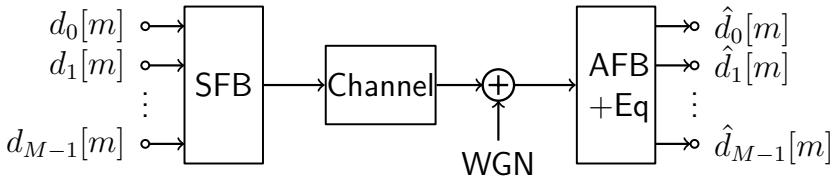

Figure 3-2: Single user single antenna FBMC System

the precoders and the receive spatial filters are jointly optimized. Then, we further propose a novel closed-form signal-to-leakage (SLR) based design of the precoders that can be conveniently extended to the case of multiple spatial streams per user. Via numerical results, it is observed that the proposed schemes achieve a very promising performance in case of highly frequency selective channels. They significantly outperform the state-of-the-art approaches that suffer from impractical restrictions on the channel frequency selectivity. By allowing multiple antennas at each user terminal, the benefits of the MIMO technology are exploited.

3.1 System model

On the transmitter side of an FBMC/OQAM system, the real part and the complex part of the QAM modulated data symbols $d_k[m] = \alpha_k[m] + \mathrm{j}\,\beta_k[m]$ are staggered by half of the symbol period $T/2$ as illustrated in Figure 3-1 for even-indexed subcarriers. The resulting signals are multiplexed by a synthesis filter bank (SFB). At the receiver, signals from the subchannels are separated by an analysis filter bank (AFB) as shown in Figure 3-2. Assuming an exponentially modulated filter bank is used for the SFB and the AFB, the pulse shaping filter of the kth subcarrier has the following form

$$\begin{aligned} h_k[l_{\mathrm{P}}] =& h_{\mathrm{P}}[l_{\mathrm{P}}]\exp\left(\jmath\frac{2\pi}{M}k\left(l_{\mathrm{P}}-\frac{L_{\mathrm{P}}-1}{2}\right)\right), \\ & l_{\mathrm{P}} = 0,1,\ldots,L_{\mathrm{P}}-1, \end{aligned} \tag{3.1}$$

where $h_{\mathrm{P}}[l_{\mathrm{P}}]$ is the prototype filter of length L_{P}, and M denotes the number of subcarriers. Here for the prototype filter we choose a root raised cosine of length $L_{\mathrm{P}} = KM+1$, where K represents the overlapping factor.

One base station serves U users simultaneously. The number of transmit antennas is denoted by N_{T}, whereas the jth user is equipped with N_{R_j} receive antennas. The total number of receive antennas of all users is denoted by $N_{\mathrm{R}} = \sum_{j=1}^{U} N_{\mathrm{R}_j}$. One data stream is transmitted to each user. Multi-tap precoding filters at the base station and equalizers at the user terminals are designed to mitigate the multi-user interference (MUI), inter-symbol interference (ISI), and inter-carrier interference (ICI) as well as to recover the desired signals. After the OQAM staggering, the signal transmitted to the jth user on the ℓth subcarrier is denoted by $x_\ell^j[n]$, $j = 1,2,\ldots,U$. The impulse response of its corresponding precoding filter is symbolized by $b_\ell^{i,j}[n]$, $i = 1,2,\ldots,N_{\mathrm{T}}$, while B denotes the length of the precoding filters. The output of the

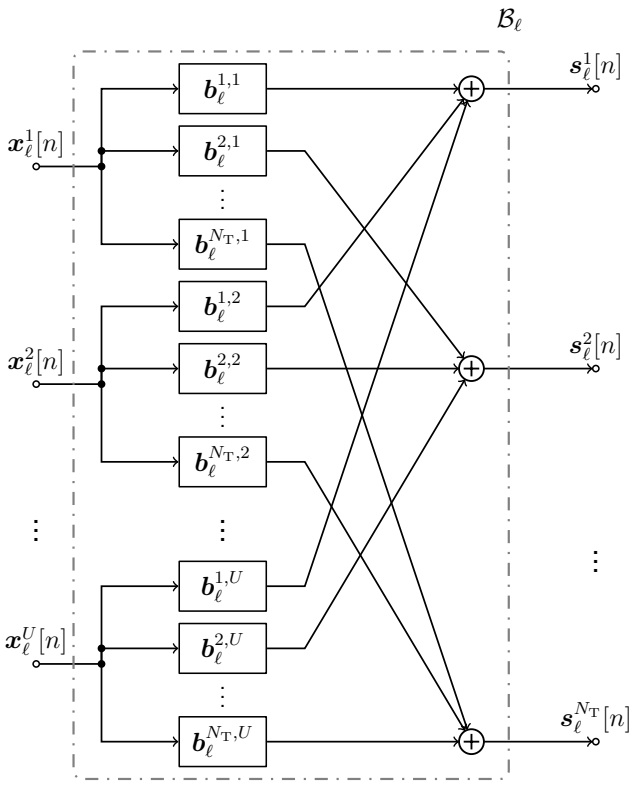

Figure 3-3: Precoding of U users onto N_T transmit antennas for subcarrier ℓ

precoders are then combined to be fed into the subcarrier filters for each subcarrier as shown in Figure 3-3. In order to derive a subcarrier model, Figure 3-4 show how the different precoder blocks $\mathcal{B}_\ell$ of Figure 3-3 are combined with the subcarrier filters and transmit antennas. In this work, highly frequency selective channels are considered, and $h_\mathrm{ch}^{i,j,r}$ represents the impulse response of the propagation channel between the ith transmit antenna and the rth receiver antenna of the jth user. The signal on the kth subcarrier is contaminated by interference from the $(k-1)$th and the $(k+1)$ subcarrier. The equivalent channel impulse response for the signal that is transmitted on the ℓth subcarrier from the ith transmit antenna to the rth receive antenna and passed through the analysis filter for the kth subcarrier can be expressed as

$$h_{\ell,k}^{i,j,r}[n] = \left[h_\ell[l_\mathrm{P}] * h_\mathrm{ch}^{i,j,r}[l_\mathrm{P}] * h_k[l_\mathrm{P}]\right]_{l_\mathrm{P}=n\frac{M}{2}}, \tag{3.2}$$

where the effects of the transmit filter, the propagation channel, the receive filter, and the upsampling and downsampling operations are included. The resulting number of taps of this equivalent channel is

$$Q = \left\lceil \frac{2(L_\mathrm{P}-1)+L_\mathrm{ch}}{M/2} \right\rceil, \tag{3.3}$$

where L_ch denotes the length of the channel impulse response. For the rth receive antenna of the jth user, an equalizer is applied, and its impulse response is represented by $g_k^{j,r}[n]$, where $j = 1, 2, \ldots, U$, and $r = 1, 2, \ldots, N_{\mathrm{R}_j}$. The subcarrier model for the receiver side is then show in 3-5. In Figure 3-6 we show the total subcarrier model for the kth subcarrier, jth user, jth transmit antenna and rth receive antenna. Equivalently, the recovered signal of the jth user

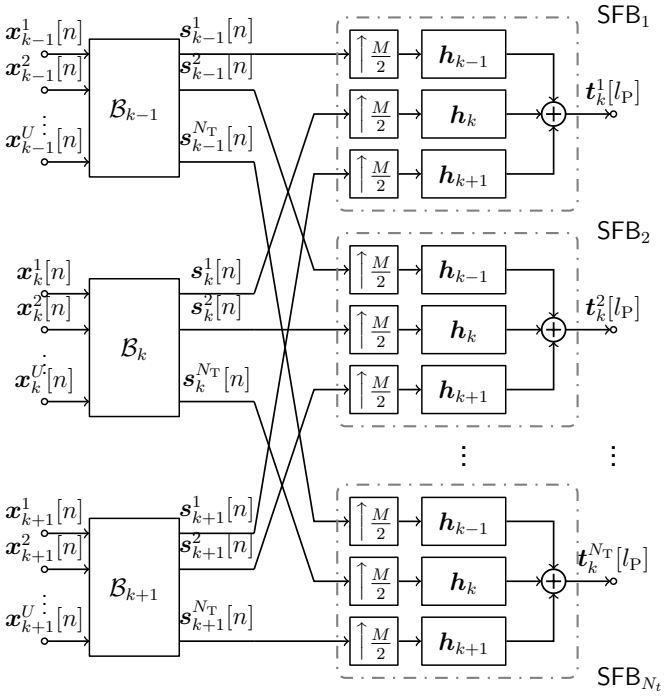

Figure 3-4: Precoded transmitter subcarrier model for N_T antennas

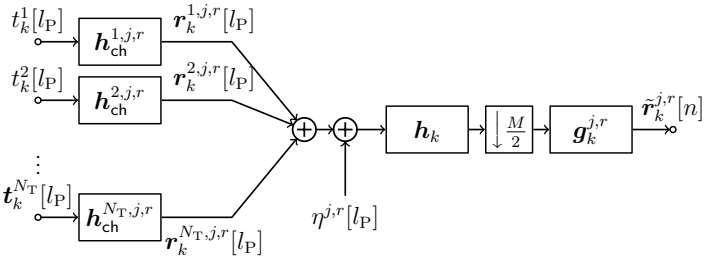

Figure 3-5: Subcarrier model for rth receive antenna

on the kth subcarrier can be written as

$$\hat{x}_k^j[n] = \sum_{r=1}^{N_{\mathrm{R}_j}} g_k^{j,r}[n] * \left(\sum_{i=1}^{N_\mathrm{T}} \sum_{\ell=k-1}^{k+1} \left(h_{\ell,k}^{i,j,r}[n] * \sum_{s=1}^{U} \left(b_\ell^{i,s}[n] * x_\ell^s[n] \right) \right) + \hat{\eta}_k^{j,r}[n] \right),$$

where $\hat{\eta}_k^{j,r}[n]$ denotes the filtered additive white Gaussian noise

$$\hat{\eta}_k^{j,r}[n] = \left[h_k[l_\mathrm{P}] * \eta^{j,r}[l_\mathrm{P}] \right]_{l_\mathrm{P}=n\frac{M}{2}}. \tag{3.4}$$

As OQAM is employed, the data sequence can be stacked in the vector $\boldsymbol{x}_k^j[n]$ as follows

$$\boldsymbol{x}_k^j[n] = \begin{cases} \begin{bmatrix} \alpha_k^j[m] & \jmath\beta_k^j[m] & \alpha_k^j[m-1] & \cdots \end{bmatrix}^\mathrm{T}, & \text{for } k \text{ odd}, \\ \begin{bmatrix} \jmath\beta_k^j[m] & \alpha_k^j[m] & \jmath\beta_k^j[m-1] & \cdots \end{bmatrix}^\mathrm{T}, & \text{for } k \text{ even}. \end{cases} \tag{3.5}$$

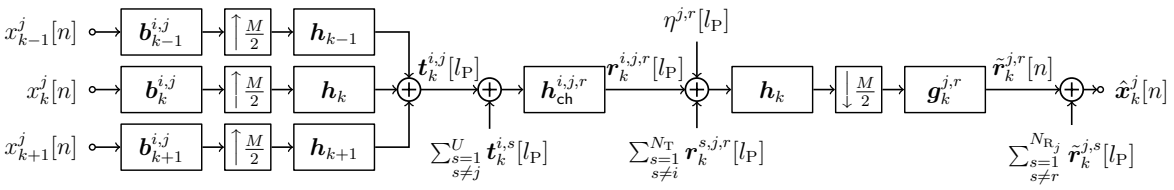

Figure 3-6: Model for subcarrier k, user j, transmit antenna i and receive antenna r

3.2 SIMO/MISO MSE-Duality based precoder design

In the particular case of MISO systems each user is equiped with only one antenna, i.e. $N_{\mathrm{R_j}} = 1$ for all j. In this section we also assume that the equalizers $g^j_k[n]$ for all users are trivial, this means that their impulse responses have length one and real valued coefficients.

In the following we will work with a purely real notation and therefore define a purely real input sequence as $\boldsymbol{x}^s_k[n] = \boldsymbol{J}_k \tilde{\boldsymbol{x}}^s_k[n]$ with

$$\boldsymbol{J}_k = \begin{cases} \mathrm{diag}\begin{bmatrix} 1 & \mathrm{j} & 1 & \mathrm{j} & \cdots \end{bmatrix}, & k \text{ is odd}, \\ \mathrm{diag}\begin{bmatrix} \mathrm{j} & 1 & \mathrm{j} & 1 & \cdots \end{bmatrix}, & k \text{ is even}. \end{cases}$$

Thereby extracting the imaginary j's from the input signal. We then multiply the transposed convolution matrix of $h^s_{l,j}[n]$ by $\boldsymbol{J}_k$ and are left with $\tilde{\boldsymbol{H}}^s_{l,j} = \boldsymbol{H}^s_{l,j}\boldsymbol{J}_k$. It can been shown, [29] and [30], that by calculating the precoder or equalizer filters with either the real or imaginary part of the input symbol both result in the same filters.

3.2.1 MU-SIMO System

For the MU-SIMO system we define a multi-tap equalizer vector $\boldsymbol{w}^s_{k,j} \in \mathbb{C}^B$ per user, per sub-carrier and per receive antenna and a single-tap precoding scalar $b^{v,\mathsf{UL}}_k$ per user. In the MU-SIMO system we have U decentralized users who transmit the $\boldsymbol{x}^1, \cdots, \boldsymbol{x}^U$ input signals over all sub-carriers to N_r centralized receive antennas. We assume there is no *Channel State Information* (CSI) in the transmitters and therefore set the MU-SIMO precoder vector equal to one, $b^{v,\mathsf{UL}}_k = 1$. The real part of our receive signal for user v in sub-carrier k is defined as

$$\hat{\alpha}^{v,\mathsf{UL}}_k[n] = \sum_{j=1}^{N_\mathsf{r}} \bar{\boldsymbol{w}}^{v,T}_{k,j} \left(\sum_{s=1}^{U} \sum_{l=k-1}^{k+1} \bar{\boldsymbol{H}}^s_{l,j} \tilde{\boldsymbol{x}}^s_l[n] + \bar{\boldsymbol{\Xi}}_{k,j} \right), \tag{3.6}$$

where we define the stacking vectors as

$$\begin{aligned} \bar{\boldsymbol{w}}^{v,T}_{k,j} &= \left[\boldsymbol{w}^{v,(R),T}_{k,j}, \quad \boldsymbol{w}^{v,(I),T}_{k,j} \right] \in \mathbb{R}^{1\times 2B}, \\ \bar{\boldsymbol{H}}^s_{l,j} &= \left[\tilde{\boldsymbol{H}}^{s,(R)}_{l,j}, \quad \tilde{\boldsymbol{H}}^{s,(I)}_{l,j} \right]^T \in \mathbb{R}^{2B\times(B+Q-1)}, \\ \bar{\boldsymbol{\Xi}}_k &= \left[(\boldsymbol{\Gamma}_k \boldsymbol{\eta}_j)^{(R)}, \quad (\boldsymbol{\Gamma}_k \boldsymbol{\eta}_j)^{(I)} \right]^T \in \mathbb{R}^{2B\times 1}, \end{aligned}$$

where we define $\bullet^{(R)} = \Re\{\bullet\}$ and $\bullet^{(I)} = \Im\{\bullet\}$. For the following derivations we will assume the input signals to be *independent and identically distributed* (i.i.d.) and Gaussian distributed. The covariance matrix before O-QAM staggering is defined as $\mathrm{E}\left[\boldsymbol{d}^s_k[m]\boldsymbol{d}^{s,H}_k[m]\right] = (\sigma^2_d/U)\boldsymbol{I}$

and after the O-QAM staggering as $\mathrm{E}\left[\tilde{\boldsymbol{x}}_k^s[n]\tilde{\boldsymbol{x}}_k^{s,T}[n]\right] = (\sigma_d^2/(2U))\boldsymbol{I} = \sigma_M^2\boldsymbol{I}$. Furthermore, we have assumed the additive noise is Gaussian distribution with $\boldsymbol{\eta}_j[n] \sim \mathcal{N}_{\mathbb{C}}\left(\boldsymbol{0}, \sigma_\eta^2\boldsymbol{I}\right)$ for each receive antenna. Additionally, the input signals and the noise are uncorrelated as well as the noise between receive antennas, i.e. $\mathrm{E}\left[\boldsymbol{x}_k^s\boldsymbol{\eta}_j^H\right] = \boldsymbol{0}\ \forall\ s,k,j$ and $\mathrm{E}\left[\boldsymbol{\eta}_i\ \boldsymbol{\eta}_j^H\right] = \boldsymbol{0}$ for $i \neq j$, respectively. The optimization problem we encounter can be expressed as an MSE we wish to minimize, defined as

$$\begin{aligned}\hat{\boldsymbol{w}}_k^v &= \underset{\hat{\boldsymbol{w}}_k^v}{\operatorname{argmin}}\, \mathrm{E}\left[\left|\hat{\alpha}_k^{v,\mathsf{UL}}[n] - \alpha_k^{v,\mathsf{UL}}[n-\nu]\right|^2\right], \\ &= \underset{\hat{\boldsymbol{w}}_k^v}{\operatorname{argmin}}\, \epsilon_k^{v,\mathsf{UL}}.\end{aligned} \tag{3.7}$$

By solving the optimization problem in (3.7) similar to [30] where an MMSE-based equalizer was calculated for a single user SISO FBMC system. We can calculate an MMSE-based equalizer filter for all receive antennas as

$$\hat{\boldsymbol{w}}_k^v = \sigma_M^2 \left(\sum_{s=1}^{U}\sum_{l=k-1}^{k+1} \sigma_M^2 \hat{\boldsymbol{H}}_l^s \hat{\boldsymbol{H}}_l^{s,T} + \hat{\boldsymbol{R}}_\eta\right)^{-1} \hat{\boldsymbol{H}}_k^v \hat{\boldsymbol{e}}_\nu. \tag{3.8}$$

Given the MMSE-based equalizer we are left with a simplified, closed form expression for the UL MSE per user and per sub-carrier defined as

$$\epsilon_k^{v,\mathsf{UL}} = \sigma_M^2 \left(1 - \boldsymbol{e}_\nu^T \hat{\boldsymbol{H}}_k^{v,T} \hat{\boldsymbol{w}}_k^v\right), \tag{3.9}$$

with the stacking matrices

$$\begin{aligned}\hat{\boldsymbol{w}}_k^{v,T} &= \begin{bmatrix}\bar{\boldsymbol{w}}_{k,1}^{v,T} & \cdots & \bar{\boldsymbol{w}}_{k,N_\mathsf{r}}^{v,T}\end{bmatrix} \in \mathbb{R}^{1\times 2BN_\mathsf{r}}, \\ \hat{\boldsymbol{H}}_l^s &= \begin{bmatrix}\bar{\boldsymbol{H}}_{l,1}^s & \cdots & \bar{\boldsymbol{H}}_{l,N_\mathsf{r}}^s\end{bmatrix}^T \in \mathbb{R}^{2BN_\mathsf{r}\times(B+Q-1)}, \\ \boldsymbol{e}_\nu &= \begin{bmatrix}0 & \cdots & 0\ 1\ 0 & \cdots & 0\end{bmatrix}^T \in \mathbb{R}^{(B+Q-1)\times 1}, \\ \hat{\boldsymbol{R}}_\eta &= \mathsf{blockdiag}\begin{bmatrix}\bar{\boldsymbol{R}}_{\eta_1} & \cdots & \bar{\boldsymbol{R}}_{\eta_{N_\mathsf{r}}}\end{bmatrix} \in \mathbb{R}^{2BN_\mathsf{r}\times 2BN_\mathsf{r}}, \\ \bar{\boldsymbol{R}}_{\eta,k} &= \begin{bmatrix}\boldsymbol{R}_{\eta,k,1} & \boldsymbol{R}_{\eta,k,2} \\ -\boldsymbol{R}_{\eta,k,2} & \boldsymbol{R}_{\eta,k,1}\end{bmatrix} \in \mathbb{R}^{2B\times 2B}, \\ \text{with } \boldsymbol{R}_{\eta,k,1} &= \frac{\sigma_\eta^2}{2}\left(\boldsymbol{\Gamma}_k^{(R)}\boldsymbol{\Gamma}_k^{(R),T} + \boldsymbol{\Gamma}_k^{(I)}\boldsymbol{\Gamma}_k^{(I),T}\right) \in \mathbb{R}^{B\times B}, \\ \boldsymbol{R}_{\eta,k,2} &= \frac{\sigma_\eta^2}{2}\left(\boldsymbol{\Gamma}_k^{(R)}\boldsymbol{\Gamma}_k^{(I),T} - \boldsymbol{\Gamma}_k^{(I)}\boldsymbol{\Gamma}_k^{(R),T}\right) \in \mathbb{R}^{B\times B}.\end{aligned}$$

3.2.2 MU-MISO System

For the MU-MISO system we define a multi-tap precoder vector $\boldsymbol{b}_{k,j}^s \in \mathbb{C}^B$ per user, per sub-carrier and per receive antenna and a single-tap equalizing scalar $w_k^{\mathsf{UL},v} \in \mathbb{R}_+$ per user and sub-carrier. In the MU-MISO system we have N_t centralized transmit antennas which transmit the $\boldsymbol{x}^1, \cdots, \boldsymbol{x}^U$ input signals over all sub-carriers to the U decentralized users. The real part

of our receive signal for user v in sub-carrier k is defined as

$$\hat{\alpha}_k^{v,\mathsf{DL}}[n] = w_k^{v,\mathsf{DL}} \left(\sum_{s=1}^{U} \sum_{l=k-1}^{k+1} \hat{\boldsymbol{b}}_l^{s,T} \hat{\boldsymbol{H}}_l^v \tilde{\boldsymbol{x}}_k^s[n] + \Re\{\boldsymbol{h}_k^H \boldsymbol{\eta}^v\} \right), \tag{3.10}$$

where we define $\hat{\boldsymbol{b}}_l^s$ and $\hat{\boldsymbol{H}}_l^v$ as the equivalent stacking vectors of $\hat{\boldsymbol{w}}_l^s$ and $\hat{\boldsymbol{H}}_l^v$ from Section 3.2.1, respectively, but with $N_\mathsf{r} = N_\mathsf{t}$. Again we have assumed that the input signals $\boldsymbol{x}_k^s$ to be i.i.d. and Gaussian distributed with an equivalent distribution to that defined in Section 3.2.1. Furthermore, we have assumed the additive noise is Gaussian distribution with $\boldsymbol{\eta}^s[n] \sim \mathcal{N}_\mathbb{C}\left(\mathbf{0}, \sigma_\eta^2 \boldsymbol{I}\right)$ for each user. Additionally, the input signals and the noise are uncorrelated as well as the noise between users, i.e. $\mathrm{E}\left[\boldsymbol{x}_k^s \boldsymbol{\eta}^{s,H}\right] = \mathbf{0}\ \forall\ s,k$ and $\mathrm{E}\left[\boldsymbol{\eta}^s \boldsymbol{\eta}^{v,H}\right] = \mathbf{0}$ for $s \neq v$, respectively.

The MSE expression we wish to minimize is defined as

$$\begin{aligned} \hat{\boldsymbol{b}}_k^v &= \underset{\hat{\boldsymbol{b}}_k^v}{\operatorname{argmin}}\, \mathrm{E}\left[|\hat{\alpha}_k^{v,\mathsf{DL}}[n] - \alpha_k^{v,\mathsf{DL}}[n-\nu]|^2 \right], \\ &= \underset{\hat{\boldsymbol{b}}_k^v}{\operatorname{argmin}}\, \epsilon_k^{v,\mathsf{DL}} \\ &\quad \text{s. t.} \sum_{v=1}^{U} \sum_{k=1}^{M_\mathsf{u}} \|\hat{\boldsymbol{b}}_k^v\|_2^2 \leq M_\mathsf{u} U. \end{aligned}$$

By plugging (3.10) into the argument of our optimization problem, we arrive at a close formed expression for the DL MSE per user and per sub-carrier as

$$\begin{aligned} \epsilon_k^{v,\mathsf{DL}} =& \sigma_M^2 w_k^{v,\mathsf{DL},2} \sum_{s=1}^{U} \sum_{l=k-1}^{k+1} \hat{\boldsymbol{b}}_l^{s,T} \hat{\boldsymbol{H}}_l^v \hat{\boldsymbol{H}}_l^{v,T} \hat{\boldsymbol{b}}_l^s \\ &- \sigma_M^2 w_k^{v,\mathsf{DL}} \hat{\boldsymbol{b}}_k^{v,T} \hat{\boldsymbol{H}}_k^v \hat{\boldsymbol{e}}_\nu - \sigma_M^2 w_k^{v,\mathsf{DL}} \hat{\boldsymbol{e}}_\nu^T \hat{\boldsymbol{H}}_k^{v,T} \hat{\boldsymbol{b}}_k^v \\ &+ w_k^{v,\mathsf{DL},2} \sigma_\eta^2 \left(\boldsymbol{h}_k^{(R),T} \boldsymbol{h}_k^{(R)} + \boldsymbol{h}_k^{(I),T} \boldsymbol{h}_k^{(I)} \right) + \sigma_M^2. \end{aligned} \tag{3.11}$$

We observe in (3.11) that the DL MSE expression for user v in sub-carrier k not only depends on the precoder vector $\hat{\boldsymbol{b}}_k^v$, but it additionally depends on the precoder vectors of the neighboring sub-carriers as well as the precoder vectors from all other users in the system. This interdependency between precoder vectors makes the minimization of the MSE more difficult than in the MU-SIMO system. In [29] a method to calculate an *quasi*-MMSE precoder was investigated and we will compare our proposed methods against it.

3.2.3 MSE-Duality Transformation

In this Section we will investigate four different methods of transforming our UL SIMO system into an equivalent DL MISO system using the duality principle as introduced in [31] and [32]. The basic principle behind an MSE-duality transformation is to switch the roles of the UL and DL filters, i.e. we interchange each receiver filter in the UL system with the respective transmitter filter in the DL system. As the dual DL system has purely transmitter processing, we must ensure that the transmit power is subsequently limited, thus we weight every transmitter filter with a strictly real value and multiply the receiver with the inverse weighting factor.

We will investigate the different levels of duality transformations similar to those defined in [32]. These different duality transformations are summarized as follows:

- In Subsection 3.2.3.1 we will attempt to preserve the *System-Wide Sum-MSE*, equivalent to a *Level 1* transformation from [32]. This is the simplest form of duality where we keep the total sum-MSE for all users and sub-carriers equal when transforming the UL to a DL system. We only require a single scaling factor which leads to an extremely low computational complexity.

- In Subsection 3.2.3.2 we will attempt to preserve the *User-Wise Sum-MSE*, equivalent to a *Level 2* transformation from [32]. This method preserves the sum-MSE per *user* resulting in an individual scaling factor per user for all sub-carriers and transmitter antennas. We have to solve a linear system of equations for the U scaling factors, thus leading to a higher computational complexity than a *Level 1* transformation.

- In Subsection 3.2.3.3 we will attempt to preserve the *Sub-Carrier-Wise Sum-MSE*, equivalent to a *Level 2* transformation from [32]. This method preserves the sum-MSE per *sub-carrier* resulting in an distinct scaling factor per sub-carrier for all users and transmitter antennas. Again, we have to solve a linear system of equations for the M_{u} scaling factors, which leads to a higher computational complexity that a *User-Wise Sum-MSE* and *Level 1* transformation.

- In Subsection 3.2.3.4 we will attempt to preserve the *User and Sub-Carrier-Wise MSE*, equivalent to a *Level 3* transformation from [32]. This method preserves the individual MSE for every single *user* and *sub-carrier*. This results in a scaling factor per user and per sub-carrier for all transmitter antennas. Evidently, a *Level 3* duality transformation requires the highest computational complexity because we have to solve for $M_{\mathsf{u}} \times U$ different scaling factors. However, this method guarantees that the individual MSEs per user, per sub-carrier will stay equal for the UL SIMO and DL MISO systems.

3.2.3.1 System-Wide Sum-MSE

First, we define a relation between the UL and DL filters with a single, real-valued scaling factor such that

$$\begin{aligned} \hat{\boldsymbol{b}}_k^s &= \gamma \hat{\boldsymbol{w}}_k^s, \\ w_k^{s,\mathsf{DL}} &= \gamma^{-1}, \end{aligned} \tag{3.12}$$

with $\gamma \in \mathbb{R}_+$ and recalling that the UL precoder filter was set such that $b_k^{v,\mathsf{UL}} = 1$. In the next step we set the system-wide sum-MSE equal between the UL and the DL system, i.e. we sum over all users and all sub-carriers and set these MSE values to be equal

$$\sum_{v=1}^{U} \sum_{k=1}^{M_{\mathsf{u}}} \epsilon_k^{\mathsf{v},\mathsf{DL}} \stackrel{!}{=} \sum_{v=1}^{U} \sum_{k=1}^{M_{\mathsf{u}}} \epsilon_k^{\mathsf{v},\mathsf{UL}}. \tag{3.13}$$

By solving (3.13) we can calculate a single scaling factor γ for all users, sub-carriers and transmit antennas

$$\gamma^2 = \frac{\sum_{k=1}^{M_{\mathsf{u}}} U \sigma_\eta^2 \|\boldsymbol{h}_k\|_2^2}{\sum_{v=1}^{U} \sum_{k=1}^{M_{\mathsf{u}}} \sigma_M^2 \left(\hat{\boldsymbol{w}}_k^{v,T} \hat{\boldsymbol{H}}_k^v \hat{\boldsymbol{e}}_\nu - \sum_{s=1}^{U} \sum_{l=k-1}^{k+1} \check{\boldsymbol{w}}_l^{s,T} \check{\boldsymbol{H}}_l^v \check{\boldsymbol{H}}_l^{v,T} \check{\boldsymbol{w}}_l^s \right)}. \tag{3.14}$$

By calculating only a single weighting factor this method of duality transformation guarantees that the system-wide sum-MSE will remain equal after the transformation but individual user MSE and sub-carrier MSE can change between the UL and DL systems. Furthermore, this method considers all users, sub-carriers and transmit antennas when spreading the total

available transmit power amongst them. This means that the users and sub-carriers with the overall worst channels in the system will get more power to compensate for their channels. However, it should be noted that if a certain user in a certain sub-carrier exhibits extremely large MSE value after the transformation this user will obtain a disproportionate amount of transmit power in regard to the other users and other sub-carriers.

3.2.3.2 User-Wise Sum-MSE

First, we define a relation between the UL and DL filters with a real-valued scaling factor per user such that

$$\begin{aligned} \hat{\boldsymbol{b}}_k^s &= \gamma^s \hat{\boldsymbol{w}}_k^s, \\ w_k^{s,\mathsf{DL}} &= \left(\gamma^s\right)^{-1}, \end{aligned} \tag{3.15}$$

with $\gamma^s \in \mathbb{R}_+$ and recalling that the UL precoder filter was set such that $b_k^{v,\mathsf{UL}} = 1$. Following this, we set the user-wise sum-MSE equal between the UL and the DL system, i.e. we sum over all sub-carriers and set them equal per user

$$\sum_{k=1}^{M_\mathsf{u}} \epsilon_k^{v,\mathsf{DL}} \stackrel{!}{=} \sum_{k=1}^{M_\mathsf{u}} \epsilon_k^{v,\mathsf{UL}}. \tag{3.16}$$

We end up with a system of linear equations for the U scaling factors γ^s per user

$$\boldsymbol{A}^s \underbrace{\begin{bmatrix} \left(\gamma^1\right)^2 \\ \vdots \\ \left(\gamma^U\right)^2 \end{bmatrix}}_{\left(\boldsymbol{\gamma}^s\right)^2} = \sum_{k=1}^{M_\mathsf{u}} \sigma_\eta^2 \|\boldsymbol{h}_k\|_2^2 \mathbf{1}_U, \tag{3.17}$$

where the matrix $\boldsymbol{A}^s \in \mathbb{R}^{U \times U}$ has strictly positive main diagonal elements and strictly negative off-diagonal elements and $\mathbf{1}_U$ is the all-one vector with length U . This matrix is defined as

$$[\boldsymbol{A}^s]_{v,y} = \begin{cases} \sum\limits_{k=1}^{M_\mathsf{u}} \sum\limits_{l=k-1}^{k+1} \sigma_M^2 \Big(\hat{\boldsymbol{w}}_k^{v,T} \hat{\boldsymbol{H}}_k^v \hat{\boldsymbol{e}}_\nu \\ -\hat{\boldsymbol{w}}_l^{v,T} \hat{\boldsymbol{H}}_l^v \hat{\boldsymbol{H}}_l^{v,T} \hat{\boldsymbol{w}}_l^v \Big), & \text{if } v = y, \\ -\sum\limits_{k=1}^{M_\mathsf{u}} \sum\limits_{l=k-1}^{k+1} \sigma_M^2 \hat{\boldsymbol{w}}_k^{y,T} \hat{\boldsymbol{H}}_l^v \hat{\boldsymbol{H}}_l^{v,T} \hat{\boldsymbol{w}}_k^y, & \text{if } v \neq y. \end{cases} \tag{3.18}$$

This form of duality transformation guarantees that each individual user's sum-MSE will stay equal in the UL and the DL system. Therefore, this method can be interpreted as allocating an equal amount of transmit power to each user whilst allowing each user to spread this transmit power across the sub-carriers as required. Again, the disadvantage of this method arises if a user has certain sub-carriers with channels with much larger MSE values, these sub-carriers will obtain a disproportionate amount of transmit power in regard to the other sub-carriers of that user.

3.2.3.3 Sub-Carrier-Wise Sum-MSE

First, we define a relation between the UL and DL filters with a real-valued scaling factor per sub-carrier such that

$$\begin{aligned} \hat{\boldsymbol{b}}_k^s &= \gamma_k \hat{\boldsymbol{w}}_k^s, \\ w_k^{s,\mathsf{DL}} &= \gamma_k^{-1}, \end{aligned} \tag{3.19}$$

with $\gamma_k \in \mathbb{R}_+$ and recalling that the UL precoder filter was set such that $b_k^{v,\mathsf{UL}} = 1$. Next we set the sub-carrier-wise sum MSE equal between the UL and the DL system, i.e. we sum over all users and set the sum-MSE values equal per sub-carrier

$$\sum_{v=1}^{U} \epsilon_k^{v,\mathsf{DL}} \stackrel{!}{=} \sum_{v=1}^{U} \epsilon_k^{v,\mathsf{UL}}. \tag{3.20}$$

We end up with a system of linear equations for the M_u scaling factors γ_k per sub-carrier

$$\boldsymbol{A}^k \underbrace{\begin{bmatrix} \gamma_1^2 \\ \vdots \\ \gamma_{M_\mathsf{u}}^2 \end{bmatrix}}_{\boldsymbol{\gamma}_k^2} = \sum_{v}^{U} \sigma_\eta^2 \|\boldsymbol{h}_\mathsf{p}\|_2^2 \mathbf{1}_{M_\mathsf{u}}, \tag{3.21}$$

with the tri-diagonal matrix $\boldsymbol{A}^k \in \mathbb{R}^{M_\mathsf{u} \times M_\mathsf{u}}$ with strictly positive elements on the main diagonal and strictly negative off-diagonal elements. This matrix is defined as

$$\left[\boldsymbol{A}^k\right]_{k,m} = \begin{cases} \sum_{v=1}^{U} \sum_{l=k-1}^{k+1} \sigma_M^2 \left(\hat{\boldsymbol{w}}_k^{v,T} \hat{\boldsymbol{H}}_k^v \hat{\boldsymbol{e}}_\nu \right. \\ \left. - \sum_{s=1}^{U} \hat{\boldsymbol{w}}_k^{s,T} \hat{\boldsymbol{H}}_k^v \hat{\boldsymbol{H}}_k^{v,T} \hat{\boldsymbol{w}}_k^s \right), & \text{if } k = m, \\ - \sum_{v,s=1}^{U} \sigma_M^2 \hat{\boldsymbol{w}}_m^{s,T} \hat{\boldsymbol{H}}_m^v \hat{\boldsymbol{H}}_m^{v,T} \hat{\boldsymbol{w}}_m^s, & \text{if } |m-k| = 1, \\ 0 & \text{else.} \end{cases} \tag{3.22}$$

This method of duality transformation guarantees that the sum-MSE per sub-carrier stays equal in the UL and the DL system. Therefore, by applying this duality transformation we allocate an equal amount of transmit power per sub-carrier but allow the transmit power to be spread across the users transmitting in that sub-carrier. Again, this transformation has the disadvantage if a certain user's MSE value is much larger than the other users for a certain sub-carrier, that user will obtain a disproportionate amount of transmit power with regards to the other users in that sub-carrier.

3.2.3.4 User and Sub-Carrier-Wise MSE

Finally, we define a relation between the UL and DL filters with a real-valued scaling factor per user and per sub-carrier such that

$$\begin{aligned} \hat{\boldsymbol{b}}_k^s &= \gamma_k^s \hat{\boldsymbol{w}}_k^s, \\ w_k^{s,\mathsf{DL}} &= \left(\gamma_k^s\right)^{-1}, \end{aligned} \tag{3.23}$$

with $\gamma_k \in \mathbb{R}_+$ and recalling that the UL precoder was set such that $b_k^{v,\mathsf{UL}} = 1$. We then set the user and sub-carrier-wise sum-MSE equal between the UL and DL system, i.e. we set the individual MSE expressions per user and per sub-carrier equal such that

$$\epsilon_k^{v,\mathsf{DL}} \stackrel{!}{=} \epsilon_k^{v,\mathsf{UL}}. \tag{3.24}$$

We end up with a system of linear equations for the $U \cdot M_{\mathsf{u}}$ scaling factors γ_k^s per user and per sub-carrier

$$\underbrace{\begin{bmatrix} \boldsymbol{A}^{1,1} & \boldsymbol{A}^{1,2} & \cdots & \boldsymbol{A}^{1,U} \\ \boldsymbol{A}^{2,1} & \boldsymbol{A}^{2,2} & \cdots & \boldsymbol{A}^{2,U} \\ \vdots & \vdots & \ddots & \vdots \\ \boldsymbol{A}^{U,1} & \boldsymbol{A}^{U,2} & \cdots & \boldsymbol{A}^{U,U} \end{bmatrix}}_{\boldsymbol{A}^{sk}} \begin{bmatrix} \boldsymbol{\gamma}^1 \\ \boldsymbol{\gamma}^2 \\ \vdots \\ \boldsymbol{\gamma}^U \end{bmatrix} = \sigma_\eta^2 \|\boldsymbol{h}_{\mathsf{p}}\|_2^2 \mathbf{1}_{M_{\mathsf{u}}U}, \tag{3.25}$$

where $\boldsymbol{A}^{v,s} \in \mathbb{R}^{M_{\mathsf{u}} \times M_{\mathsf{u}}}$ and $\boldsymbol{\gamma}^v \in \mathbb{R}_+^{M_{\mathsf{u}}}$. We stack the scaling factors per user and define the following vectors

$$\boldsymbol{\gamma}^v = \left[\left(\gamma_1^v\right)^2, \quad \left(\gamma_2^v\right)^2, \quad \cdots \quad \left(\gamma_{M_{\mathsf{u}}}^v\right)^2 \right]^T. \tag{3.26}$$

We define the matrix tri-diagonal matrices $\boldsymbol{A}^{v,v}$ and $\boldsymbol{A}^{v,s}$ for $s \neq v$ as follows

$$[\boldsymbol{A}^{v,v}]_{k,j} = \begin{cases} \sigma_M^2 \left(\hat{\boldsymbol{w}}_k^{v,T} \hat{\boldsymbol{H}}_k^v \hat{\boldsymbol{e}}_\nu - \hat{\boldsymbol{w}}_k^{v,T} \hat{\boldsymbol{H}}_k^v \hat{\boldsymbol{H}}_k^{v,T} \hat{\boldsymbol{w}}_k^v \right), & \text{if } k = j, \\ -\sigma_M^2 \hat{\boldsymbol{w}}_{k-1}^{v,T} \hat{\boldsymbol{H}}_{k-1}^v \hat{\boldsymbol{H}}_{k-1}^{v,T} \hat{\boldsymbol{w}}_{k-1}^v, & \text{if } j = k-1, \\ -\sigma_M^2 \hat{\boldsymbol{w}}_{k+1}^{v,T} \hat{\boldsymbol{H}}_{k+1}^v \hat{\boldsymbol{H}}_{k+1}^{v,T} \hat{\boldsymbol{w}}_{k+1}^v, & \text{if } j = k+1, \\ 0, & \text{else.} \end{cases} \tag{3.27}$$

$$[\boldsymbol{A}^{v,s}]_{k,j} = \begin{cases} -\sigma_M^2 \hat{\boldsymbol{w}}_k^{s,T} \hat{\boldsymbol{H}}_k^v \hat{\boldsymbol{H}}_k^{v,T} \hat{\boldsymbol{w}}_k^s, & \text{if } k = j, \\ -\sigma_M^2 \hat{\boldsymbol{w}}_{k-1}^{s,T} \hat{\boldsymbol{H}}_{k-1}^v \hat{\boldsymbol{H}}_{k-1}^{v,T} \hat{\boldsymbol{w}}_{k-1}^s, & \text{if } j = k-1, \\ -\sigma_M^2 \hat{\boldsymbol{w}}_{k+1}^{s,T} \hat{\boldsymbol{H}}_{k+1}^v \hat{\boldsymbol{H}}_{k+1}^{v,T} \hat{\boldsymbol{w}}_{k+1}^s, & \text{if } j = k+1, \\ 0 & \text{else.} \end{cases} \tag{3.28}$$

By calculating a weighting factor per user and per sub-carrier, this method of duality transformation guarantees that the individual MSE values stay equal between the UL and the DL system. Therefore by applying this method of duality transformation we cannot spread the transmit power amongst the users or sub-carriers but each user and sub-carrier will be normalized individually.

3.3 Iterative design of MMSE based precoder and real-valued receive spatial filter

The precoder is designed to mitigate the MUI, ISI, and ICI. At each user terminal, only a real-valued single-tap spatial filter is applied. The recovered desired signal $\hat{\alpha}_k^j[m]$ is expressed in a matrix-vector formulation as follows

$$\hat{\alpha}_k^j[m] = \sum_{r=1}^{N_{\mathrm{R}_j}} g_k^{j,r} \cdot \mathrm{Re}\left\{ \left(\sum_{\ell=k-1}^{k+1} \sum_{s=1}^{U} \boldsymbol{x}_\ell^{s\,\mathrm{T}}[n] \cdot \boldsymbol{H}_{\ell,k}^{j,r} \cdot \boldsymbol{b}_\ell^s + \hat{\eta}_k^{j,r}[n] \right) \right\}, \tag{3.29}$$

where

$$\boldsymbol{b}_\ell^s = \left[\begin{array}{cccc} \boldsymbol{b}_\ell^{1,s^{\mathrm{T}}} & \boldsymbol{b}_\ell^{2,s^{\mathrm{T}}} & \cdots & \boldsymbol{b}_\ell^{N_{\mathrm{T}},s^{\mathrm{T}}} \end{array} \right]^{\mathrm{T}} \in \mathbb{C}^{N_{\mathrm{T}} \cdot B} \tag{3.30}$$

contains the N_{T} coefficients of the precoding filter for the sth user on the ℓth subcarrier, and

$$\boldsymbol{H}_{\ell,k}^{j,r} = \left[\begin{array}{cccc} \boldsymbol{H}_{\ell,k}^{1,j,r} & \boldsymbol{H}_{\ell,k}^{2,j,r} & \cdots & \boldsymbol{H}_{\ell,k}^{N_{\mathrm{T}},j,r} \end{array} \right] \in \mathbb{C}^{(B+Q-1)\times N_{\mathrm{T}} \cdot B} \tag{3.31}$$

with $\boldsymbol{H}_{\ell,k}^{i,j,r} \in \mathbb{C}^{(B+Q-1)\times B}$, $i = 1, 2, \ldots, N_{\mathrm{T}}$, representing a Toeplitz matrix of the equivalent channel coefficients $h_{\ell,k}^{i,j,r}[n]$. The data vector $\boldsymbol{x}_\ell^s[n] \in \mathbb{C}^{B+Q-1}$ contains consecutive data symbols, whereas $g_k^{j,r}$ denotes the real-valued coefficient of the spatial filter for the signal on the kth subcarrier received by the rth receive antenna of the jth user. In case of $\hat{\beta}_k^j[m]$, it is obtained by taking the imaginary part of (3.4). Since both cases are equivalent to each other, we focus on the case of $\hat{\alpha}_k^j[m]$ in the sequel.

In this iterative design, the precoders and the spatial filters are updated alternately. First given the spatial filter, the expression of the estimated desired signal of the jth user on the kth subcarrier can be written as

$$\hat{\alpha}_k^j[m] = \mathrm{Re}\left\{ \sum_{\ell=k-1}^{k+1} \sum_{s=1}^{U} \boldsymbol{x}_\ell^{s^{\mathrm{T}}}[n] \cdot \breve{\boldsymbol{H}}_{\ell,k}^j \cdot \boldsymbol{b}_\ell^s + \sum_{r=1}^{N_{\mathrm{R}_j}} g_k^{j,r} \cdot \hat{\eta}_k^{j,r}[n] \right\}, \tag{3.32}$$

where $\breve{\boldsymbol{H}}_{\ell,k}^j = \sum_{r=1}^{N_{\mathrm{R}_j}} g_k^{j,r} \cdot \boldsymbol{H}_{\ell,k}^{j,r}$ is a short-hand notation. The precoder for the jth user on the kth subcarrier that minimizes the mean square error and the leakage can be obtained via the following optimization problem [29]

$$\boldsymbol{b}_k^j = \arg\min_{\boldsymbol{b}_k^j} \mathrm{E}\left\{ \left| \hat{\alpha}_k^j[m] - \alpha_k^j[m-\nu] \right|^2 + c_k^j + u_k^j \right\}, \tag{3.33}$$

where $\nu = \left\lceil \frac{B+Q-1}{2} \right\rceil$ is the (integer) delay of the system. The terms c_k^j and u_k^j measure the interference caused by the signal for the jth user on the kth subcarrier to the adjacent subcarriers and the other users. They take the following forms

$$c_k^j = \sum_{r=1}^{N_{\mathrm{R}_j}} \sum_{\ell=k-1,\ell\neq k}^{k+1} \left| \mathrm{Im}\left\{ \boldsymbol{x}_k^{j^{\mathrm{T}}}[n] \cdot \boldsymbol{H}_{\ell,k}^{j,r} \cdot \boldsymbol{b}_k^j \right\} \right|^2 \tag{3.34}$$

$$\begin{aligned} u_k^j = \sum_{s=1,s\neq j}^{U} \sum_{r=1}^{N_{\mathrm{R}_s}} \Bigg(& \sum_{\ell=k-1,\ell\neq k}^{k+1} \left| \mathrm{Im}\left\{ \boldsymbol{x}_k^{j^{\mathrm{T}}}[n] \cdot \boldsymbol{H}_{\ell,k}^{s,r} \cdot \boldsymbol{b}_k^j \right\} \right|^2 \\ & + \left| \mathrm{Re}\left\{ \boldsymbol{x}_k^{j^{\mathrm{T}}}[n] \cdot \boldsymbol{H}_{k,k}^{s,r} \cdot \boldsymbol{b}_k^j \right\} \right|^2 \Bigg). \end{aligned} \tag{3.35}$$

Let us define $\widetilde{\boldsymbol{x}}_k^j \in \mathbb{R}^{B+Q-1}$ such that

$$\boldsymbol{x}_k^j = \boldsymbol{J}_k \cdot \widetilde{\boldsymbol{x}}_k^j, \tag{3.36}$$

where the diagonal matrix $\boldsymbol{J}_k \in \mathbb{C}^{(B+Q-1)\times(B+Q-1)}$ has "1" and "$\jmath$" alternately appearing on its diagonal. Similarly as in [29], the following linear expressions for the real part and the imaginary part of the interference terms in (3.34) and (3.35) can be obtained

$$\mathrm{Re}\left\{ \boldsymbol{x}_k^{j^{\mathrm{T}}}[n] \cdot \boldsymbol{H}_{k,k}^{s,r} \cdot \boldsymbol{b}_k^j \right\} = \widetilde{\boldsymbol{x}}_k^{j^{\mathrm{T}}} \cdot \boldsymbol{\Psi}_{k,k}^{s,r} \cdot \boldsymbol{\xi}_k^j \tag{3.37}$$

$$\mathrm{Im}\left\{ \boldsymbol{x}_k^{j^{\mathrm{T}}}[n] \cdot \boldsymbol{H}_{\ell,k}^{s,r} \cdot \boldsymbol{b}_k^j \right\} = \widetilde{\boldsymbol{x}}_k^{j^{\mathrm{T}}} \cdot \boldsymbol{\Phi}_{\ell,k}^{s,r} \cdot \boldsymbol{\xi}_k^j \tag{3.38}$$

where

$$\boldsymbol{\Psi}_{k,k}^{s,r} = \left[\begin{array}{cc} \mathrm{Re}\left\{\boldsymbol{J}_k \cdot \boldsymbol{H}_{k,k}^{s,r}\right\} & -\mathrm{Im}\left\{\boldsymbol{J}_k \cdot \boldsymbol{H}_{k,k}^{s,r}\right\} \end{array} \right] \tag{3.39}$$

$$\boldsymbol{\Phi}_{\ell,k}^{s,r} = \left[\begin{array}{cc} \mathrm{Im}\left\{\boldsymbol{J}_k \cdot \boldsymbol{H}_{\ell,k}^{s,r}\right\} & \mathrm{Re}\left\{\boldsymbol{J}_k \cdot \boldsymbol{H}_{\ell,k}^{s,r}\right\} \end{array} \right] \tag{3.40}$$

$$\boldsymbol{\xi}_k^j = \left[\begin{array}{c} \mathrm{Re}\left\{\boldsymbol{b}_k^j\right\} \\ \mathrm{Im}\left\{\boldsymbol{b}_k^j\right\} \end{array} \right]. \tag{3.41}$$

The linear formulation for the operation of taking the real part in (3.32) can be similarly obtained via defining

$$\breve{\boldsymbol{\Psi}}_{\ell,k}^j = \left[\begin{array}{cc} \mathrm{Re}\left\{\boldsymbol{J}_k \cdot \breve{\boldsymbol{H}}_{\ell,k}^j\right\} & -\mathrm{Im}\left\{\boldsymbol{J}_k \cdot \breve{\boldsymbol{H}}_{\ell,k}^j\right\} \end{array} \right]. \tag{3.42}$$

Assume that data symbols are uncorrelated, and the desired signal and the noise are uncorrelated. After inserting (3.32), (3.34), and (3.35) into the optimization problem defined via (3.33), it can be further reformulated using (3.37) – (3.42). Then, taking the derivative with respect to $\boldsymbol{\xi}_k^j$ and setting it to zero yield

$$\begin{aligned} \boldsymbol{\xi}_k^j = & \left(\breve{\boldsymbol{\Psi}}_{k,k}^{j^{\mathrm{T}}} \cdot \breve{\boldsymbol{\Psi}}_{k,k}^j + \sum_{s=1}^{U} \sum_{r=1}^{N_{\mathrm{R}_s}} \sum_{\ell=k-1, \ell \neq k}^{k+1} \boldsymbol{\Phi}_{\ell,k}^{s,r^{\mathrm{T}}} \cdot \boldsymbol{\Phi}_{\ell,k}^{s,r} \right. \\ & \left. + \sum_{s=1, s \neq j}^{U} \sum_{r=1}^{N_{\mathrm{R}_s}} \boldsymbol{\Psi}_{k,k}^{s,r^{\mathrm{T}}} \cdot \boldsymbol{\Psi}_{k,k}^{s,r} \right)^{-1} \cdot \breve{\boldsymbol{\Psi}}_{k,k}^{j^{\mathrm{T}}} \cdot \boldsymbol{e}_\nu, \end{aligned} \tag{3.43}$$

where $\boldsymbol{e}_\nu \in \mathbb{C}^{B+Q-1}$ is a unit vector with its νth element as one. To solve the problem that the matrix might be ill-conditioned, we add $\alpha \cdot \boldsymbol{I}_{2 \cdot N_{\mathrm{T}} \cdot B}$ in the matrix inversion involved in (3.43) with $\alpha > 0$ as a regularization factor.

After computing the precoders, we turn to update the spatial filters assuming that the MUI, ISI, and ICI have been canceled completely, i.e., $\hat{\alpha}_k^j[m]$ takes the following form in the noiseless case

$$\hat{\alpha}_k^j[m] = \mathrm{Re}\left\{ \boldsymbol{x}_k^{j^{\mathrm{T}}}[n] \cdot \sum_{r=1}^{N_{\mathrm{R}_j}} g_k^{j,r} \cdot \boldsymbol{H}_{k,k}^{j,r} \cdot \boldsymbol{b}_k^j \right\}. \tag{3.44}$$

Define a vector $\boldsymbol{g}_k^j \in \mathbb{R}^{N_{\mathrm{R}_j}}$ that contains the N_{R_j} coefficients of the spatial filter of the jth user on the kth subcarrier, i.e.,

$$\boldsymbol{g}_k^j = \left[\begin{array}{ccccc} g_k^{j,1} & g_k^{j,2} & \cdots & g_k^{j,N_{\mathrm{R}_j}} \end{array} \right]^{\mathrm{T}}. \tag{3.45}$$

The maximal-ratio combining (MRC) is used as the criterion for the spatial filter. Therefore, $\boldsymbol{g}_k^j$ can be obtained as

$$\boldsymbol{g}_k^j = \check{\boldsymbol{h}}_{k,k}^j, \tag{3.46}$$

where the rth element of $\check{\boldsymbol{h}}_{k,k}^j$, $r = 1, 2, \ldots, N_{\mathrm{R}_j}$, is given by

$$\check{\boldsymbol{h}}_{k,k}^{j,r} = \mathrm{Re}\left\{ \boldsymbol{e}_\nu^{\mathrm{T}} \cdot \boldsymbol{H}_{k,k}^{j,r} \cdot \boldsymbol{b}_k^j \right\}. \tag{3.47}$$

In this proposed iterative scheme, $\boldsymbol{g}_k^s$ $(s = 1, 2, \ldots, U)$ that contains the N_{R_s} real-valued coefficients of the receive spatial filter of the sth user on the kth subcarrier is initialized randomly. To determine the termination of the iterative procedure, we propose to use the following stopping criterion. The term $\Delta(\boldsymbol{g})$ that tracks the change of the receive spatial filters is defined as

$$\Delta(\boldsymbol{g}) = \sum_{s=1}^{U} \left| \boldsymbol{g}_k^{s^{(p)}} - \boldsymbol{g}_k^{s^{(p-1)}} \right|^2, \tag{3.48}$$

where $\boldsymbol{g}_k^{s^{(p)}}$ and $\boldsymbol{g}_k^{s^{(p-1)}} \in \mathbb{R}^{N_{\mathrm{R}s}}$ contain the coefficients of the receive spatial filter of the sth user computed in the pth iteration and the $(p-1)$th iteration, respectively. A threshold denoted by ϵ is set to 10^{-5} in the simulations. At the end of each iteration, $\Delta(\boldsymbol{g})$ is calculated and compared to ϵ. If $\Delta(\boldsymbol{g}) < \epsilon$, the algorithm terminates, and the precoders are obtained. Otherwise, the iterative procedure continues, and the precoders as well as the receive filters are further updated.

3.4 Signal-to-leakage (SLR) based precoder and real-valued receive spatial filter

Similar to the iterative design, we again consider a real-valued spatial filter at each user node. Instead of jointly and iteratively updating the precoder and the spatial filter, we propose a closed-form SLR based linear precoder. A MRC based spatial filter is employed at each user node. The effective channel with respect to the rth receive antenna of the jth user for the kth subcarrier is given by

$$\boldsymbol{h}_{k,k}^{(\mathrm{eff}),j,r} = \boldsymbol{\Psi}_{k,k}^{j,r^{\mathrm{T}}} \cdot \boldsymbol{e}_\nu \in \mathbb{R}^{2 \cdot N_{\mathrm{T}} \cdot B}. \tag{3.49}$$

The ISI for the signal of the jth user on the kth subcarrier is measured via

$$\begin{aligned} \mathrm{ISI}_k^j &= \mathrm{E}\left\{ \sum_{r=1}^{N_{\mathrm{R}_j}} \left| \widetilde{\boldsymbol{x}}_k^{j^{\mathrm{T}}} \cdot \boldsymbol{\Psi}_{k,k}^{(\mathrm{int}),j,r} \cdot \boldsymbol{\xi}_k^j \right|^2 \right\} \\ &= \boldsymbol{\xi}_k^{j^{\mathrm{T}}} \cdot \sum_{r=1}^{N_{\mathrm{R}_j}} \boldsymbol{\Psi}_{k,k}^{(\mathrm{int}),j,r^{\mathrm{T}}} \cdot \boldsymbol{\Psi}_{k,k}^{(\mathrm{int}),j,r} \cdot \boldsymbol{\xi}_k^j, \end{aligned} \tag{3.50}$$

where

$$\boldsymbol{\Psi}_{k,k}^{(\mathrm{int}),j,r} = \boldsymbol{J}_{\mathrm{int}}^{(\nu)} \cdot \boldsymbol{\Psi}_{k,k}^{j,r} \in \mathbb{R}^{(B+Q-1) \times 2 \cdot N_{\mathrm{T}} \cdot B}. \tag{3.51}$$

Here $\boldsymbol{J}_{\mathrm{int}}^{(\nu)} \in \mathbb{R}^{(B+Q-1) \times (B+Q-1)}$ is constructed by replacing the νth row of a $(B+Q-1)$-by-$(B+Q-1)$ identity matrix by an all-zeros vector. The interference that is leaked to the adjacent subcarriers and other users by the signal for the jth user on the kth subcarrier can be represented as $\mathrm{E}\left\{c_k^j + u_k^j\right\}$, where c_k^j and u_k^j are given by (3.34) and (3.35), respectively. Consequently, the SLR on the kth subcarrier for the jth user denoted by SLR_k^j has the form given in (3.52). The precoder for the jth user on the kth subcarrier can be obtained via

$$\boldsymbol{\xi}_k^j = \underset{\boldsymbol{\xi}_k^j}{\arg\max}\ \mathrm{SLR}_k^j. \tag{3.53}$$

$$\mathrm{SLR}_k^j = \frac{\boldsymbol{\xi}_k^{j^{\mathrm{T}}} \cdot \overbrace{\sum_{r=1}^{N_{\mathrm{R}_j}} \boldsymbol{h}_{k,k}^{(\mathrm{eff}),j,r} \cdot \boldsymbol{h}_{k,k}^{(\mathrm{eff}),j,r^{\mathrm{T}}}}^{\boldsymbol{A}} \cdot \boldsymbol{\xi}_k^j}{\boldsymbol{\xi}_k^{j^{\mathrm{T}}} \cdot \underbrace{\left(\sum_{s=1}^{U} \sum_{r=1}^{N_{\mathrm{R}_s}} \sum_{\ell=k-1,\ell\neq k}^{k+1} \boldsymbol{\Phi}_{\ell,k}^{s,r^{\mathrm{T}}} \cdot \boldsymbol{\Phi}_{\ell,k}^{s,r} + \sum_{s=1,s\neq j}^{U} \sum_{r=1}^{N_{\mathrm{R}_s}} \boldsymbol{\Psi}_{k,k}^{s,r^{\mathrm{T}}} \cdot \boldsymbol{\Psi}_{k,k}^{s,r} + \sum_{r=1}^{N_{\mathrm{R}_j}} \boldsymbol{\Psi}_{k,k}^{(\mathrm{int}),j,r^{\mathrm{T}}} \cdot \boldsymbol{\Psi}_{k,k}^{(\mathrm{int}),j,r} \right)}_{\boldsymbol{C}} \cdot \boldsymbol{\xi}_k^j} \tag{3.52}$$

The solution is given by

$$\boldsymbol{\xi}_k^j = \mathcal{P}\left\{ \boldsymbol{C}^{-1} \cdot \boldsymbol{A} \right\}, \tag{3.54}$$

where $\mathcal{P}\{\cdot\}$ represents the operator of computing the principal eigenvector of a matrix which corresponds to the maximal eigenvalue. Similarly as for the iterative design, we introduce a regularization factor α in the matrix inversion involved in (3.54). Note that the extension of this SLR based scheme to the case of multiple spatial streams per user can be conveniently conducted based on a similar philosophy introduced in [33].

As the MUI, ISI and ICI are mitigated by the SLR based precoders at the base station, each user terminal then applies the MRC based spatial filter given by (3.46) and (3.47).

3.5 Simulation results

3.5.1 FBMC/OQAM based multi-user MISO downlink

In this Section we will discuss the simulation results of all four MSE-duality transformation taking the MMSE-based precoder design from [29] as a reference. For the MU-MISO FBMC system we used channel realizations from the *Wireless World Initiative New Radio* (WINNER II) project which is an extension to the *Spacial Channel Model* (SCM) [34] developed by *3rd Generation Partnership Project* (3GPP) . Using WINNER II in MATLAB, we had an array of libraries to generate both different layouts and channels, dependent on the sampling rate, f_s, the number of transmit antennas, N_{t}, and the total number of users, U.

Throughout our simulations we transmitted data across $M_{\mathsf{u}} = 210$ of the available $M = 256$ sub-carriers per user and per transmit antenna. We used a sampling rate of $f_s = 11.2$MHz. We used randomly generated 16-QAM symbols and took a block length of 1000 symbols per sub-carrier. We had a channel impulse response of $L_{\mathsf{ch}} = 124$ taps. Throughout the simulations we will take the quantity of E_b/N_0 being a near-signal-to-noise ratio per user and antenna for MU-MISO simulations and we took the *Bit Error Rate* (BER) and *Mean Square Error* (MSE) as an average over all users. We took an average over 200 randomly generated channel realizations to remove the dependency on the individual ones.

We will investigated a system with a precoder vector of length $B = 5$ taps. We set $N_{\mathsf{t}} = 4$, whilst varying the number of users $U \in \{1, 2, 3, 4\}$ in the system. For the following MSE plots we will use a solid line to represent the measured MSE and a dotted line to represent the analytical MSE from our formulas. We have added the analytical MSE for the UL system to show that after all the duality transformations the MSE has in fact stayed unchanged.

In Figure 3-7 we see the results of the MSE-duality versus the precoder-[29] design with two methods of transmit power normalization for $U = 1, 2$. The precoder-[29] design with a solid

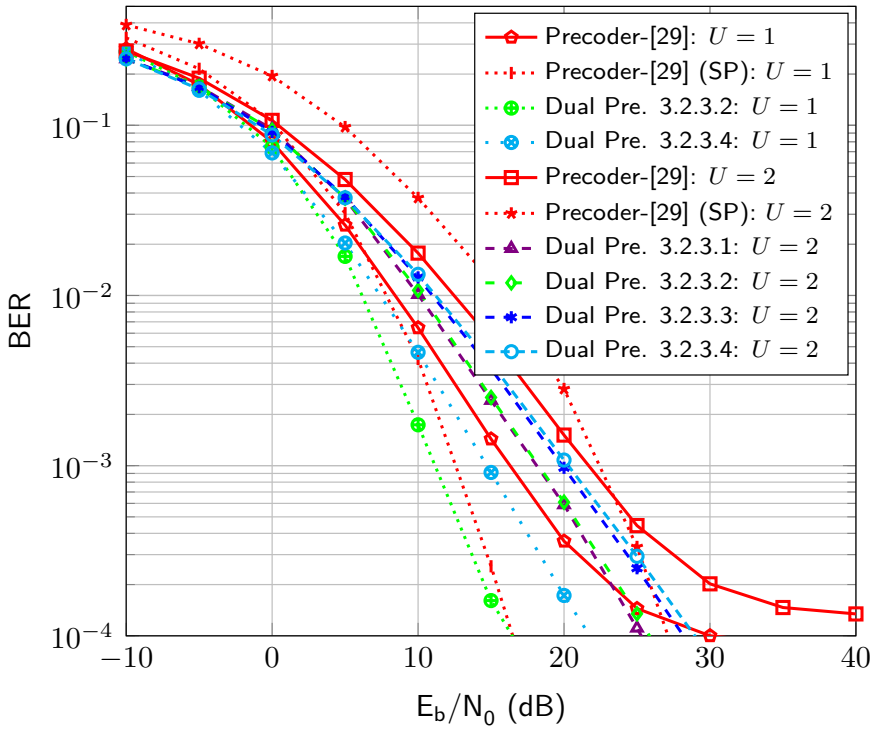

Figure 3-7: BER of the Precoder-[29] and the four Dual Precoder designs for $N_t = 4$ and varying $U = 1$ and $U = 2$

line used a user and sub-carrier wise normalization and the dotted plot with a *Sum-Power* (SP) normalization of the transmit power. Both the precoder-[29] design and all the dual precoder design benefit from the diversity gain or antenna gain. Furthermore, it should be noted that for $U = 1$ the dual precoder 3.2.3.1 is equivalent to the dual precoder 3.2.3.2 and the dual precoder 3.2.3.3 is equivalent to the dual precoder 3.2.3.4 since we are summing over one user, therefore only one of each was plotted. In general, the dual precoders outperform the precoder-[29] design throughout most of the E_b/N_0 regime. The systems where we used the 3.2.3.1 and the 3.2.3.2 transformation showed the most extreme performance improvements. This is due to the fact that these methods will use an inverse water filling technique to divide the most transmit power to those sub-carriers with the worst channels. A similar behaviour is observed in the precoder-[29] (SP) design where we spread the transmit power over all users and sub-carriers. As we increase the number of users in the system we observe a clear degradation of performance which is observed in the gradient of the plots. Nevertheless, the dual precoders outperform the precoder-[29] design with user and sub-carrier transmit power normalization. The precoder-[29] (SP) design showed improvements in higher E_b/N_0 values.

After we increase the number of users to $U = 3, 4$ in Figure 3-8 we observe further degradation in the system performance as well as a smaller difference between the different dual precoders. The dual precoders outperformed the precoder-[29] design for most system assemblies and over most E_b/N_0 values. This is probably due to the fact that the precoder-[29] design suffers from extra ICI since the precoders have only minimized the *near*-MSE and this method of precoder calculation does not take the noise covariance matrix into account. However, when we normalize the SP of the precoder-[29] design we notice improved BER for high E_b/N_0 values. When the system is at full capacity in Figure 3-8, i.e. when $N_t = U = 4$, the different dual transformations show little difference in terms of BER performance. However, for this system assembly the precoder-[29] design with both forms of normalization showed improved BER for

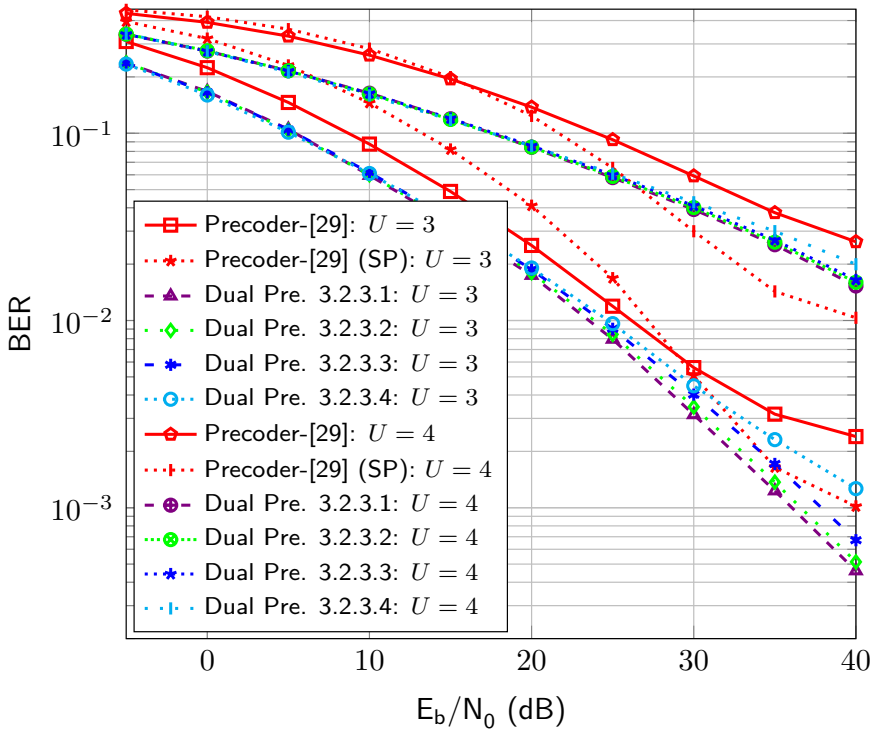

Figure 3-8: BER of the Precoder-[29] and the four Dual Precoder designs for $N_t = 4$ and varying $U = 3$ and $U = 4$

high E_b/N_0 values.

Now we will discuss the MSE simulation results in Figure 3-9 and 3-10. The MSE plots show again that the precoder-[29] design does not saturate for low E_b/N_0 values, unlike the dual precoders. This is due to the fact that the precoder-[29] method does not take the noise into its calculations and will therefore not saturate for any value of E_b/N_0. We also observe that the more users in the system, the greater the difference in MSE values between the dual precoders and the precoder-[29] design. Furthermore, it should be observed in Figure 3-9 and 3-10 that both the analytical and simulated MSE results stay equal between the UL and DL systems for all duality transformations.

It should be noted that during the calculation of the equalizing vectors in the SIMO system and the scaling factors for the 3.2.3.4 duality transformation, we observed ill-conditioned matrices. Due to the ill-conditioned matrices we heuristically investigated a threshold for the Moore-Penrose pseudo-inverse and the ideal parameter for a regularization matrix. Due to sub-optimal parameters, we observed a slight inconsistency in the MSE results for the 3.2.3.4 duality transformation.

3.5.2 FBMC/OQAM based multi-user MIMO downlink

In this section, we evaluate the performance of the proposed transmitter and receiver designs in various multi-user MIMO downlink settings. The total number of subcarriers is 128, whereas the number of subcarriers with data symbols is 72. The subcarrier spacing is set to 15 kHz, and the bandwidth is 1.4 MHz. The data symbols are drawn from the 16 QAM constellation. We employ the WINNER Phase II spatial channel model based on the 3GPP as in [29]. The maximum channel impulse response length is approximately $L_{\text{ch}} = 22$ samples. For all examples, 1000 channel realizations have been performed with 1000 symbols per subcarrier, and a single

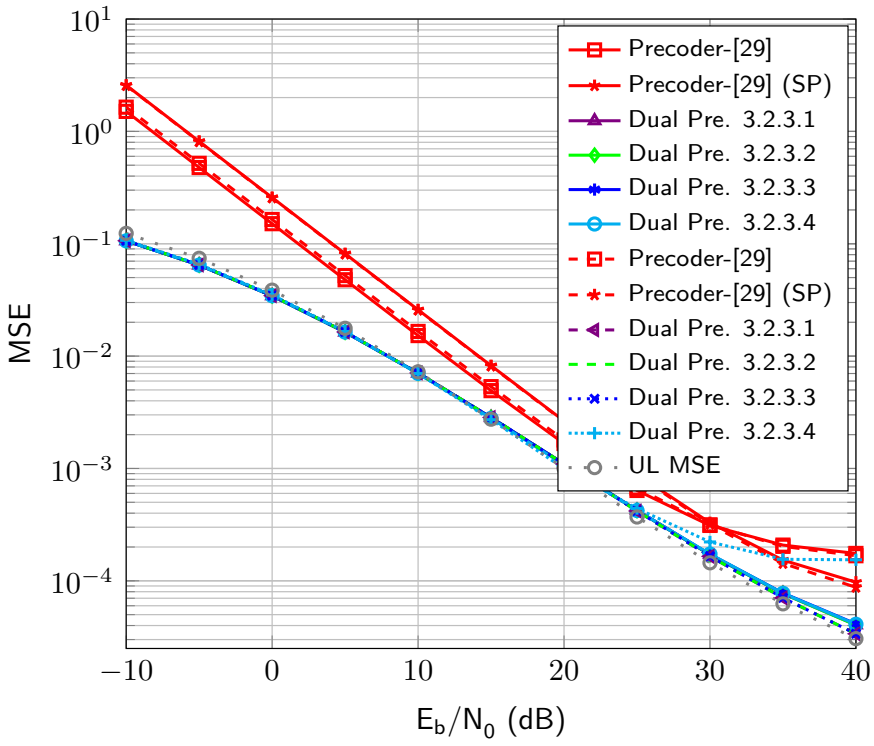

Figure 3-9: Analytical (Dotted) and Simulated (Solid) MSE of the Precoder-[29] and the four Dual Precoder designs for $N_{\mathrm{t}} = 4$ and $U = 2$

spatial stream is sent to each user.

Fig. 3-11 depicts the BER performances of the MMSE based iterative design and the closed-form SLR based design. The former slightly outperforms the latter with the price of a higher computational complexity due to the iterative procedure. Still, the average number of iterations required for convergence is only around three. Moreover, it is observed that as the number of transmit antennas increases, the BER performance is better. A larger number of transmit antennas leads to greater spatial degrees of freedom for the users that are simultaneously served in such SDMA settings. Consequently, the MUI caused by each users to the other users is more effectively mitigated. The resulting inter-carrier interference is smaller, too. On the other hand, even with only a single tap, i.e., $B = 1$, the performance superiority of the both proposed schemes over the BD based technique [18] is significant.

In addition, the CCDF of the number of iterations required for convergence is illustrated at the top of Fig. 3-12, while the CCDF of the final value (recorded as the algorithm terminates) of the term $\Delta(\boldsymbol{g})$ is shown at the bottom of Fig. 3-12. Here we consider a two-user scenario, and each user is equipped with two receive antennas, i.e., $U = 2$, and $N_{\mathrm{R}_1} = N_{\mathrm{R}_2} = 2$. The number of transmit antennas at the base station $N_{\mathrm{T}} = 8$, 6, or 4. The length of the precoder B is set to 5, whereas the matrix inversion regularization factor is chosen as 0.01. It can be seen that the algorithm converges within five iterations at a probability of around 90% regardless of the number of transmit antennas considered in this example. It is also worth noting that the number of iterations required for convergence is barely affected by the length of the precoders or the MIMO settings.

Via Fig. 3-13, the impact of the number of taps and the choice of the regularization factor is investigated. Longer precoders contribute to a superior capability in mitigating the MUI, ICI, and ISI. Hence, the BER performance of the proposed iterative approach becomes better, as

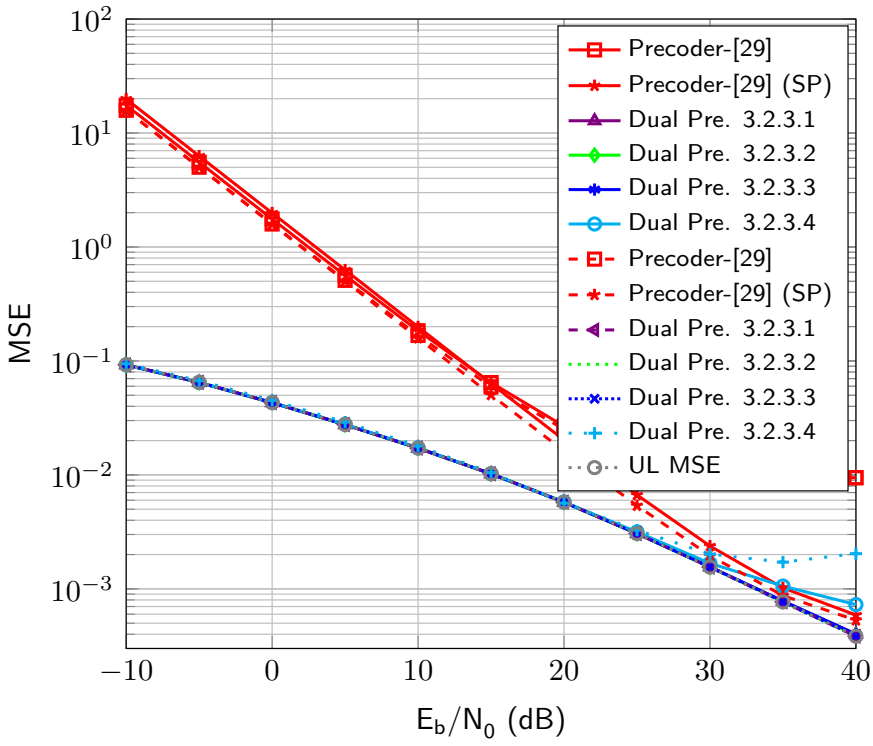

Figure 3-10: Analytical (Dotted) and Simulated (Solid) MSE of the Precoder-[29] and the four Dual Precoder designs for $N_{\mathrm{t}} = 4$ and $U = 3$

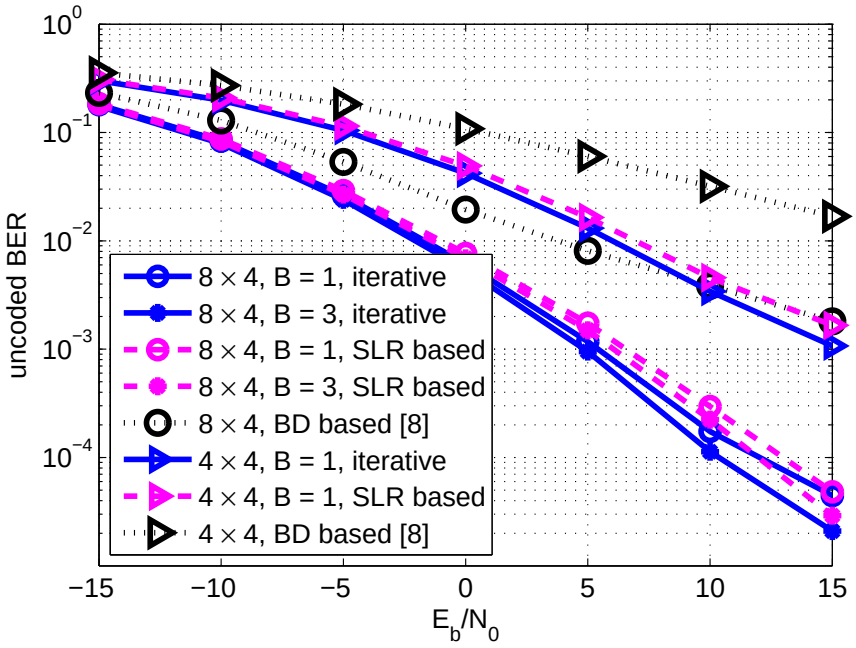

Figure 3-11: BER performance in different multi-user MIMO downlink settings where $U = 2$, $N_{\mathrm{R}_1} = N_{\mathrm{R}_2} = 2$, $N_{\mathrm{T}} = 8$, or 4, and $\alpha = 0.025$

the length of the precoding filters increases. Nevertheless, by increasing the length from five

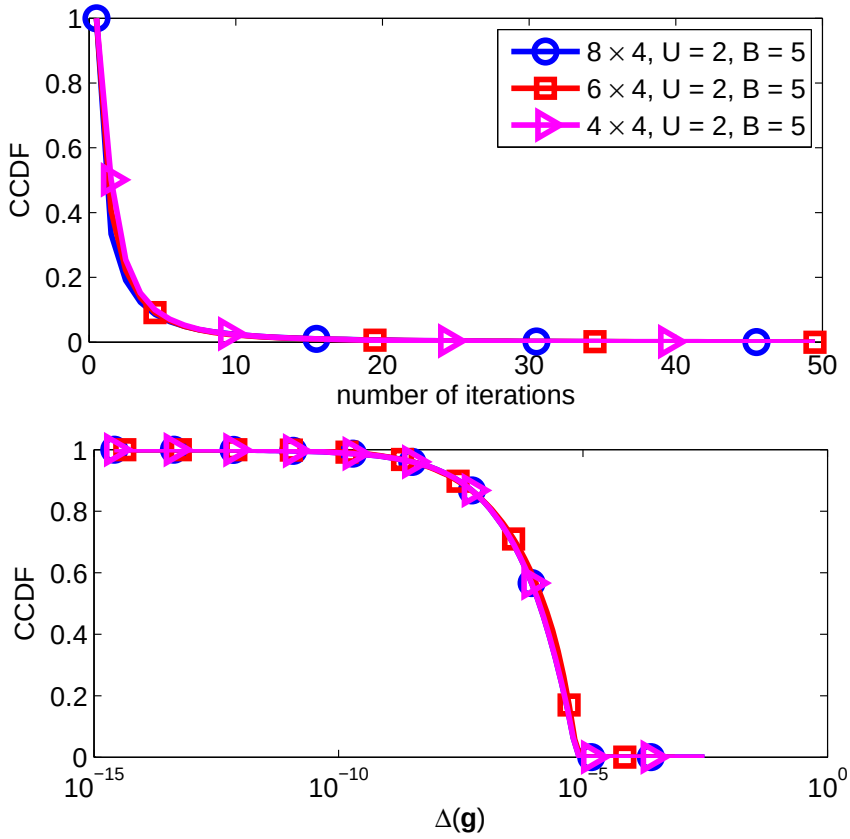

Figure 3-12: CCDF of the number of iterations and the final value of $\Delta(\boldsymbol{g})$ in different multi-user MIMO downlink settings where $U = 2$, $N_{\mathrm{R}_1} = N_{\mathrm{R}_2} = 2$, $N_{\mathrm{T}} = 8$, 6, or 4, $B = 5$, and $\alpha = 0.01$

to nine, the performance improvement is already very small. In addition, it is observed that a larger value for the matrix inversion regularization factor leads to a better performance in the low signal-to-noise-ratio (SNR) regime, while there is an error floor in the high SNR regime. The reason is that a larger value for the regularization factor results in larger residual ISI and residual leakage due to approximation errors induced by the regularization procedure. Unlike the low SNR regime, in the high SNR regime the residual interference (residual ISI and leakage) dominates instead of the noise. Hence, this observation inspires the design of an SNR-related regularization factor as future work. For all the values of the lengths of the precoders and the choices of the regularization factor considered in this example, the iterative scheme achieves a much better performance compared to the IIM-CBF 1 scheme in [27] and the BD based technique [18].

3.6 Summary

We have proposed a new method to design dual precoders for a MU-MISO FBMC system from the equalizers of a MU-SIMO FBMC system. The techniques investigated were based on the MSE-duality transformation between an UL and a DL system, where we attempt to conserve either the *System-Wide Sum-MSE*, the *User-Wise Sum-MSE*, the *Sub-Carrier-Wise Sum-MSE*

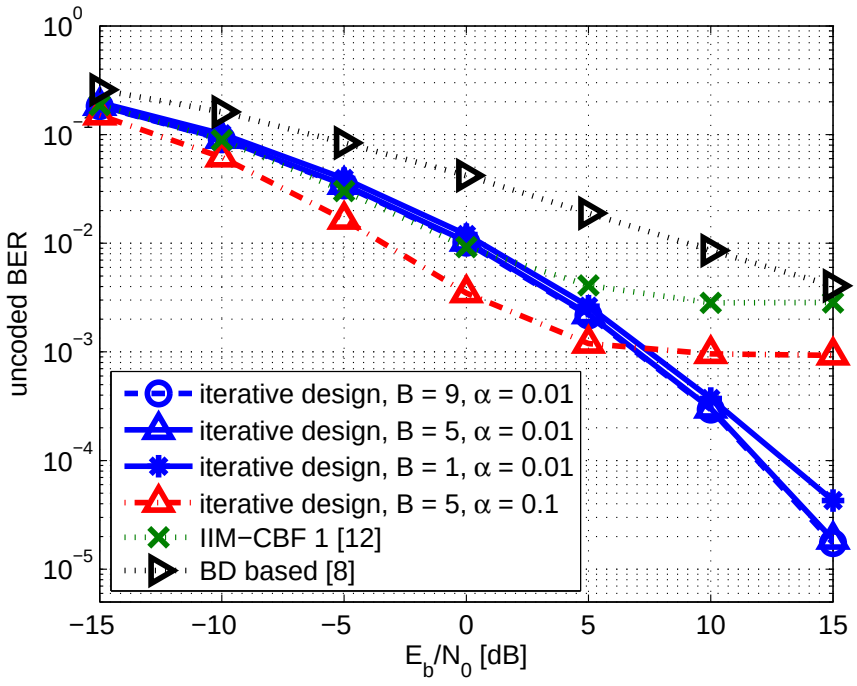

Figure 3-13: BER performance in a multi-user MIMO downlink setting where $U = 2$, $N_{\mathrm{R}_1} = N_{\mathrm{R}_2} = 3$, $N_{\mathrm{T}} = 6$

or the *User and Sub-Carrier-Wise MSE*. Throughout our simulations we observed that the *System-Wide Sum-MSE* performed the best over the whole E_b/N_0 regime, which could be explained by its equivalence to an inverse water-filling technique, i.e. giving the worst channels most power to improve their performance. By first designing equalizer filters for the MU-SIMO FBMC system on a per sub-carrier basis to compensate for ISI, ICI and MUI and then applying the MSE-duality transformation, we are able to eliminate the inter-user and inter-sub-carrier dependencies of the precoder filter in the design of MMSE- based precoder filters as seen in [29]. The dual precoders all outperform the original precoder-[29] design in terms of BER and MSE over a wide SNR range. Furthermore, the MSE values of the dual precoder designs all outperform the precoder-[29] design and saturate where the precoder-[29] design does not since it does not take the noise into account during the calculations.

We have proposed two designs of precoders and equalizers for FBMC/OQAM based multi-user MIMO downlink systems. The first one is an iterative approach where the MMSE based precoders and the MRC based receive spatial filters are jointly computed. In the second scheme, we have devised closed-form SLR based precoders for the base station and a similar MRC based receive processing for each user terminal. Both schemes are developed to effectively mitigate the MUI, ISI, and ICI in critical highly frequency selective propagation conditions.

From the numerical results it can be concluded that the first approach provides a slightly better performance compared to the second method, at the cost of a higher complexity due to the joint transceiver design. Moreover, both approaches show a considerable improvement over two state-of-the-art schemes that do not consider the channel frequency selectivity inside each subcarrier.

4. Channel estimation in OFDM/FBMC based distributed MIMO systems

4.1 Introduction

All precoding and beamforming methods presented in previous sections rely on CSI. So it is necessary to investigate how this channel information can be obtained, in particular in the distributed case where full coordination and full synchronization between the base stations (BS) is not necessarily available.

In this Section, we investigate the issue of the channel estimation in a distributed MIMO context. To this end, a preamble-based channel estimation is considered. The important consequence is that, during the channel estimation procedure, CSI is not known yet and synchronization may not be known either. Hence we have to work under the assumption that the precoding is not yet possible during the preamble duration and that the preamble streams to the different users can suffer from multi-stream interference (MSI). Similarly, it is also important to investigate the effect of imperfect synchronization among the various base stations. In order to overcome the issue of this MSI, we propose to use two different subcarriers assignment schemes (SAS) during the preamble phase. It is worth mentioning that each BS is using the entire frequency bandwidth to transmit its useful data signal. At the same time, the utilization of these SAS during the preamble means that the receiver can recover only a part of the channel frequency response (CFR) for each transmitter. In order to reconstruct the entire CFR, we consider two methods exploiting the sparsity of the channel impulse response (CIR). The performances in terms of mean squared error (MSE) of both methods are investigated using both SAS in synchronous and asynchronous contexts.

4.2 System Model

We consider the downlink of a distributed MIMO system having K_t base stations (transmitters) and Q users (receivers), as depicted in Figure 4-1[1]. We assume that each node is equipped with a single transmit/receive antenna. Two multicarrier techniques are considered: the Cyclic Prefix based Orthogonal Frequency Division multiplexing (CP-OFDM) and the Offset-QAM based Filter Bank MultiCarrier scheme (FBMC-OQAM). We assume that the channel is mildly frequency selective and that the number of subcarriers M is sufficiently big so that each subcarrier experiences a flat fading channel. We also assume that the propagation channels are stationary during the downlink frame period. This is the case for time-invariant or slowly varying channels.

Our aim is to study the issue of estimating the distributed MIMO channel when both CP-OFDM and FBMC-OQAM are used. As presented in previous sections, in order to ensure a MSI free transmission, a precoding technique can be applied. However, computing the precoding matrix for the subcarrier of interest requires the knowledge of the Channel State Information (CSI) between each couple BS-user. Since the channel is unknown to both BSs and users, precoding or decoding is not yet possible.

4.3 Subcarrier assignment schemes used in the preamble

In order to ensure a multi-stream interference free channel estimation. We propose the utilization of subcarrier assignment schemes (SAS) ensuring that each subcarrier is assigned to at

[1]For the clarity, only two users are shown.

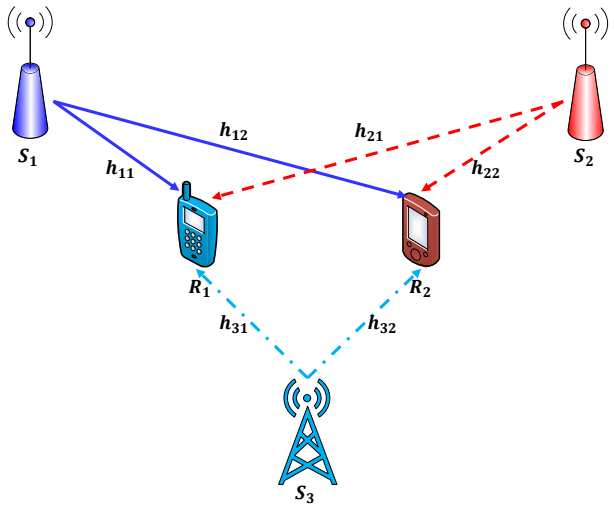

Figure 4-1: OFDM/FBMC distributed MIMO system: K_t BSs (transmitters) and Q users (receivers)

most one base station, during the preamble phase. At the reception, each user computes an estimation of the channel between this user and each BS. After receiving the users feedback by all base stations, a precoding technique can be applied allowing thus the utilization of the entire frequency bandwidth by each BS.
Assuming that the number of subcarriers M is bigger than the number of transmitted streams K_t with $\lfloor \frac{M}{K_t} \rfloor = m$, each user obtains at best m measurements of each channel frequency response (CFR). In order to ensure the recovery of the transmitted information, it is obvious that we need the knowledge of all M points of each CFR. These M points can be computed from the m measurements thanks to the time domain channel response sparsity[2].
Consequently, exploiting the sparsity of each CIR, we are able to reconstruct the required M frequency response points provided that the number of measurements m is bigger than the number of non-zero impulse response coefficients.

We focus here on two subcarriers assignment schemes (SAS) depicted in Figure 4-2, namely, the block SAS and the equispaced SAS:

- Equispaced SAS: In this scheme, the assigned subcarriers to each user are allocated uniformly over the whole bandwidth. In order to avoid inter-BS (multi-stream) interference, δ free subcarriers serve as guard bands between the different pilot subcarriers. The advantage of this scheme is that the pilot subcarriers are well distributed over the whole bandwidth inducing very little correlation between each other. However, one can note that this scheme results in a large number of subcarriers used as guard bands : maximum $\lfloor \frac{M}{(\delta+1)K_t} \rfloor$ subcarrier pilots can be assigned to each BS. The next assignment scheme mitigate this issue by using blocks of subcarriers.

- Block SAS: In this scheme, several blocks of consecutive adjacent subcarriers in the preamble are allocated to each base station. δ free subcarriers adjacent to each block serve as guard bands between the different blocks. The ratio of pilot subcarriers $\lfloor \frac{M}{(\delta+L_{block})K_t} \rfloor$ versus guard band subcarriers is much more favorable in this case compared to the latter. However, this scheme may lead to performance degradation given that the subcarriers are more correlated and give a worse overview of the whole bandwidth.

[2]A $M \times 1$ vector $\mathbf{x}$ is S-sparse, if only $S < M$ elements are non-zero.

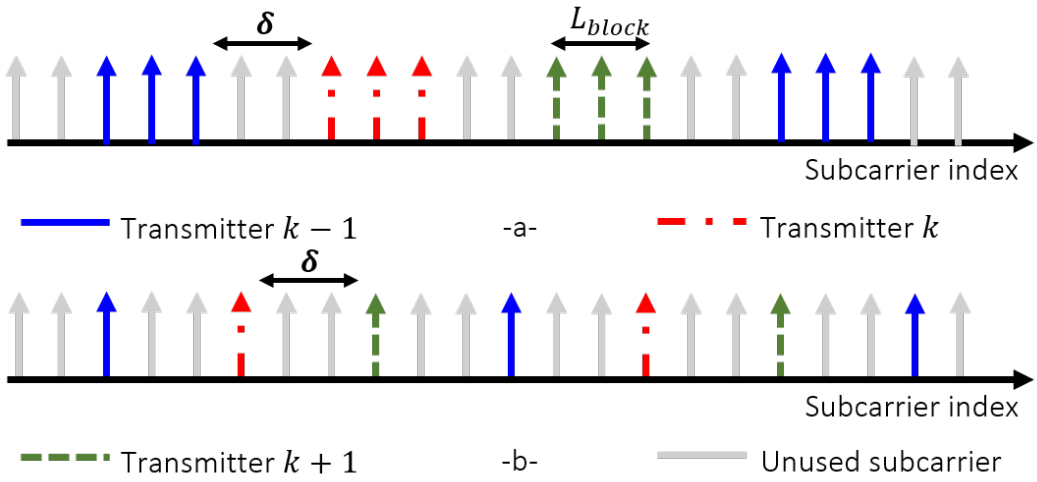

Figure 4-2: Subcarriers assignment schemes: -a- block (block size $L_{block} = 3$ subcarriers), -b- equispaced, (guard band size $\delta = 2$ subcarriers)

In [35], the authors show that for both CP-OFDM and FBMC-OQAM systems, all equispaced preambles with a number of pilots L_p larger or equal than the channel length L_h minimize the MSE of the CFR estimates, subject to a constraint on the total transmitted energy. Indeed, block SAS leads to noise amplification degrading the final CFR MSE. However, it should be noted that the optimization of [35] is conducted in the SISO case only. It does not investigate the synchronization issues that can occur in the present distributed MIMO scenario. Furthermore, it assumes there is always enough pilots to be able to recover the entire CIR $L_p = \lfloor \frac{M}{(\delta+1)K_t} \rfloor \geq L_h$, which is not always true in our MIMO case, especially for a large number of users.
Now let us write the discrete-time signal at the output of a given FBMC-OQAM base station i,

$$s^i[l] = \sum_{n=-\infty}^{+\infty} \sum_{k \in \mathcal{F}_i} d_k^i[n] g_{k,n}[l], \tag{4.1}$$

where, $d_k^i[n]$ are the transmitted real-valued PAM symbols with variance $\sigma_d^2 = 1/2$ representing both in-phase and quadrature phase components of QAM symbols. $\mathcal{F}_i$ stands for the subcarriers assigned to the i-th base station and $g_{k,n}[l]$ is a time/frequency shifted version of the symmetric real-valued prototype filter impulse response g,

$$g_{k,n}[l] = g[l - nM/2] e^{j\frac{2\pi}{M}k\left(l - \frac{L_g - 1}{2}\right)} e^{j\varphi_{k,n}}, \tag{4.2}$$

where the phase $\varphi_{k,n} = \frac{\pi}{2}(k+n) - \pi kn$ is introduced to ensure a phase shift of $\frac{\pi}{2}$ between the adjacent transmitted PAM symbols along time and frequency [8] and $L_g = K \times M$ is the length of g with K being the overlapping factor.
All signals propagate through different multipath channels using a similar propagation model, where the impulse response of the multipath channel between the i-th base station and the q-th user is given by $h^{i,q}[l]$, $l = 0, ..., L_h - 1$. The complex channel path gains $h^{i,q}[l]$ are assumed to be mutually independent: $\mathbb{E}\left[h^{i,q}[l] h^{*i',q'}[l']\right] = \gamma[l]\delta_{l-l'}\delta_{i-i'}\delta_{q-q'}$. We further assume that the power is normalized for each channel such that $\sum_{l=0}^{L_h-1} \gamma[l] = 1$.

The composite signal received at a given user q can be written as follows,

$$y^q[l] = \sum_{i=1}^{K_t} s^i[l] \star h^{i,q}[l] + n^q[l] \tag{4.3}$$

The operator $\star$ stands for the convolution product and $n^q[l]$ is the additive white Gaussian noise (AWGN) at the q-th user with a zero mean and a variance σ_n^2.
Assuming that the CFR is approximately constant at the subcarrier level and constant during the duration of the prototype filter, we can write the demodulated signal of the q_0-th user at the k_0-th subcarrier and n_0-th signaling period as,

$$y_{k_0}^{q_0}[n_0] = H_{k_0}^{i_0,q_0} d_{k_0}^{i_0}[n_0] + j \sum_{i=1}^{K_t} \sum_{\substack{k \in \mathcal{F}_i \\ k \neq k_0}} \sum_{\substack{n \\ n \neq n_0}} H_k^{i,q_0} d_k^i[n] \langle g \rangle_{k,n}^{k_0,n_0} + n_{k_0}^{q_0}[n_0] \tag{4.4}$$

where $\sum_l g_{k,n}[l] g^*_{k_0,n_0}[l] = j \langle g \rangle_{k,n}^{k_0,n_0}$ and $H_{k_0}^{i_0,q_0}$ is the k_0-th component of the CFR between the i_0-th base station and the q_0-th user.

We can further simplify this expression by assuming also that the CFR is approximately constant in the neighborhood Ω_{k_0,n_0} around (k_0, n_0). Moreover, the demodulated signal is free from inter-user interference thanks to the guard-bands. Hence, we can write

$$\begin{aligned} y_{k_0}^{q_0}[n_0] &= H_{k_0}^{i_0,q_0} \left(d_{k_0}^{i_0}[n_0] + j \sum_{(k,n) \in \Omega_{k_0,n_0}} d_k^{i_0}[n] \langle g \rangle_{k,n}^{k_0,n_0} \right) + n_{k_0}^{q_0}[n_0] \\ &= H_{k_0}^{i_0,q_0} c_{k_0}^{i_0}[n_0] + n_{k_0}^{q_0}[n_0] \end{aligned} \tag{4.5}$$

where $c_{k_0}^{i_0}[n_0]$ is referred to as the pseudo-pilot and can be computed based on one of the preamble-based channel estimation method developed in the literature [36]. In the end, we can obtain an estimate of a part of each BS-user CFR,

$$\hat{H}_k^{i,q_0} = \frac{y_k^{q_0}[n_0]}{c_k^i[n_0]} = H_k^{i,q_0} + \frac{n_{k,n_0}^{q_0}}{c_k^i[n_0]} = H_k^{i,q_0} + \eta_k^{i,q_0}[n_0], \quad k \in \mathcal{F}_i, \quad i = 1, ..., K_t \tag{4.6}$$

Similarly to FBMC, the discrete-time signal at the output of a given OFDM base station i,

$$s^i[l] = \sum_{n=-\infty}^{+\infty} \sum_{k \in \mathcal{F}_i} b_k^i[n] f_k[l - n(M + CP)], \tag{4.7}$$

where, M stands for the useful OFDM symbol time and $b_{k_0}^{i_0}[n_0]$ is a complex-valued QAM symbol with a variance $\sigma_b^2 = 1/2$. Moreover, CP is the cyclic prefix duration and $f_k[l]$ is given by,

$$f_k[l] = \frac{1}{\sqrt{M}} \begin{cases} e^{j\frac{2\pi}{M}kl} & l \in [0, M + CP] \\ 0 & \text{elsewhere} \end{cases} \tag{4.8}$$

After CP removal and demodulation, the k_0-th output of the q_0-th user reads,

$$y_{k_0}^{q_0}[n_0] = H_{k_0}^{i_0,q_0} b_{k_0}^{i_0}[n_0] + n_{k_0}^{q_0}[n_0] \tag{4.9}$$

Therefore, an estimate of a part of each BS-user CFR can be obtained as described in (4.6).

Stacking the CFR estimates $\hat{H}_k^{i_0,q_0}$, $\forall k \in \mathcal{F}_{i_0}$ in a vector $\hat{\boldsymbol{H}}_{\boldsymbol{L_p}}$ and the noise samples $\eta_k^{i_0,q_0}[n_0]$, $\forall k \in \mathcal{F}_{i_0}$ in a vector $\boldsymbol{\eta}_{\boldsymbol{L_p}}$, we obtain for the channel between the i_0-th base station and the q_0-th user[3]

$$\hat{\boldsymbol{H}}_{\boldsymbol{L_p}} = \boldsymbol{F}_{\boldsymbol{L_p \times L_h}} \boldsymbol{h} + \boldsymbol{\eta}_{\boldsymbol{L_p}} \tag{4.10}$$

where the $L_h \times 1$ vector $\boldsymbol{h}$ is the true CIR, $\boldsymbol{F}_{\boldsymbol{L_p \times L_h}}$ is the $L_p \times L_h$ sub-matrix of the full $M \times M$ DFT matrix $\boldsymbol{F}$ consisting of its L_h first columns and its rows corresponding to the pilot subcarriers indexes in $\mathcal{F}_k$.

4.4 Channel estimation algorithms

We here describe and compare two methods for reconstructing the entire CFR based on the pilot estimates in (4.10). Furthermore, an analytical comparison of block and equispaced SAS is conducted.

4.4.1 Minimum mean squared error estimator

We use the MMSE criterion to reconstruct the CIR estimate $\hat{\boldsymbol{h}} = \boldsymbol{G}\hat{\boldsymbol{H}}_{\boldsymbol{L_p}}$ of $\boldsymbol{h}$

$$\boldsymbol{G} = arg\min \ \text{tr}\left\{E\left((\boldsymbol{h} - \hat{\boldsymbol{h}})(\boldsymbol{h} - \hat{\boldsymbol{h}})^H\right)\right\} \tag{4.11}$$

which gives by the orthogonality principle

$$\boldsymbol{G} = \boldsymbol{C_h} \boldsymbol{F}^{\boldsymbol{H}}_{\boldsymbol{L_p \times L_h}} \left(\boldsymbol{F}_{\boldsymbol{L_p \times L_h}} \boldsymbol{C_h} \boldsymbol{F}^{\boldsymbol{H}}_{\boldsymbol{L_p \times L_h}} + \boldsymbol{C_\eta}\right)^{-1} \tag{4.12}$$

assuming the channel has a certain power delay profile (PDP) inducing a covariance matrix of the form $E(\boldsymbol{h}\boldsymbol{h}^{\boldsymbol{H}}) = \boldsymbol{C_h}$ and a noise covariance matrix $E(\boldsymbol{\eta}_{\boldsymbol{L_p}}\boldsymbol{\eta}^{\boldsymbol{H}}_{\boldsymbol{L_p}}) = \boldsymbol{C_\eta}$. One can check that the noise covariance matrix is equal to $\boldsymbol{C_\eta} = \frac{\sigma^2}{E_{Pilot}} \boldsymbol{I}_{\boldsymbol{L_p}}$ for CP-OFDM. However, in FBMC-OQAM, this is only true for the equispaced SAS since in the block SAS, the noise samples are correlated with the samples coming from the adjacent subcarriers.

In the case of a uniform PDP $\boldsymbol{C_h} = \frac{1}{L_h} \boldsymbol{I}_{\boldsymbol{L_h}}$, we finally obtain

$$\hat{\boldsymbol{h}} = \boldsymbol{G}\hat{\boldsymbol{H}}_{\boldsymbol{L_p}} = \boldsymbol{F}^{\boldsymbol{H}}_{\boldsymbol{L_p \times L_h}} \left(\boldsymbol{F}_{\boldsymbol{L_p \times L_h}} \boldsymbol{F}^{\boldsymbol{H}}_{\boldsymbol{L_p \times L_h}} + L_h \boldsymbol{C_\eta}\right)^{-1} \hat{\boldsymbol{H}}_{\boldsymbol{L_p}} \tag{4.13}$$

Finally, the CFR at each subcarrier is found by DFT on the estimated CIR as

$$\hat{\boldsymbol{H}} = \boldsymbol{F}_{\boldsymbol{M \times L_h}} \hat{\boldsymbol{h}} = \boldsymbol{F}_{\boldsymbol{M \times L_h}} \boldsymbol{F}^{\boldsymbol{H}}_{\boldsymbol{L_p \times L_h}} \left(\boldsymbol{F}_{\boldsymbol{L_p \times L_h}} \boldsymbol{F}^{\boldsymbol{H}}_{\boldsymbol{L_p \times L_h}} + L_h \boldsymbol{C_\eta}\right)^{-1} \hat{\boldsymbol{H}}_{\boldsymbol{L_p}} \tag{4.14}$$

At low SNR or when the matrix $\boldsymbol{F}_{\boldsymbol{L_p \times L_h}} \boldsymbol{F}^{\boldsymbol{H}}_{\boldsymbol{L_p \times L_h}}$ is ill-conditioned, $\hat{\boldsymbol{h}}$ becomes

$$\hat{\boldsymbol{h}}^{\boldsymbol{low}} = \boldsymbol{F}^{\boldsymbol{H}}_{\boldsymbol{L_p \times L_h}} (L_h \boldsymbol{C_\eta})^{-1} \hat{\boldsymbol{H}}_{\boldsymbol{L_p}} \approx \frac{E_{Pilot}}{L_h \sigma^2} \boldsymbol{F}^{\boldsymbol{H}}_{\boldsymbol{L_p \times L_h}} \hat{\boldsymbol{H}}_{\boldsymbol{L_p}} \tag{4.15}$$

where the last simplification neglects the correlation between noise samples occurring in FBMC-OQAM. This last expression means that it is preferable to perform a direct IDFT on the pilot estimates and thus assuming the channel frequency response at all non pilots subcarriers is zero

[3] From now on, we drop the indexes i_0 and q_0 for the sake of clarity.

rather than performing an additional processing requiring the inversion of an ill-conditioned matrix and thus amplifying the noise.

At high SNR, the ill-conditioning and the noise level do not influence anymore the estimator which becomes nothing else than the pseudo inverse of the DFT matrix $\boldsymbol{F}_{\boldsymbol{L_p}\times\boldsymbol{L_h}}$ giving

$$\begin{aligned}\hat{\boldsymbol{h}}^{high} &= \boldsymbol{F}^{\boldsymbol{H}}_{\boldsymbol{L_p}\times\boldsymbol{L_h}}\left(\boldsymbol{F}_{\boldsymbol{L_p}\times\boldsymbol{L_h}}\boldsymbol{F}^{\boldsymbol{H}}_{\boldsymbol{L_p}\times\boldsymbol{L_h}}\right)^{-1}\hat{\boldsymbol{H}}_{\boldsymbol{L_p}} \\ &= \boldsymbol{h} + (\boldsymbol{F}^{\boldsymbol{H}}_{\boldsymbol{L_p}\times\boldsymbol{L_h}}\boldsymbol{F}_{\boldsymbol{L_p}\times\boldsymbol{L_h}})^{-1}\boldsymbol{F}^{\boldsymbol{H}}_{\boldsymbol{L_p}\times\boldsymbol{L_h}}\boldsymbol{\eta}_{\boldsymbol{L_p}}\end{aligned} \tag{4.16}$$

At very high SNR, this estimator will converge towards the true CFR. Actually, this is only true for CP-OFDM but not for FBMC-OQAM. Indeed, the hypothesis about the channel frequency flatness leading to our system model given by (4.5) is only true for a one tap channel. At high SNR, the noise power becomes smaller than the degradation power induced by the channel selectivity and causes a performance floor.

In the end, the performance of our channel estimation algorithm will directly depend on the SNR level and the conditioning of the matrix $\boldsymbol{F}_{\boldsymbol{L_p}\times\boldsymbol{L_h}}\boldsymbol{F}^{\boldsymbol{H}}_{\boldsymbol{L_p}\times\boldsymbol{L_h}}$.

4.4.2 Iterative channel estimator

We here describe an alternative technique based on the iterative channel estimation described in [37] and [38]. Furthermore, we derive the relation between the steady state of the algorithm and the MMSE estimator at high SNR. The algorithm is given by the following steps:

1. Compute the initial pilot estimates described by (4.10)
$$\hat{\boldsymbol{H}}_{\boldsymbol{L_p}} = \boldsymbol{F}_{\boldsymbol{L_p}\times\boldsymbol{L_h}}\boldsymbol{h} + \boldsymbol{\eta}_{\boldsymbol{L_p}} \tag{4.17}$$
2. Compute the IDFT of the CFR estimate considering all non pilots subcarriers are zeros for the first iteration only. We only compute the L_h first taps assuming that we know the channel length.
3. Compute the DFT of the CIR estimate obtained at previous step to obtain the CFR at each subcarrier.
4. Replace the CFR at pilot positions by their estimated value in step 1. $\hat{\boldsymbol{H}}_{\boldsymbol{L_p}}$.
5. Repeat steps 2. to 4. The final CFR estimate is given by step 3. of last iteration.

The advantage of this algorithm is that it is hardware efficient and was therefore standardized for HIPERLAN/2. Furthermore, it does not require the channel and the noise covariance matrices.

4.4.2.1 Steady state

We here investigate the steady state CIR of the method $\hat{\boldsymbol{h}}^{(\infty)}$ which if reached would not be deviated from afterwards. At the i-th iteration, step 2. is given by

$$\begin{aligned}\hat{\boldsymbol{h}}^{(i)} &= \frac{1}{M}\boldsymbol{F}^{\boldsymbol{H}}_{\boldsymbol{M}\times\boldsymbol{L_h}}\hat{\boldsymbol{H}}^{(\boldsymbol{i-1})} \\ &= \frac{1}{M}\boldsymbol{F}^{\boldsymbol{H}}_{\boldsymbol{L_p}\times\boldsymbol{L_h}}\hat{\boldsymbol{H}}_{\boldsymbol{L_p}} + \frac{1}{M}\boldsymbol{F}^{\boldsymbol{H}}_{\bar{\boldsymbol{L}}_{\boldsymbol{p}}\times\boldsymbol{L_h}}\hat{\boldsymbol{H}}^{(\boldsymbol{i-1})}_{\bar{\boldsymbol{L}}_{\boldsymbol{p}}} \\ &= \frac{1}{M}\boldsymbol{F}^{\boldsymbol{H}}_{\boldsymbol{L_p}\times\boldsymbol{L_h}}\hat{\boldsymbol{H}}_{\boldsymbol{L_p}} + \frac{1}{M}\boldsymbol{F}^{\boldsymbol{H}}_{\bar{\boldsymbol{L}}_{\boldsymbol{p}}\times\boldsymbol{L_h}}\boldsymbol{F}_{\bar{\boldsymbol{L}}_{\boldsymbol{p}}\times\boldsymbol{L_h}}\hat{\boldsymbol{h}}^{(\boldsymbol{i-1})}\end{aligned} \tag{4.18}$$

where $\boldsymbol{F}_{\bar{L_p}\times \boldsymbol{L_h}}$ denotes the $\bar{L_p} \times L_h$ submatrix of the full $M \times M$ DFT matrix $\boldsymbol{F}$ consisting of its L_h first columns and its rows corresponding to the non pilot subcarriers indexes. $\hat{\boldsymbol{H}}_{\boldsymbol{L_p}}$ and $\hat{\boldsymbol{H}}^{(\boldsymbol{i-1})}_{\bar{\boldsymbol{L}}_{\boldsymbol{p}}}$ are the CFR at pilot subcarriers and non pilot subcarriers respectively.

At steady state, we have $\hat{\boldsymbol{h}}^{(i)} = \hat{\boldsymbol{h}}^{(i-1)} = \hat{\boldsymbol{h}}^{(\infty)}$ leading to

$$\begin{aligned}\hat{\boldsymbol{h}}^{(\infty)} &= \frac{1}{M}\boldsymbol{F}^{\boldsymbol{H}}_{\boldsymbol{L_p}\times \boldsymbol{L_h}}\hat{\boldsymbol{H}}_{\boldsymbol{L_p}} + \frac{1}{M}\boldsymbol{F}^{\boldsymbol{H}}_{\bar{\boldsymbol{L}}_{\boldsymbol{p}}\times \boldsymbol{L_h}}\boldsymbol{F}_{\bar{\boldsymbol{L}}_{\boldsymbol{p}}\times \boldsymbol{L_h}}\hat{\boldsymbol{h}}^{(\infty)} \\ &= (\boldsymbol{I}_{\boldsymbol{L_h}} - \frac{1}{M}\boldsymbol{F}^{\boldsymbol{H}}_{\bar{\boldsymbol{L}}_{\boldsymbol{p}}\times \boldsymbol{L_h}}\boldsymbol{F}_{\bar{\boldsymbol{L}}_{\boldsymbol{p}}\times \boldsymbol{L_h}})^{-1}\frac{1}{M}\boldsymbol{F}^{\boldsymbol{H}}_{\boldsymbol{L_p}\times \boldsymbol{L_h}}\hat{\boldsymbol{H}}_{\boldsymbol{L_p}} \\ &= (\boldsymbol{F}^{\boldsymbol{H}}_{\boldsymbol{L_p}\times \boldsymbol{L_h}}\boldsymbol{F}_{\boldsymbol{L_p}\times \boldsymbol{L_h}})^{-1}\boldsymbol{F}^{\boldsymbol{H}}_{\boldsymbol{L_p}\times \boldsymbol{L_h}}\hat{\boldsymbol{H}}_{\boldsymbol{L_p}} \\ &= \boldsymbol{h} + (\boldsymbol{F}^{\boldsymbol{H}}_{\boldsymbol{L_p}\times \boldsymbol{L_h}}\boldsymbol{F}_{\boldsymbol{L_p}\times \boldsymbol{L_h}})^{-1}\boldsymbol{F}^{\boldsymbol{H}}_{\boldsymbol{L_p}\times \boldsymbol{L_h}}\boldsymbol{\eta}_{\boldsymbol{L_p}}\end{aligned} \tag{4.19}$$

This CIR estimate is no different than performing the pseudo inverse of the DFT matrix $\boldsymbol{F}_{\boldsymbol{L_p}\times \boldsymbol{L_h}}$ derived for the MMSE estimator at high SNR in (4.16). At very high SNR, when stable, it will then converge towards the exact CFR. Actually, as for the MMSE estimator, this is only true for CP-OFDM but not for FBMC-OQAM due to the assumption of the CFR flatness at the subcarrier level leading to our system model given by (4.5).

4.4.3 Analytical comparison of equispaced and block SAS

In this section we aim at comparing the equispaced and block SAS. Therefore, we make the assumption that we are at high SNR for the MMSE estimator or that we are at steady state for the iterative estimator. This means that the estimation of the channel is given by the pseudo inverse giving

$$\hat{\boldsymbol{H}} = \boldsymbol{H} + \boldsymbol{F}_{M\times \boldsymbol{L_h}}(\boldsymbol{F}^{\boldsymbol{H}}_{\boldsymbol{L_p}\times \boldsymbol{L_h}}\boldsymbol{F}_{\boldsymbol{L_p}\times \boldsymbol{L_h}})^{-1}\boldsymbol{F}^{\boldsymbol{H}}_{\boldsymbol{L_p}\times \boldsymbol{L_h}}\boldsymbol{\eta}_{\boldsymbol{L_p}} \tag{4.20}$$

Then the remaining MSE can be calculated as

$$\begin{aligned}MSE &= E(||\boldsymbol{H} - \hat{\boldsymbol{H}}||^2) \\ &= tr\left(\boldsymbol{F}_{M\times \boldsymbol{L_h}}(\boldsymbol{F}^{\boldsymbol{H}}_{\boldsymbol{L_p}\times \boldsymbol{L_h}}\boldsymbol{F}_{\boldsymbol{L_p}\times \boldsymbol{L_h}})^{-1}\boldsymbol{F}^{\boldsymbol{H}}_{\boldsymbol{L_p}\times \boldsymbol{L_h}}\boldsymbol{C}_{\boldsymbol{\eta}}\boldsymbol{F}_{\boldsymbol{L_p}\times \boldsymbol{L_h}}(\boldsymbol{F}^{\boldsymbol{H}}_{\boldsymbol{L_p}\times \boldsymbol{L_h}}\boldsymbol{F}_{\boldsymbol{L_p}\times \boldsymbol{L_h}})^{-1}\boldsymbol{F}^{\boldsymbol{H}}_{M\times \boldsymbol{L_h}}\right) \\ &= \frac{\sigma^2 L_p}{E_T}tr\left(\boldsymbol{F}_{M\times \boldsymbol{L_h}}(\boldsymbol{F}^{\boldsymbol{H}}_{\boldsymbol{L_p}\times \boldsymbol{L_h}}\boldsymbol{F}_{\boldsymbol{L_p}\times \boldsymbol{L_h}})^{-1}\boldsymbol{F}^{\boldsymbol{H}}_{M\times \boldsymbol{L_h}}\right)\end{aligned} \tag{4.21}$$

where we supposed a preamble with random equal pilots known by the users leading to $\boldsymbol{C}_{\boldsymbol{\eta}} = \frac{\sigma^2}{E_{Pilot}}\boldsymbol{I}_{\boldsymbol{L_p}} = \frac{\sigma^2 L_p}{E_T}\boldsymbol{I}_{\boldsymbol{L_p}}$[4]. This expression can be further simplified for the equispaced SAS supposing that there is no lack of pilots, $\lfloor \frac{M}{(\delta+1)K_t} \rfloor \geq L_h$ and noting then that $\boldsymbol{F}^{\boldsymbol{H}}_{\boldsymbol{L_p}\times \boldsymbol{L_h}}\boldsymbol{F}_{\boldsymbol{L_p}\times \boldsymbol{L_h}} \approx L_p\boldsymbol{I}_{\boldsymbol{L_h}}$[5].

$$MSE_{Equispaced} = \frac{\sigma^2 M L_h}{E_T} \tag{4.22}$$

One can note that this expression does not depend on the number of pilots L_p. It only depends on the channel length L_h. This means that as the channel length increases, the estimation

[4]We here again neglect the correlation between adjacent noise samples in FBMC-OQAM with block SAS.

[5]The strict equality actually only holds if $(\delta+1)K_t$ divides M. If it does not, it will gives something that is almost but not perfectly diagonal.

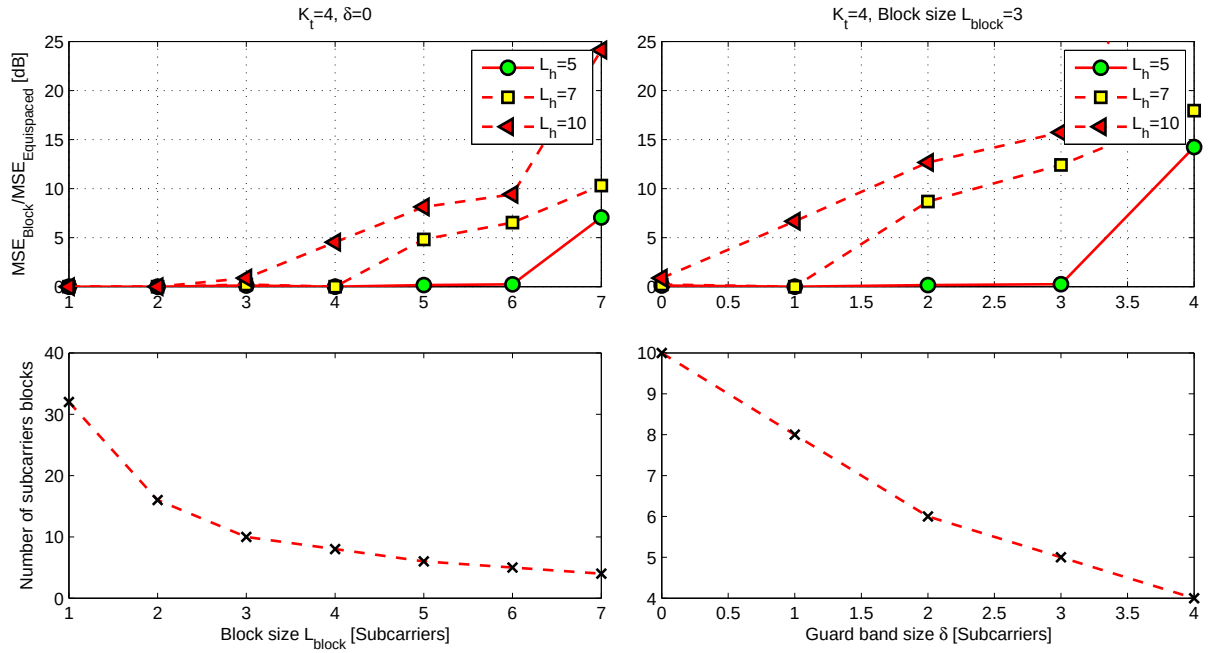

Figure 4-3: Performance comparison of the block and subcarrier SAS

will degrade because the useful per-tap energy decreases. In the end, we get the following block-equispaced ratio

$$\frac{MSE_{Block}}{MSE_{Equispaced}} = \frac{L_p tr\left(\boldsymbol{F}_{M\times L_h}(\boldsymbol{F}^{\boldsymbol{H}}_{\boldsymbol{L_p}\times \boldsymbol{L_h}}\boldsymbol{F}_{\boldsymbol{L_p}\times \boldsymbol{L_h}})^{-1}\boldsymbol{F}^{\boldsymbol{H}}_{\boldsymbol{M}\times \boldsymbol{L_h}}\right)}{ML_h} \tag{4.23}$$

[35] shows that the equispaced SAS is optimal when there is no lack of pilots meaning that this last expression is always greater or equal to 1. Then, the goodness of the block SAS will directly depend on the conditioning of $\boldsymbol{F}^{\boldsymbol{H}}_{\boldsymbol{L_p}\times \boldsymbol{L_h}}\boldsymbol{F}_{\boldsymbol{L_p}\times \boldsymbol{L_h}}$. This is further analyzed in Figure 4-3. The subfigure on top left shows the result of this ratio for increasing block sizes L_{block} with no guard band inserted ($\delta = 0$) and for different channel lengths L_h. One can see that the block SAS performs as well as the equispaced SAS up to a certain point depending on L_h. Looking at bottom left subfigure, we can see that this degradation actually occurs when the number of blocks is smaller than the channel length L_h: $\lfloor \frac{M}{(\delta+L_{block})K_t} \rfloor < L_h$. In other words, there is a lack of pilot blocks. This is further confirmed by the two subfigures on the right where the block size L_{block} is fixed to 3 subcarriers and the guard band size δ varies from 0 to 4 subcarriers. Again, we see that the 3-block SAS performs well up to a point determined by $\lfloor \frac{M}{(\delta+L_{block})K_t} \rfloor < L_h$.

One should note that the results of Figure 4-3 rely on strong assumptions such as perfect orthogonality, perfect synchronization, no lack of pilots for the equispaced method, no correlation between adjacent noise samples in FBMC-OQAM... It also does not address low SNR situations when the MMSE estimator is not equal to the pseudo inverse. However, it gives a good intuition of the global behavior of the block SAS compared to the equispaced SAS and it allows to better analyze the simulation results of the next section.

4.5 Simulation results

In this section, we investigate the performance of the proposed channel estimation algorithms depending on the SAS for scenarios with or without synchronization.

All presented simulations are performed in quasi-static conditions, that is each channel realization is considered constant over the preamble duration. A uniform PDP of the channel is assumed. No data is sent after the preamble in the simulations. Indeed, we assume that the preamble is protected from the data by a sufficient guard time. The subcarrier spacing is set to $\Delta f = 1/T_0 = 15kHz$ with $M = 128$ subcarriers leading to a sampling period $T_s = T_0/M = 520ns$. The prototype filter used is the PHYDYAS filter [9] which has a roll-off factor $\rho = 1$ and an overlapping factor $K = 4$. The preambles for every different schemes are scaled so to have a same transmit power at the SFB output.

In the next simulations, we aim at comparing CP-OFDM and FBMC-OQAM. However, obtaining a perfectly fair comparison between both schemes is difficult. Both modulation schemes are relying on different parameters and have different characteristics. The choice being made here is to normalize each system so that the same total energy is sent over a frame transmission. This means that FBMC-OQAM is more energy efficient since it does not "waste" energy transmitting the CP and it also means that the throughput rate of CP-OFDM is smaller than that of FBMC-OQAM. In the simulations, a CP length of $CP = M/4$ is considered.

4.5.1 Synchronized scenario

Since perfect synchronization is assumed, there is no need for CP-OFDM to insert guard bands between the different blocks or subcarriers because the orthogonality is ensured in the complex domain. On the other hand, the FBMC-OQAM technique is only restricted to the real domain. Therefore, guard bands are needed between different blocks or subcarriers to ensure orthogonality. Since the prototype filter has a roll-off factor of $\rho = 1$, it is sufficient to use a guard band size of $\delta = 1$.

Figure 4-4 shows the MSE of the MMSE CFR estimate for different SAS, namely the equispaced SAS and the block SAS with a size of 4 or 8 subcarriers. The number of base stations is fixed to $K_t = 4$ and two channel lengths are investigated, namely $L_h = 5$ and $L_h = 10$ taps. The number of users in the simulation is actually not important since only the number of base stations will impact the system performance.

As could be expected, at low SNR, FBMC-OQAM outperforms CP-OFDM thanks to its better energy efficiency. However, as discussed in the previous section, at large SNR, FBMC-OQAM experiences interference imposing a performance floor. This floor comes faster for a longer channel. This is reasonable since our hypothesis leading to our system model (4.5) relies on the channel frequency flatness.

We can also note that the equispaced SAS always outperforms the block SAS as expected from previous section. The reason is that the ill-conditioning of the inverse matrix in (4.13) is worse for the block assignments leading to a larger noise amplification. This ill-conditioning gets worser for a longer channel and a larger block size. Moreover, the performance floor due to FBMC-OQAM interference becomes more important for an increasing block size, this comes from two effects. The first one is the appearance of stronger ICI due to contiguous subcarrier allocation and our hypothesis on the CFR flatness on adjacent subcarriers. The second effect is the fact that both noise and interference are amplified by the ill-conditioned inverse.

Figure 4-5 compares the performance of the MMSE and the iterative algorithms for CP-OFDM and FBMC-OQAM, respectively. One can see that the MMSE estimator always outper-

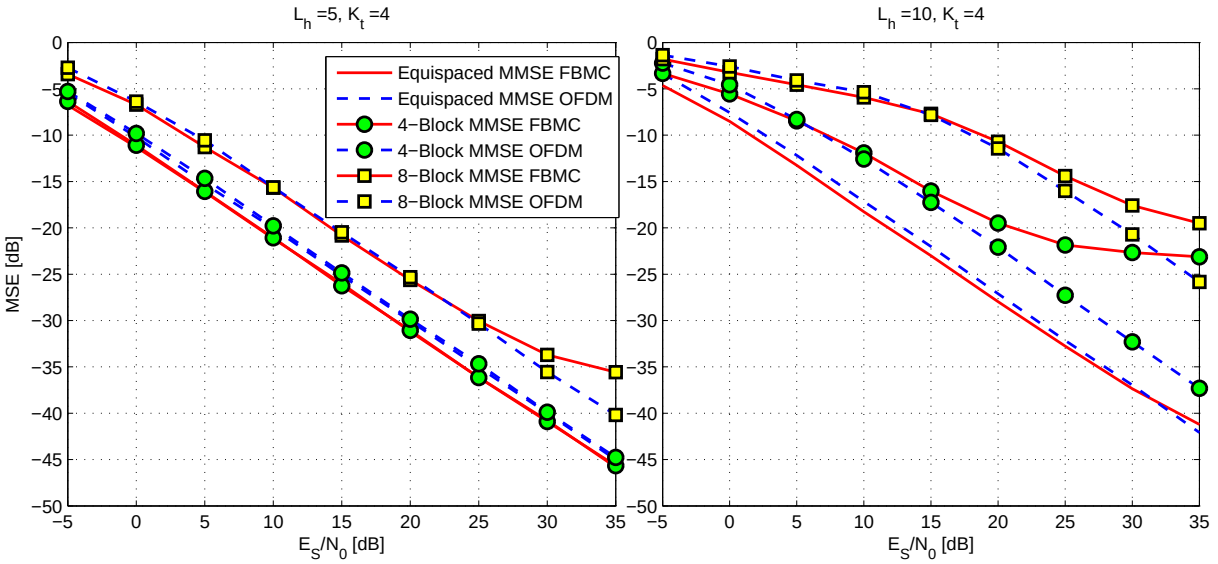

Figure 4-4: Subcarriers assignment schemes performance analysis in a perfectly synchronized scenario for $K_t = 4$ base stations and a channel lengths $L_h = 5$ and $L_h = 10$ ($\lfloor \frac{M}{(\delta+1)K_t} \rfloor \geq L_h$)

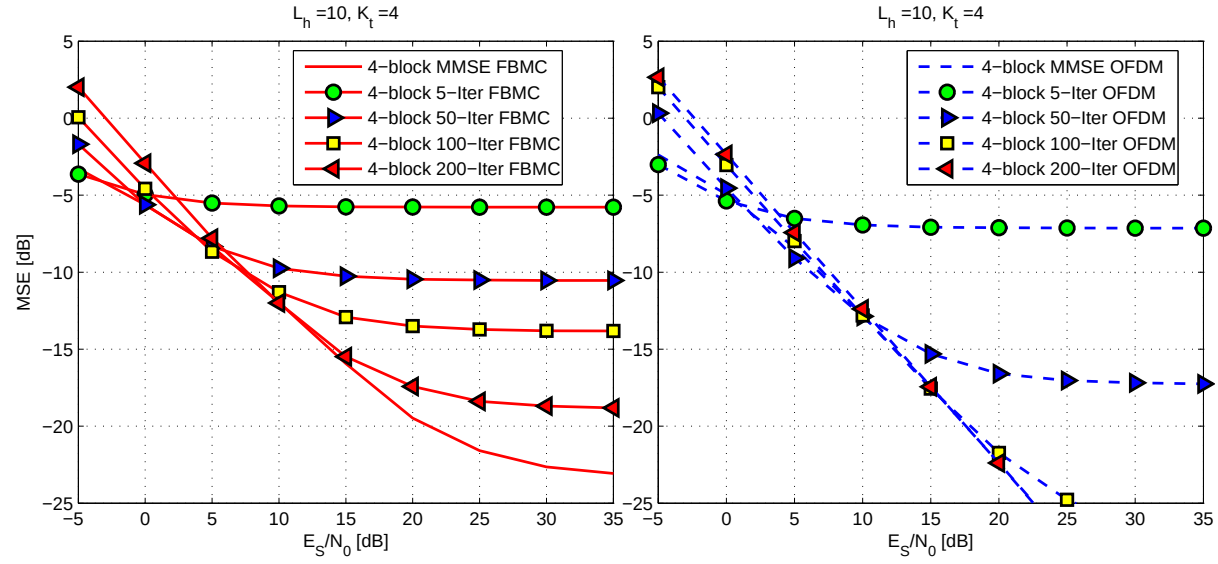

Figure 4-5: Iterative and MMSE channel estimation performance analysis in a perfectly synchronized scenario for $K_t = 4$ base stations and a channel lengths $L_h = 10$ ($\lfloor \frac{M}{(\delta+1)K_t} \rfloor \geq L_h$)

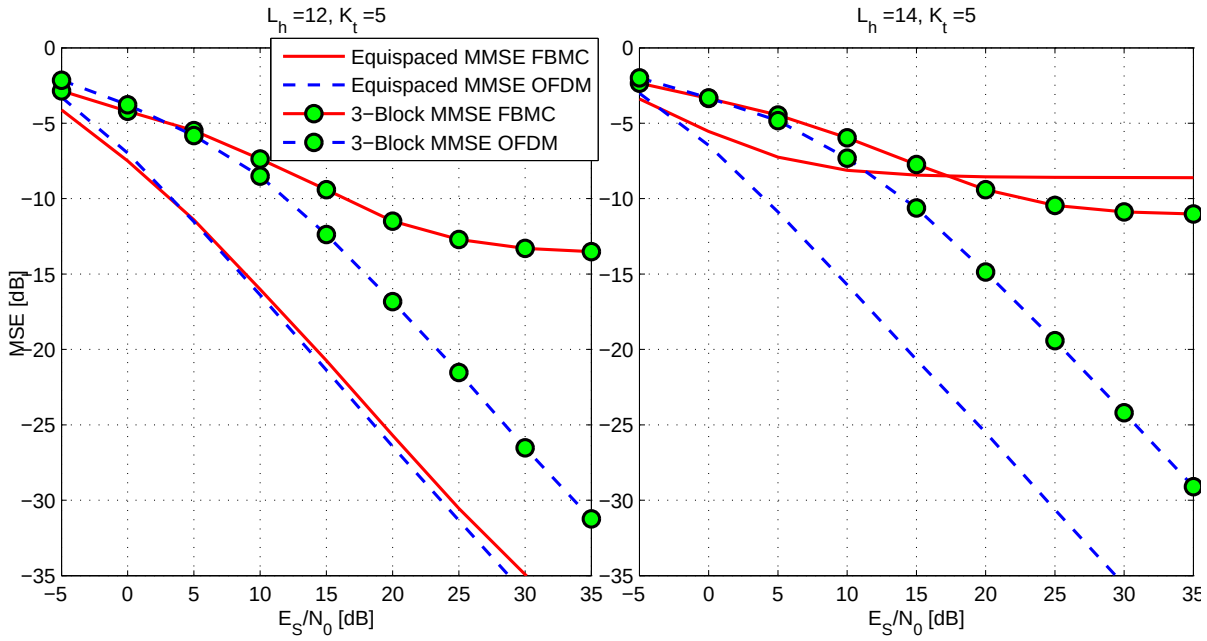

Figure 4-6: Subcarriers assignment schemes performance analysis in a perfectly synchronized scenario for $K_t = 5$ base stations and a channel lengths $L_h = 12$ ($\lfloor \frac{M}{(\delta+1)K_t} \rfloor \geq L_h$) and $L_h = 14$ ($\lfloor \frac{M}{(\delta+1)K_t} \rfloor < L_h$)

forms the iterative estimator. This is due to the fact that the MMSE estimator adapts itself to the SNR level. The iterative estimator is only tangent to the MMSE estimator at a certain SNR for a certain iterations number. We can also check that for a large number of iterations, the iterative estimator converges towards the pseudo inverse which is the MMSE estimator at high SNR. An improvement of the iterative algorithm would then be to fix the number of iterations as a function of the SNR. Furthermore, the iterative channel estimator needs less iterations to converge in CP-OFDM compared to FBMC-OQAM. This comes from the better conditioning of CP-OFDM which uses no guard band and has more pilots subcarriers leading to a faster convergence of the iterative algorithm.

One can also notice that in both cases of Figure 4-4 and Figure 4-5, we have $\lfloor \frac{M}{(\delta+1)K_t} \rfloor \geq L_h$ so that there are enough pilots for each base station-user channel to recover the entire CIR for the FBMC-OQAM equispaced method. Figure 4-6 shows the MSE of the MMSE CFR estimate for different SAS. The number of base stations is fixed to $K_t = 5$ and two channel lengths are investigated, namely $L_h = 12$ and $L_h = 14$ taps. For the $L_h = 12$ taps channel, we have $\lfloor \frac{M}{(\delta+1)K_t} \rfloor = 12 \geq L_h = 12$. This means that the FBMC-OQAM equispaced assignment has just enough pilots for each base station-user channel to recover the CIR. However, for the $L_h = 14$ taps channel, we have $\lfloor \frac{M}{(\delta+1)K_t} \rfloor = 12 < L_h = 14$. This means that there is a lack of subcarriers, there are only 12 pilots to recover a CIR of length 14. This causes a performance floor of the FBMC-OQAM equispaced SAS. However, one can see that the FBMC-OQAM block SAS outperforms the equispaced SAS at high SNR. This is due to the fact that there is need for less guard bands in the block assignment leading to a larger number of pilots. The block SAS can then recover the entire CIR. In CP-OFDM, since there is no need for guard bands, there is enough room to put a sufficient number of pilots to recover the entire CIR and there is thus no performance floor except the one due to the assumption about frequency flatness at subcarrier level of FBMC.

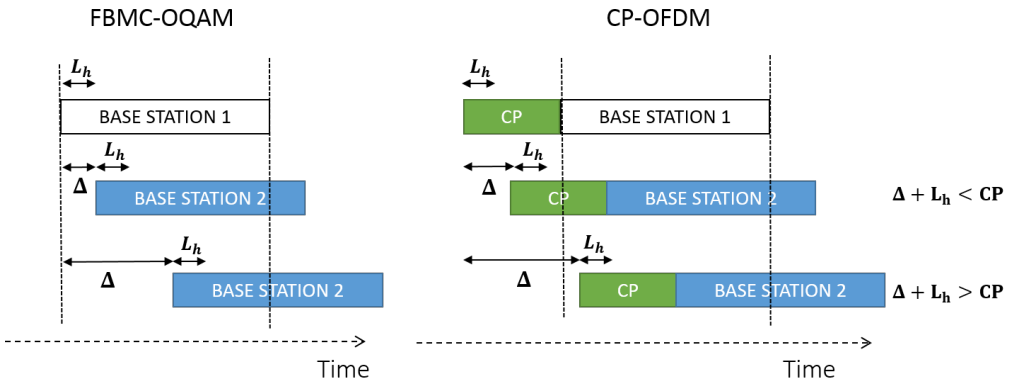

Figure 4-7: Unsynchronized scenario with two base stations ($K_t = 2$) and one receiver for all base stations

4.5.2 Unsynchronized scenario

We now address situations occurring when the different base stations are not synchronized. Each base station transmits its signal with a specific delay Δ_k. We assume this delay is an integer number of sampling periods T_s which is known by the different users. In the following sections, we investigate the effect of this delay on the estimation performance in two scenarios at the user level. In the first one, each user uses only one receiver for all base stations which means that only one time processing window is used to estimate the signals coming from each base station. In the second, each user uses one receiver per base station and each receiver is assumed to be perfectly synchronized with its corresponding base station. Furthermore, we investigate the potential advantages of increasing the guard band size δ.

4.5.2.1 One receiver for all base stations

Figure 4-7 illustrates the studied scenario for the case of two base stations $K_t = 2$. We use only one processing window centered on the first signal that arrives. We assume that there is no data sent before and after the preamble so that there is no interference with the previous and next transmitted blocks. Figure 4-8 gives the corresponding MSE for the channel estimated of each base station as a function of the delay difference $\Delta = \Delta_2 - \Delta_1$. The channel length of the true channel $\boldsymbol{h}$ to estimate considered is $L_h = 16$.

In FBMC-OQAM, since a one subcarrier guard band $\delta = 1$ is used, there is no MSI between the signals coming from both base stations. Therefore, the signal coming from base station 1 does not suffer any degradation from its delay Δ_1. However, the signal coming from base station 2 passes through an effective channel of length $\Delta + L_h$ instead of a true channel length L_h for base station 1. The first consequence of this delay Δ is the need to correct the phase rotation $e^{-j\frac{2\pi}{M}m\Delta}, m \in \mathcal{F}_2$ induced on the subcarrier pilots in order to estimate the true channel $\boldsymbol{h}$ of length L_h. The second consequence is that the effective channel gets more frequency selective making our system model (4.5) less accurate which degrades the performance for base station 2. Finally, the useful energy is smaller for base station 2 given that the window is not centered where the energy is maximum. Those considerations can be checked in Figure 4-8 : base station 1 is not affected by the delay of synchronization while base station 2 suffers a lot from it. A fairer way assuring the same MSE for each base station would have been to center the processing window at the middle of the delay difference $\Delta/2$.

In CP-OFDM, depending on the delay difference Δ and the true channel length L_h, there

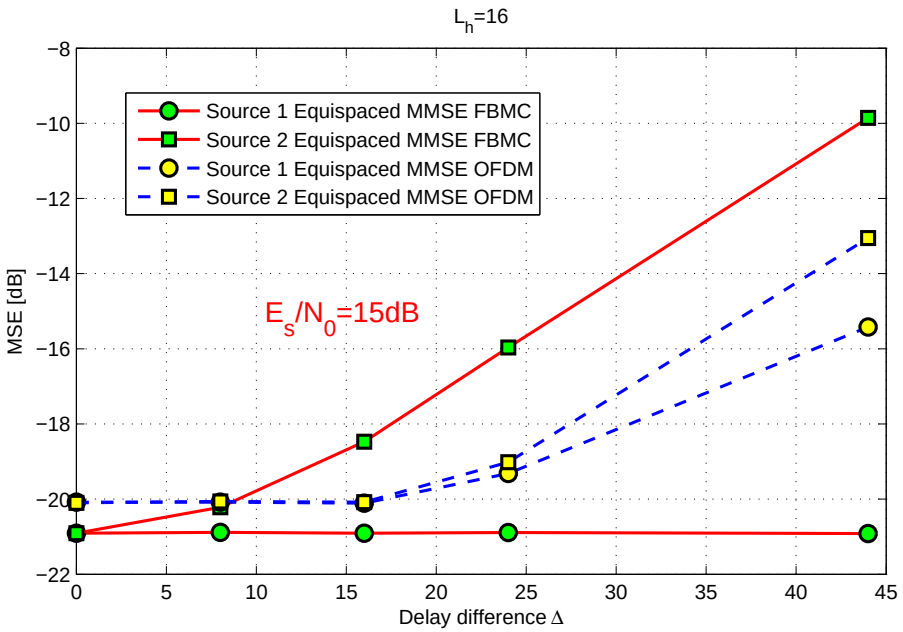

Figure 4-8: Synchronization delay $\Delta = \Delta_2 - \Delta_1$ effect on performance in the case of one receiver for all base stations

are two cases to investigate. On the one hand, when $\Delta + L_h < CP$, the orthogonality is preserved and there is no MSI. The pilots of base station 2 should just be compensated for the phase rotation $e^{-j\frac{2\pi}{M}m\Delta}, m \in \mathcal{F}_2$. On the other hand, as soon as $\Delta + L_h > CP$, the orthogonality is lost. Base station 1 suffers only from MSI coming from the pilot subcarriers of base station 2. However, base station 2 not only suffers from MSI coming from base station 1. Another degradation comes from the true channel $\boldsymbol{h}$ spreading causing the signal processed not to be circulant anymore which is another source of interference on base station 2 coming from its own subcarriers. Furthermore, for large delay differences Δ, less energy is contained in the processing window for base station 2 than for base station 1. Figure 4-8 illustrates the fact that as $\Delta + L_h > CP \Leftrightarrow \Delta > 16$, the performance degrades faster for base station 2 than for base station 1. In this Figure, no guard band is inserted in CP-OFDM ($\delta = 0$).

4.5.2.2 One receiver per base station

Figure 4-9 illustrates the studied scenario for the case of multiple base stations. We now use a different window to process the signals coming from each base station. We assume that there is no data sent before and immediately after the preamble so that there is no interference with the previous and next transmitted blocks. Figure 4-10 gives the corresponding MSE for the channel estimated of all base stations ($K_t = 4$) as a function of the SNR for two channel lengths, $L_h = 5$ and $L_h = 10$. We assume the synchronization delay Δ_k of each base station is an independent random variable uniformly distributed over the interval $[0, M]$. The final MSE is averaged over all base stations, 1000 channel realizations of $\boldsymbol{h}$ and 1000 delays $\Delta_k, k = 1, ..., K_t$ realizations.

As mentioned before, FBMC-OQAM does not suffer from MSI thanks to the well localized prototype filter and the guard band size $\delta = 1$. Now that the processing windows are centered on the signals of each base station, there is no degradation anymore induced by the asynchronism. As can be checked on Figure 4-10, FBMC-OQAM does not suffer from any synchronization

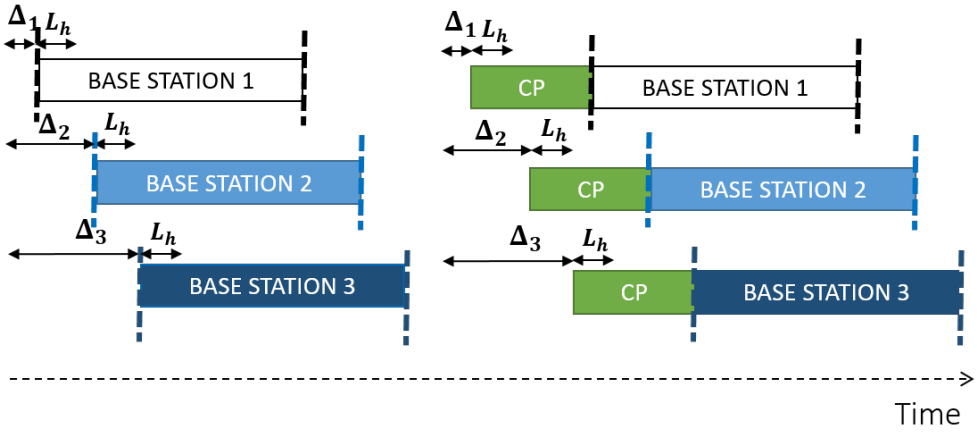

Figure 4-9: Unsynchronized scenario with multiple base stations and one receiver for each base station

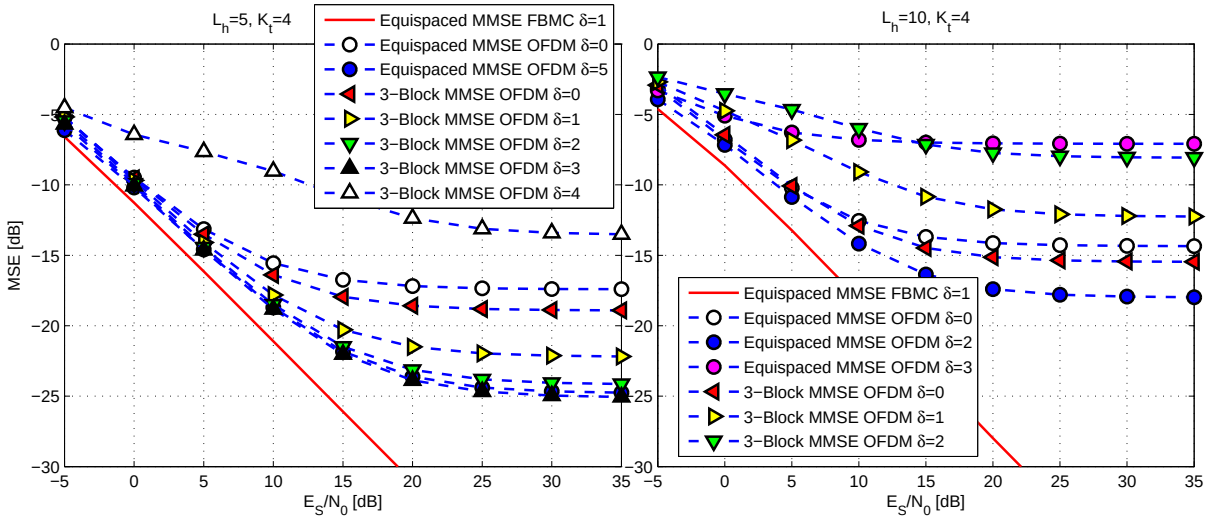

Figure 4-10: Effect of unsynchronized base stations on performance in the case of one receiver per base station

degradation when using one processing window for each base station.

However, given that CP-OFDM suffers from very high spectral leakage, it will still suffer from asynchronism leading to MSI even if the processing windows are centered on each base station. One solution to decrease the MSI power is to insert guard bands between the pilot subcarriers. Figure 4-10 shows the resulting performance of inserting guard bands of different sizes δ subcarriers in CP-OFDM and using either equispaced SAS either block SAS.

For the $L_h = 5$ channel length, we can see that the equispaced SAS with no guard bands ($\delta = 0$) is outperformed by the corresponding block SAS with no guard bands ($\delta = 0$). Indeed, the block SAS is more robust against asynchronism since the pilot subcarriers in the middle of the block suffer less from MSI.

Furthermore, one can note that using an increasing guard band size δ in CP-OFDM is always beneficial to the equispaced SAS if there is no lack of pilots $\lfloor \frac{M}{(\delta+1)K_t} \rfloor \geq L_h$. This allows to decrease the signal to interference ratio (SIR) of each pilot[6] and at the same time, it does not change the conditioning of the matrix $\boldsymbol{F}^{\boldsymbol{H}}_{\boldsymbol{L_p}\times\boldsymbol{L_h}}\boldsymbol{F}_{\boldsymbol{L_p}\times\boldsymbol{L_h}} = L_p\boldsymbol{I}_{\boldsymbol{L_h}}$. One can check for both channel lengths $L_h = 5$ and $L_h = 10$, using a larger δ improves the performance except the $\delta = 3$ case for $L_h = 10$. Indeed, in this case, there is a lack of pilots $\lfloor \frac{M}{(\delta+1)K_t} \rfloor < L_h$, the user cannot reconstruct the entire CIR from the received pilots.

However, the last remarks for the equispaced SAS do not always hold for the block SAS. For the $L_h = 5$, we can note that using an increasing δ up to three subcarriers is beneficial thanks to the corresponding decrease of the MSI power. However, the performance degrades a lot for $\delta = 4$ getting even worse that the $\delta = 0$ case. This effect does not come this time from the lack of pilots but from the matrix $\boldsymbol{F}^{\boldsymbol{H}}_{\boldsymbol{L_p}\times\boldsymbol{L_h}}\boldsymbol{F}_{\boldsymbol{L_p}\times\boldsymbol{L_h}}$ which gets ill-conditioned as soon as there is a lack of pilot blocks $\lfloor \frac{M}{(\delta+L_{block})K_t} \rfloor < L_h$ as shown in Section 4.4.3. For the $L_h = 10$ channel, $\boldsymbol{F}^{\boldsymbol{H}}_{\boldsymbol{L_p}\times\boldsymbol{L_h}}\boldsymbol{F}_{\boldsymbol{L_p}\times\boldsymbol{L_h}}$ has just enough pilot blocks for a $\delta = 0$ guard band size. Then, for an increasing δ, the decrease in MSI power will not counterweight the worse ill-conditioning caused by a larger guard band size δ. Those results confirm our analytical study of the block-equispaced SAS in Section 4.4.3.

In the end, the last consideration on Figure 4-9 bring us to the conclusion that the best SAS in an asynchronous CP-OFDM system is the sparsest $L_p = L_h$ equispaced SAS. Indeed, this the SAS that maximizes the guard band size δ while keeping a well conditioned $\boldsymbol{F}^{\boldsymbol{H}}_{\boldsymbol{L_p}\times\boldsymbol{L_h}}\boldsymbol{F}_{\boldsymbol{L_p}\times\boldsymbol{L_h}}$ matrix.

4.6 Conclusion

We investigated channel estimation in OFDM/FBMC based distributed MIMO systems. During this phase, CSI is not known yet at the base stations and full synchronization is not necessarily available. Precoding is then not yet possible and MSI can appear. Therefore, we have proposed preamble-based channel estimation using either equispaced SAS either block SAS. Each user recovers a part of the CFR from each base station. We then considered two methods to reconstruct the whole CFR exploiting the sparsity of the CIR. The first approach consists of a MMSE estimator which requires one matrix inversion and information on the channel and noise covariance matrices. The second approach is an iterative estimator which is hardware efficient and requires only information on the channel length.

[6]Using a larger δ means less pilots over the whole bandwidth. It then leads to a larger per-pilot power given the total transmitted power constraint and also to a corresponding increase of the MSI power. However, given that the pilots are now placed further apart, the MSI will decrease faster leading to a more favorable SIR ratio in the end.

It has been shown that the MMSE estimator always outperforms the iterative estimator while for a given number of iterations, the iterative estimator performs as well as the MMSE estimator at a certain SNR. We have also demonstrated that the iterative estimator if stable and for a large number of iterations converges towards the MMSE estimator at large SNR. Furthermore, we concluded from synchronized and unsynchronized numerical simulations that the sparsest equispaced SAS is generally the best SAS to use except in FBMC-OQAM when a lack of pilots occurs.

5. Low feedback downlink MIMO channel estimation for distributed FBMC systems using SNR measurements

5.1 Introduction

Preamble-based channel estimation has been investigated in section 4. It is based however on the assumption that the channels remain constant on the duration of the packet. Depending on the mobility in the system and the length of the packets, some additional adaptation of the channel estimation may be required in many scenarios. To this end, this section investigates the issue of regular estimation of the MIMO channel during data transmission, for a distributed MIMO scenario when FBMC-OQAM modulation is used. Most estimation methods for this purpose in multicarrier communications systems are based on pilots [36]. However, in the case of FBMC-OQAM, the complicated interference structure present at the receiver makes the use of pilots slightly more difficult and requires additional techniques such as POP (Pair of pilots), or auxiliary pilots [39].

In this section, a new estimation method is presented that is no longer making use of pilots. It is based on the application of several well designed perturbations of the transmitted signals. The changes brought by these perturbations on the observed SNR's at the different receivers are measured and fed back to the basestations. The information for different perturbations is collected at the basestation and then used to perform the channel estimation at regular intervals during data transmission. With this method, the receivers are simply estimating their SNR in a normal way and need not be aware of the created perturbation. It has the advantage of requiring a low overhead (only the SNR's need to be fed back). On another hand, the perturbation has an impact on the transmission of normal data, and has to be kept small enough to allow continuous transmission. Similar methods have already been presented in the context of VDSL (Very high bit-rate Digital Subscriber Lines) with DMT (Discrete Multitone) transmission [40], or for multi-cell OFDM systems [41]. In this section, it is shown how the method can be applied to the more complicated case of FBMC-OQAM with several adjustments. The principle of the method is first presented in section 5.3, then some analytical performance evaluations are derived in section 5.4 and finally the efficiency of the method is shown in section 5.5 through several simulation results.

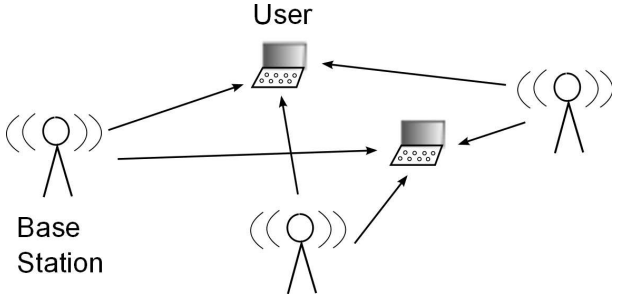

Figure 5-1: General model of distributed beamforming

5.2 System model and precoding

A distributed MIMO environment is considered where FBMC-OQAM modulation [8] is employed. The considered model is depicted in Figure 5-1. There are N basestations (transmitters) in the system and N users. For simplicity, the model is here limited to the case of equal number of basestations and number of users. The basestations cooperatively send their signals (similarly to a single transmitter with multiple antennas) to transmit N independent streams of information to the N users. For simplicity, it is also assumed that each transmitter and receiver only uses one antenna, but it can be generalized to the case of multiple antennas at some or all of the nodes. The choice of the MIMO precoding method is discussed in earlier sections for the case of FBMC. In this section, a linear precoder (see (5.1) below) is considered. It is assumed that the channel is mildly selective and the number M of subcarriers is sufficient so that the channel can be considered flat inside each subcarrier. The inter-subcarrier interference is therefore negligible. All operations can be applied per-subcarrier so only one given subcarrier is considered. It is also assumed that the channel is slowly time-varying so that it can be considered constant on the duration of the various measurements.

The system model used here takes as inputs the real data entries [23]. The real information symbols to be transmitted to the different users on subcarrier k at instant n are denoted by $d_{k,i}(n),\ i = 1, \ldots, N$ and are grouped into a vector $\boldsymbol{d}_k(n) = [d_{k,1}(n) \ldots d_{k,N}(n)]^T$. The variance of the symbols is denoted by σ_d^2. For simplicity of notations, it is assumed to be the same for all symbols. The transmitters precode the information in order to be able to transmit N streams independently (or with as little inter-user interference as possible). The $N \times N$ precoding matrix for the subcarrier of interest is denoted by $\mathbf{F}$. Hence the following symbols are transmitted on subcarrier k from the different basestations at instant n

$$\boldsymbol{x}_k(n) = \mathbf{F}\, \boldsymbol{d}_k(n). \tag{5.1}$$

Taking into account the particular interference structure resulting from the FBMC-OQAM modulation, and assuming that the channel is flat inside each subcarrier, the transmission model can be written as [8, 23]

$$\boldsymbol{y}_k(n) = \mathbf{C}\, \boldsymbol{x}_k(n) + j\mathbf{C} \sum_{k'=k-1}^{k+1} \sum_{n'} t_{k,k'}(n - n')\boldsymbol{x}_{k'}(n') + \boldsymbol{\nu}(n)\,, \tag{5.2}$$

where $\boldsymbol{y}_k(n)$ denotes the N-dimensional vector of received symbols at the different receivers. $\mathbf{C}$ is the $N \times N$ channel matrix for the subcarrier of interest (subscript k is omitted here for readability). It is assumed that the channel is mildly selective so that the channel matrix for neighboring subcarriers can be considered approximately equal. The channel matrix is also assumed constant on the duration of the estimation procedure. $t_{kk'}(n - n')$ represents the transmultiplexer response of the filterbank, it is responsible for the complex interference appearing at the receiver from the FBMC-OQAM modulation which can usually be rendered purely imaginary by proper equalization and then removed when taking the real part to obtain the symbol of interest. Finally, $\boldsymbol{\nu}(n)$ is the vector of noise samples at the different receivers. The additive noise is assumed to be Gaussian with independent elements.

Because the receivers are not collocated, the i-th receiver only has access to the i-th entry of $\boldsymbol{y}_k(n)$ for detection and/or estimation purposes, so the objective of the precoder is to cancel all interference coming from other users. When the precoder is active, a new global model can

be obtained to take into account the presence of the precoder:

$$\boldsymbol{y}_k(n) = \mathbf{H}\boldsymbol{d}_k(n) + j\mathbf{H}\sum_{k'=k-1}^{k+1}\sum_{n'} t_{k,k'}(n-n')\boldsymbol{d}_{k'}(n') + \boldsymbol{\nu}(n) \tag{5.3}$$

where

$$\mathbf{H} = \mathbf{CF} \tag{5.4}$$

is the combined precoder-channel matrix. It is the combined matrix $\mathbf{H}$ that the proposed method tries to estimate (or more precisely the normalized version with respect to the diagonal elements, see below). This is a square $N \times N$ matrix. It is interesting to note that in a tracking scenario (i.e. when some preamble-based estimation has already been performed), the current precoding can be assumed to offer a reasonable inter-user interference cancellation and $\mathbf{H}$ is close to a diagonal matrix.

At the receiver, per-subcarrier equalization is performed and then the real part is extracted to recover the transmitted symbols. The (real) output symbol for user i at instant n can be written as

$$z_{k,i}(n) = \Re\left\{\frac{y_{k,i}(n)}{H_{ii}}\right\} \tag{5.5}$$

$$= \sum_{l=1}^{N} \bar{H}_{il,\Re} d_{k,l}(n) + \mu_i(n) + \sum_{k'=k-1}^{k+1}\sum_{n'} t_{kk'}(n-n')\sum_{l=1}^{N}\bar{H}_{il,\Im} d_{k,l}(n') \tag{5.6}$$

where

$$\mu_i(n) = \Re\left\{\frac{\nu_i(n)}{H_{ii}}\right\} \tag{5.7}$$

$$\bar{H}_{il,\Re} = \Re\left\{\frac{H_{il}}{H_{ii}}\right\} \tag{5.8}$$

$$\bar{H}_{il,\Im} = \Re\left\{\frac{jH_{il}}{H_{ii}}\right\} = -\Im\left\{\frac{H_{il}}{H_{ii}}\right\}. \tag{5.9}$$

The variance of the noise sample $\mu_i(m)$ for receiver i is denoted by $\sigma^2_{\mu,i}$. Note that if equalization is assumed to be perfect:

$$\bar{H}_{ii,\Re} = 1 \tag{5.10}$$

$$\bar{H}_{ii,\Im} = 0 \tag{5.11}$$

and the objective of the precoder is to obtain $\bar{H}_{il,\Re} \approx \bar{H}_{il,\Im} \approx 0$,for all $l \neq i$. Due to the scaling performed at the receiver, only the *normalized* matrix coefficients $\bar{H}_{il,\Re}$ and $\bar{H}_{il,\Im}$ are important in order to design the precoder, so the estimation procedure can be restricted to these normalized matrix coefficients (in other words any scaling coefficient that is applied at the receiver i will scale the coefficients of row i of matrix $\mathbf{H}$ accordingly but it has no impact on the interference that is received from the other users).

5.3 Estimation method based on small perturbation

For illustration purpose, consider the estimation of the normalized channel matrix coefficients of index (i, N), that is estimation of $\bar{H}_{iN,\Re}$ and $\bar{H}_{iN,\Im}$ for a given user i. The basic principle of this method is to add a small perturbation to the symbols of the victim user i coming from the data stream of user N. The effect of this small perturbation on the SNR of user i is observed, and from the corresponding changes in SNR, the (normalized) channel matrix coefficients of interest can be estimated.

First, the SNR is measured for normal transmission with all users active (including user N). Note that to be more precise, we could call it the SINR as it includes both additive noise and interference. For simplicity of the notations however, we write it simply as SNR, emphasizing the fact that the receiver itself cannot make the difference between these two sources of degradation. The SNR observed at receiver i during normal transmission, that is before the insertion of any perturbation is given by (remember that all symbols are assumed to have a fixed variance)

$$\begin{aligned}\frac{1}{\mathsf{SNR}_{i,0}} &= \sum_{l\neq i} \bar{H}^2_{il,\Re} + \frac{\sigma^2_{\mu,i}}{\sigma^2_d} \\ &\quad + \sum_{k'} \sum_{n'} \sum_{l} t^2_{kk'}(n-n')\bar{H}^2_{il,\Im}. \end{aligned} \tag{5.12}$$

After this first SNR measurement, a second situation is considered where, instead of transmitting the usual data symbol $d_{k,i}(n)$ for user i, a perturbation is added proportionally to the symbols from user N. The transmitted symbols are now:

$$d'_{k,i}(n) = d_{k,i}(n) + \epsilon_{iN} d_{k,N}(n) \tag{5.13}$$

where the coefficients ϵ_{iN} are real coefficients of small amplitude to avoid disturbing the normal transmission too much. After the perturbation is inserted, the new received model becomes

$$\begin{aligned} z_{k,i}(n) &= d_{k,i}(n) + d_{k,N}(n)\left[\bar{H}_{iN,\Re} + \epsilon_{iN}\right] + \sum_{l\neq N; l\neq i} \bar{H}_{il,\Re} d_{k,l}(n) \\ &\quad + \sum_{k'} \sum_{n'} \sum_{l} t_{kk'}(n-n')\bar{H}_{il,\Im} d_{k',l}(n') + \mu_i(n). \end{aligned} \tag{5.14}$$

The new SNR for user i can thus be approximated by

$$\begin{aligned}\frac{1}{\mathsf{SNR}_{i,1}} = \\ &\left[\bar{H}_{iN,\Re} + \epsilon_{iN}\right]^2 + \sum_{l\neq i; l\neq N} \bar{H}^2_{il,\Re} + \frac{\sigma^2_{\mu,i}}{\sigma^2_d} \\ &+ \sum_{k'} \sum_{n'} \sum_{l} t^2_{kk'}(n-n')\bar{H}^2_{il,\Im}. \end{aligned} \tag{5.15}$$

As can be observed, the perturbation has an impact on the SNR by modifying the apparent normalized coefficient $\bar{H}_{iN,\Re}$. From the receiver point of view, and because of the perturbation, everything happens as if the coefficient had been changed to the new value $\bar{H}_{iN,\Re} + \epsilon_{iN}$. All other coefficients remain unaffected.

A third measure of SNR is necessary to obtain the complete normalized matrix coefficient (real and imaginary parts), using a second perturbation. In this third situation, a slightly modified perturbation is added to the symbols. The new transmitted symbols are

$$d''_{k,i}(n) = d_{k,i}(n) + \epsilon_{iN} t_{kk}(1) d_{k,N}(n-1). \tag{5.16}$$

Note that $d_{k,N}(n-1)$ is used here instead of $d_{k,N}(n)$ as well as an additional coefficient $t_{kk}(1)$, the purpose of which will be apparent later on. Once again, the new received model can be rewritten

$$\begin{aligned} z_{k,i}(n) &= d_{k,i}(n) + \sum_{l \neq i} \bar{H}_{il,\Re} d_{k,l}(n) \\ &\quad + d_{k,N}(n-1)\, t_{kk}(1) \left[\bar{H}_{iN,\Im} + \epsilon_{iN} \right] + \mu_i(n) \\ &\quad + \sum_{(k',n',l) \neq (k,n-1,N)} \sum \sum \sum t_{kk'}(n-n') \bar{H}_{il,\Im} d_{k',l}(n'). \end{aligned} \tag{5.17}$$

In this case, it can easily be observed that everything happens as if the normalized channel coefficient $\bar{H}_{iN,\Im}$ is replaced with $\bar{H}_{iN,\Im} + \epsilon_{iN}$

The SNR with the second perturbation satisfies

$$\begin{aligned} \frac{1}{\mathsf{SNR}_{i,2}} = & \\ & \left[\bar{H}_{iN,\Im} + \epsilon_{iN} \right]^2 t_{kk}^2(1) + \sum_{l \neq i} \bar{H}_{il,\Re}^2 + \frac{\sigma_{\mu,i}^2}{\sigma_d^2} \\ & + \sum_{(k',n',l) \neq (k,n-1,N)} \sum \sum \sum t_{kk'}^2(n-n') \bar{H}_{il,\Im}^2. \end{aligned} \tag{5.18}$$

Now based on these 3 measurements, it is possible to obtain the normalized channel coefficients $\bar{H}_{iN,\Re}$ and $\bar{H}_{iN,\Im}$ (real and imaginary parts). After a few computations, the following estimators are obtained:

$$\hat{H}_{iN,\Re} = \frac{1}{2\epsilon_{iN}} \left(\frac{1}{\mathsf{SNR}_{i,1}} - \frac{1}{\mathsf{SNR}_{i,0}} \right) - \epsilon_{iN}/2. \tag{5.19}$$

Similarly,

$$\hat{H}_{iN,\Im} = \frac{1}{2\epsilon_{iN} t_{kk}^2(1)} \left(\frac{1}{\mathsf{SNR}_{i,2}} - \frac{1}{\mathsf{SNR}_{i,0}} \right) - \epsilon_{iN}/2. \tag{5.20}$$

These equations provide the estimation method for the real and imaginary parts of the normalized channel matrix coefficient. It is valid even when other users are present, as long as their power remains constant during all 3 SNR measurements. It only requires the 3 SNR measurements described above, for a value of ϵ_{iN} that can be chosen arbitrarily. For the estimation to be as precise as possible, ϵ_{iN} has to be chosen as big as possible, so that a significant impact on the SNR can be measured. On the other hand, if ϵ_{iN} is too big, there is a risk to decrease the SNR excessively and prevent the normal transmission of the data symbols. A simple and reasonable choice is to impose that the amplitude of $\epsilon_{iN}|H_{ii}|$ is approximately half of the coefficient $|H_{iN}|$

$$\epsilon_{iN} = \frac{1}{2} \frac{|H_{iN}|}{|H_{ii}|} \tag{5.21}$$

or in other words that ϵ_{iN} is on the order of half the normalized coefficients. Overall, this choice of ϵ_i ensures that the SNR degradation remains acceptable while providing a value sufficiently high to have a visible impact on the SNR. Obviously, it is not always possible to evaluate this as it would require a coarse estimation already, but it provides a general order of magnitude.

5.4 Accuracy of the channel estimate

In this section, the performance of the method is analyzed theoretically by computing the average accuracy of the estimate obtained by (5.19) and (5.20). Since all the estimations are based on SNR measurements, the general results of accuracy for SNR measurements are first reviewed. It is assumed that the SNR is estimated during data transmission by averaging the observed noise (including interference) at the output of the demodulator over K_e realizations (the number of observed symbols), and then computing the ratio between the useful signal variance and the noise variance. Now as shown above, expressions for the channel coefficient estimations use the inverse of the estimated SNR. So the value of interest is the estimation error variance on the *inverse* of the SNR. For this kind of estimator, and assuming that the noise is approximately Gaussian at the output of the demodulator, the variance on the estimation of $(1/SNR)$ can be shown to be equal to

$$\text{var}\left(\frac{\hat{1}}{\text{SNR}}\right) = \frac{2}{K_e(\text{SNR})^2} \tag{5.22}$$

where it appears clearly that the estimation variance depends on the SNR itself[1]. The total noise on the received samples is usually not Gaussian when the inter-user interference is dominant (it depends on the constellations used), and in fact the resulting error variance is then generally lower than (5.22). So (5.22) provides a worst-case approximation.

Based on these results, the accuracy of the method can easily be derived. It is assumed that the constellation amplitude is normalized, so that the symbols coming from different users have a fixed variance. Therefore the variance of the channel estimation is given by

$$\text{var}\left(\hat{H}_{iN,\Re}\right) = \frac{1}{2\epsilon_{iN}^2 K_e}\left(\frac{1}{\text{SNR}_{i,1}^2} + \frac{1}{\text{SNR}_{i,0}^2}\right) \tag{5.23}$$

for the real part, and similarly for the imaginary part. The estimation variance is thus inversely proportional to ϵ_{iN}^2 but is also highly dependent on the values of SNR in the two considered situations.

Finally, the useful performance measure is the rejection of the inter-user interference after the precoding is applied, based on the provided estimate. In order to evaluate it, several approximations are made. A tracking scenario is considered where the combined channel matrix $\mathbf{H}$ is already close to a diagonal matrix (so that $H_{ii} >> H_{ij}$, for $j \neq i$). It is also assumed that a zero-forcing precoder is applied after estimating the channel matrix, in order to correct the precoder and remove the inter-user interference as much as possible. Based on these approximations, it can be easily shown that, for estimation error variances $\sigma_{e_{ij}}^2$ on channel coefficients H_{ij}, the resulting SIR (signal to interference ratio) after correcting the precoder is well approximated by

$$\text{SIR}_i = \frac{|H_{ii}|^2}{\sum_j \sigma_{e_{ij}}^2}. \tag{5.24}$$

This represents the ratio between the signal power, and the remaining inter-user interference power, thus not taking the additive noise into account. Using the error variance on the real part and imaginary part of the normalized channel coefficients (5.23), and assuming that the

[1] once again, including the interference from other users

SNR does not change too much between the different perturbation steps, the performance of the precoder based on SNR estimates is obtained as

$$\mathsf{SIR}_i = \frac{K_e \mathsf{SNR}_i^2}{2\sum_j \frac{1}{\epsilon_{ij}^2}} \tag{5.25}$$

$$= \frac{K_e \epsilon_i^2 \mathsf{SNR}_i^2}{2(N-1)}, \tag{5.26}$$

where the last line corresponds to the case where all coefficients $\epsilon_{ij} = \epsilon_i$ are identical.

5.5 Simulation Results

In this section, simulation results for the proposed method are presented. They are compared to the theoretical evaluation of the performance presented in the previous section.

A system with 5 users and 5 basestations is considered and for the simplicity only one given subcarrier is investigated. Several noise and interference power situations are investigated (corresponding to different accuracies or different stages of the channel tracking). For each situation, a large number of simulations (5000) is performed. The channel matrix is generated randomly for each simulation according to a log-normal model, fulfilling the noise and interference conditions. The perturbation coefficients ϵ_{ij} are chosen according to the rule (5.21). The variance of the channel coefficient estimates is computed by averaging over all simulations. Instead of representing the variance estimate itself, the results are presented with the more meaningful value of the resulting SIR, using the approximation of (5.24). It provides an evaluation of how well the inter-user interference is decreased by the obtained precoder, with respect to the signal power. Figure 5-2 shows the obtained SIR as a function of the number of blocks K_e used for each measurement, expressed in terms of the total needed time (in number of FBMC symbols). Three noise and interference situations are represented where the inter-user interference is dominant. An additional situation is represented (labelled Add N) where the additive noise is dominant. Also shown in circles is the predicted performance, as obtained with the results of section 5.4. As can be observed, the performance prediction seems very good except with high inter-user interference (SINR=12).

Influence of the perturbation amplitude: Figure 5-3 shows the influence of the amplitude of the perturbation. The parameter ϵ_{ij} is varying around the choice described earlier (which is around 0.1). As expected, the performance increases with an increased perturbation, up to a point where the perturbation is so large that it causes a significant degradation in the SNR, and thus in the estimation. The theoretical performance measure (circles) based on (5.23) assumes that the SNR does not change too much between measurements, and becomes thus inaccurate for large perturbations. The point where the perturbation becomes too large depends on the noise level, as can be seen in figure 5-3. For higher noise, this degradation effect appears later.

5.6 Summary

In this section, we have presented a method to estimate MIMO channel coefficients in a distributed MIMO system using FBMC-OQAM modulation in a tracking scenario. The method is based on the application of small perturbations to the signal by the basestations. It only

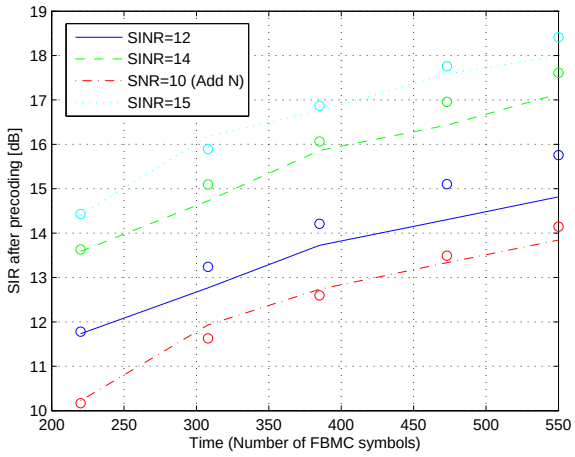

Figure 5-2: Results of the SNR method: resulting SIR as a function of the total time used for estimation, for different noise and interference situations. In 3 out of 4 situations, the inter-user interference is dominant (the additive noise is approximately 15 dB below the signal). For the situation labelled 'Add N', the additive noise is dominant and the inter-user interference is low. The theoretical performance predictions are represented with circles.

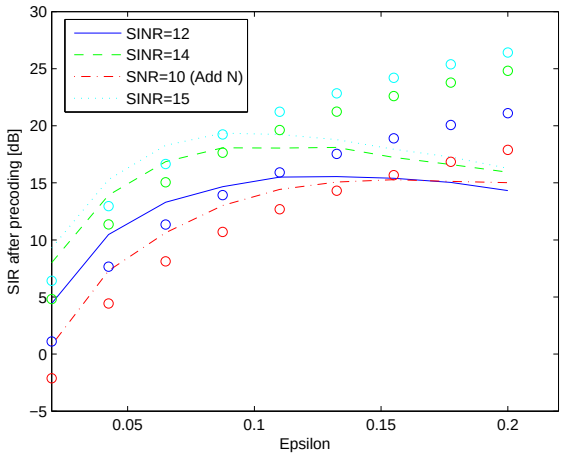

Figure 5-3: Results of the SNR method as a function of the parameter ϵ_{ij} for different SINR situations. The theoretical performance predictions are represented with circles.

requires SNR measurements to be fed back from the receivers. Simulation results show that a good estimate can be obtained in a reasonable amount of time. Theoretical performance evaluation have been given and match the simulation results well.

6. Conclusions

This deliverable presented the main contributions of task 6.2 related to the application of the CoMP and distributed beamforming principles for distributed multi-user MIMO systems using FBMC/OQAM in a PMR scenario. Beamforming design and channel estimation issues have both been investigated.

In section 2, three IIM-CBF transmission schemes have been presented for the dowlink of FBMC/OQAM-based multi-user MIMO and CoMP systems. These schemes are designed to cope with the case where the total number of receive antennas of the different users served is larger or equal to the total number of transmit antennas. The case of partial cooperation of adjacent cells has also been tackled with the scheme IIM-CBF 3. These three proposed IIM-CBF schemes are effective in mitigating the intrinsic interference that is inherent in FBMC/OQAM based systems in addition to the suppression of the multi-user interference, without relying on the assumption that the channel is almost frequency flat. Through simulation results, it has been shown that the FBMC/OQAM based multi-user MIMO and CoMP downlink systems where IIM-CBF 1, IIM-CBF 2, or IIM-CBF 3 is employed achieve a similar performance compared to their CP-OFDM based counterparts but with a higher spectral efficiency and a greater robustness against misalignments in the frequency domain. In addition, the convergence of the IIM-CBF techniques has been analyzed numerically. It leads to the conclusion that the complexity is quite acceptable.

In section 3, two new methods have been presented to jointly design precoders and receivers for a MU-MIMO FBMC downlink system when the channel is highly selective. The first method is iterative and successively optimizes the precoder and equalizer using the MSE uplink-downlink duality with various constraints. Throughout the simulations, the *System-Wide Sum-MSE* constraint performed the best over the whole E_b/N_0 regime. The dual precoders were compared to an existing precoder design [29] for highly selective channel. All outperform the precoder-[29] design in terms of BER and MSE over a wide SNR range as they are better able to mitigate the different types of interference as well as the noise. The second method is based on a SLR (signal-to-leakage ratio) criterion. It is no longer iterative and closed-form expressions of the precoder have been developed. From the numerical results it can be concluded that the first approach provides a slightly better performance compared to the second, at the cost of a higher complexity due to the iterative joint transceiver design. Both approaches show a considerable improvement over two state-of-the-art schemes that do not consider the channel frequency selectivity inside each subcarrier.

Section 4 analyzed the issue of *preamble-based* channel estimation in a distributed MIMO downlink scenario using either OFDM or FBMC/OQAM. Because precoding is impossible during the preamble (channel is not known yet), it was suggested to use some subcarrier assignment to the different basestations during the preamble only in order to avoid the multistream interference. Two channel estimation methods and two subcarrier assignments were compared. It has been shown that the MMSE estimator always outperforms the iterative estimator although the iterative estimator is able to reach comparable performance with a well-chosen number of iterations (depending on the SNR). Furthermore, it was shown through simulation results that the equispaced subcarrier assignment scheme performs the best in both synchronized and unsynchronized scenario, except in FBMC-OQAM when a lack of pilots occurs. The simulation results also confirmed the significant advantage of FBMC-OQAM in unsynchronized scenarios.

Finally, section 5 investigated the tracking of distributed MIMO dowlink channel estimates. A method was proposed that does not rely on scattered pilots but only requires the feedback of SNR measurements, and is based on small perturbations applied to the transmitted signal.

Simulation results have shown that a good estimate can be obtained in a reasonable amount of time with a limited impact on the data transmission. Theoretical performance evaluations have been given and match the simulation results well.

7. References

[1] R. Zakaria, D. le Ruyet, and M. Bellanger. Maximum Likelihood Detection in spatial multiplexing with FBMC. In *Proc. 2010 European Wireless*, June 2010.

[2] Y. Cheng and M. Haardt. Widely Linear Processing in MIMO FBMC/OQAM Systems. In *Proc. ISWCS 2013*, Aug. 2013.

[3] D. Lee, H. Seo, B. Clerckx, E. Hardouin, D. Mazzarese, S. Nagata, and K. Sayana. Coordinated multipoint transmission and reception in LTE-advanced deployment scenarios and operational challenges. *IEEE Communications Magazine*, 50(2):148 – 155, Feb. 2012.

[4] L. Venturino, N. Prasad, and X. Wang. Coordinated linear beamforming in downlink multi-cell wireless networks. *IEEE Trans. on Wireless Communications*, 9(4):1536 – 1276, Apr. 2010.

[5] B. Song, F. Roemer, and M. Haardt. Flexible coordinated beamforming (FlexCoBF) for the downlink of multi-user MIMO systems in single and clustered multiple cells. *Elsevier Signal Processing*, 93:2462 – 2473, Sept. 2013.

[6] J. Zhang, R. Chen, and J. G. Andrews. Networked MIMO with clustered linear precoding. *IEEE Trans. on Wireless Communications*, 8(4):1910 – 1921, Apr. 2009.

[7] K. Kim, J. Lee, C. Lee, N. Jeon, and S. Kim. Coordinated beamforming with limited BS cooperation for multicell multiuser MIMO broadcast channel. In *Proc. IEEE Vehicular Technology Conference (VTC) Spring*, Apr. 2009.

[8] P. Siohan, C. Siclet, and N. Lacaille. Analysis and design of OFDM/OQAM systems based on filterbank theory. *IEEE Transactions on Signal Processing*, 50(5):1170 – 1183, May 2002.

[9] M.G. Bellanger. Specification and design of a prototype filter for filter bank based multicarrier transmission. In *Acoustics, Speech, and Signal Processing, 2001. Proceedings. (ICASSP '01). 2001 IEEE International Conference on*, volume 4, pages 2417–2420 vol.4, 2001.

[10] T. Fusco, A. Petrella, and M. Tanda. Sensitivity of multi-user filter-bank multicarrier systems to synchronization errors. In *Proc. ISCCSP*, Mar. 2008.

[11] H. Saeedi-Sourck, Y. Wu, J. W. M. Bergmans, S. Sadri, and B. Farhang-Boroujeny. Complexity and performance comparison of filter bank multicarrier and OFDM in uplink of multicarrier multiple access networks. *IEEE Transactions on Signal Processing*, 59(4):1907–1912, Apr. 2011.

[12] M. Shaat and F. Bader. Computationally efficient power allocation algorithm in multicarrier-based cognitive radio networks: OFDM and FBMC systems. *EURASIP Journal on Advances in Signal Processing*, 2010, Mar. 2010.

[13] M. Renfors, F. Bader, L. Baltar, D. Le Ruyet, D. Roviras, P. Mege, and M. Haardt. On the use of filter bank based multicarrier modulation for professional mobile radio. In *Proc. 77th IEEE Vehicular Technology Conf. (VTC 2013 Spring)*, June 2013.

[14] M. G. Bellanger. FBMC physical layer: a primer, June 2010.

[15] M. Caus and A. I. Perez-Neira. Multi-stream transmission in MIMO-FBMC systems. In *Proc. ICASSP 2013*, May 2013.

[16] M. Caus and A. I. Perez-Neira. Comparison of linear and widely linear processing in MIMO-FBMC systems. In *Proc. ISWCS 2013*, Aug. 2013.

[17] M. Caus and A. I. Perez-Neira. SDMA for filterbank with Tomlinson Harashima precoding. In *Proc. ICC 2013*, June 2013.

[18] M. Caus, A. I. Perez-Neira, and M. Moretti. SDMA for FBMC with block diagonalization. In *Proc. SPAWC 2013*, June 2013.

[19] Q. H. Spencer, A. L. Swindlehurst, and M. Haardt. Zero-forcing methods for downlink spatial multiplexing in multi-user MIMO channels. *IEEE Trans. Signal Process.*, 52(2):461–471, Feb. 2004.

[20] F. Boccardi and H. Huang. Limited downlink network coordination in cellular network. In *Proc. IEEE International Symposium on Personal Indoor and Mobile Radio Communications*, Sept. 2007.

[21] H. Zhang, N. B. Mehta, A. F. Molisch, J. Zhang, and H. Dai. Asynchronous Interference mitigation in Cooperative Base Station Systems. *IEEE Trans. on Wireless Communications*, 7(1):155–164, Jan. 2008.

[22] Y. Cheng, S. Li, J. Zhang, F. Roemer, B. Song, M. Haardt, Y. Zhou, and M. Dong. An Efficient and Flexible Transmission Strategy for the Multi-carrier Multi-user MIMO Downlink. *IEEE Transactions on Vehicular Technology*, 63(2):628 – 642, Feb. 2014.

[23] FP7-ICT Project PHYDYAS - Physical Layer for Dynamic Spectrum Access and Cognitive Radio. http://www.ict-phydyas.org.

[24] V. Stankovic and M. Haardt. Generalized design of multi-user MIMO precoding matrices. *IEEE Trans. Wireless Commun.*, 7(3):953 – 961, Mar. 2008.

[25] ITU-R Recommendation M.1225. Guidelines for evaluation of radio transmission technologies for IMT-2000, 1997.

[26] Y. Cheng, P. Li, and M. Haardt. Coordinated beamforming in MIMO FBMC/OQAM systems. In *Proc. IEEE Int. Conference on Acoustics, Speech, and Signal Processing (ICASSP)*, May 2014.

[27] Y. Cheng, P. Li, and M. Haardt. Intrinsic interference mitigating coordinated beamforming for the FBMC/OQAM based downlink. *EURASIP Journal on Advances in Signal Processing*, May 2014.

[28] F. Horlin, J. Fickers, T. Deleu, and J. Louveaux. Interference-free SDMA for FBMC-OQAM. *EURASIP Journal on Advances in Signal Processing*, 46, Mar. 2013.

[29] M. Newinger, L. G. Baltar, A. L. Swindlehurst, and J. A. Nossek. MISO Broadcasting FBMC System for Highly Frequency Selective Channels. In *Proc. International ITG Workshop on Smart Antennas (WSA 2014)*, Mar. 2014.

[30] D. S. Waldhauser, L. G. Baltar, and J. A. Nossek. MMSE subcarrier equalization for filter bank based multicarrier systems. In *Proc. IEEE 9th Workshop Signal Proc. Advances in Wireless Comm. SPAWC 2008*.

[31] A. Mezghani, M. Joham, R. Hunger, and W. Utschick. Transceiver design for multi-user MIMO systems. In *International ITG Workshop on Smart Antennas*, 2006. Ulm, Germany.

[32] R. Hunger, M. Joham, and W. Utschick. On the MSE-duality of the broadcast channel and the multiple access channel. *WSA*, 57(2):698–713, 2009.

[33] M. Sadek, A. Tarighat, and A. Sayed. A Leakage-Based Precoding Scheme for Downlink Multi-User MIMO Channels. *IEEE Trans. Wireless Commun.*, 6(5):1711 – 1721, May 2007.

[34] L. Hentilä, P. Kyösti, M. Käske, M. Narandzic, and M. Alatossava. MATLAB implementation of the WINNER Phase II Channel Model ver1.1, December 2007.

[35] D. Katselis, E. Kofidis, A. Rontogiannis, and S. Theodoridis. Preamble-Based Channel Estimation for CP-OFDM and OFDM/OQAM Systems: A Comparative Study. *IEEE Transactions on Signal Processing*, 58:2911–2916, May 2010.

[36] Eleftherios Kofidis, Dimitrios Katselis, Athanasios Rontogiannis, and Sergios Theodoridis. Preamble-based channel estimation in OFDM/OQAM systems: a review. *Signal Process.*, 93(7):2038–2054, July 2013.

[37] M. Belotserkovsky. An equalizer initialization algorithm for OFDM receivers. In *Consumer Electronics, 2002. ICCE. 2002 Digest of Technical Papers. International Conference on*, pages 372–373, June 2002.

[38] Jiun Siew, Robert Piechocki, Andrew Nix, and Simon Armour. A Channel Estimation Method for MIMO-OFDM Systems. 2002.

[39] C. Lélé, J.-P. Javaudin, R. Legouable, A. Skrzypczak, and P. Siohan. Channel estimation methods for preamble-based OFDM/OQAM modulation. *European Transactions on Telecommunications*, 19:741–750, September 2008.

[40] J. Louveaux, A. Kalakech, M. Guenach, J. Maes, M. Peeters, and L. Vandendorpe. An SNR-Assisted Crosstalk Channel Estimation Technique. In *Proc. IEEE International Conference on Communications (ICC '09)*, June 2009.

[41] L. Vandendorpe and J. Louveaux. ML co-channel interference estimation from SINR measurements for multicell OFDM downlink: bounds and performance analysis. In *Proc. International Conference on Acoustics Speech and Signal Processing (ICASSP'2010)*, pages 3298–3301, March 2010.

Glossary and Definitions

Acronym	Meaning
AFB	Analysis Filter Bank
AWGN	Additive White Gaussian Noise
BD	Block Diagonalization
BER	Bit Error Rate
BS	Base Station
CCDF	Complimentary Cumulative Distribution Function
CFR	Channel Frequency Response
CIR	Channel Impulse Response
CP	Cyclic Prefix
CP-OFDM	Orthogonal Frequency Division Multiplexing with the Cyclic Prefix insertion
CSI	Channel State Information
CSIT	Channel State Information at Transmitter
DFT	Discrete Fourier Transform
FB-MC	Filter Bank based Multi-Carrier modulation
FBMC/OQAM	Filter Bank based Multi-Carrier with Offset Quadrature Amplitude Modulation
ICI	Inter-Carrier Interference
IIM-CBF	Intrinsic Interference Mitigating Coordinated Beamforming
ISI	Inter-Symbol Interference
LoCCoBF	Low Complexity Coordinated Beamforming
MIMO	Multiple-Input-Multiple-Output
MISO	Multiple-Input-Single-Output
MISO-BC	Multiple-Input-Single-Output-Broadcast-Channel
MMSE	Minimum Mean Square Error
MRC	Maximum Ratio Combining
MSE	Mean Square Error
MSI	Multi-Stream Interference
MUI	Multi-User Interference
OQAM	Offset Quadrature Amplitude Modulation
Ped-A	Pedestrian-A [channel model]

PHYDYAS	PHYsical layer for DYnamic AccesS and cognitive radio, ICT PHYDYAS project,
PMR	Professional Mobile Radio
QAM	Quadrature Amplitude Modulation
QPSK	Quadrature Phase Shift Keying
RX	Receiver
SAS	Subcarrier Assignment scheme
SDMA	Space Division Multiple Access
SFB	Synthesis Filter Bank
SIMO	Single-Input-Multiple-Output
SISO	Single-Input-Single-Output
SINR	Signal to Interference and Noise Ratio
SIR	Signal to Interference Ratio
SNR	Signal to Noise Ratio
STHP	Spatial Tomlinson Harashima Precoder
SVD	Singular Value Decomposition
TX	Transmitter
UE	User Equipment
Veh-A	Vehicular-A [channel model]
Veh-B	Vehicular-B [channel model]
ZF	Zero-Forcing